FEDERAL UNIVERSITY OF PARANÁ

JÚLIO XAVIER VIANNA NETO

WIND TURBINE BLADE GEOMETRY DESIGN BASED ON MULTI-OBJECTIVE OPTIMIZATION USING METAHEURISTICS

CURITIBA

2013

JÚLIO XAVIER VIANNA NETO

WIND TURBINE BLADE GEOMETRY DESIGN BASED ON MULTI-OBJECTIVE OPTIMIZATION USING METAHEURISTICS

Dissertation submitted to the Graduate Program in Electrical Engineering from the Federal University of Paraná, as partial fulfilment of the requirements for the degree of Master of Science in Electrical Engineering.

Supervisor: Prof. Dr. Leandro dos Santos Coelho

CURITIBA

2013

Vianna Neto, Júlio Xavier
Wind turbine blade geometry design based on multi-objective optimization using metaheuristics / Júlio Xavier Vianna Neto. – Curitiba, 2013.
116 f. : il.; graf., tab.

Thesis (Master of Science) – Federal University of Paraná, Technology Sector, Post Graduate Program in Electrical Engineering.
Supervisor: Leandro dos Santos Coelho

1. Wind power - Turbines. I. Coelho, Leandro dos Santos. II. Título.

CDD 621.312136

Statement of Approval

JÚLIO XAVIER VIANNA NETO

WIND TURBINE BLADE GEOMETRY DESIGN BASED ON MULTI-OBJECTIVE OPTIMIZATION USING METAHEURISTICS

Dissertation approved by the following examining committee, as partial fulfilment of the requirements for the degree of Master of Science in Electrical Engineering, of the Graduate Program in Electrical Engineering from the Federal University of Paraná:

Dr. Leandro dos Santos Coelho
Department of Electrical Engineering, UFPR

Ph.D. Alessandro Lameiras Koerich
Department of Electrical Engineering, UFPR

Dr. Alexandre Rasi Aoki
Department of Electrical Engineering, UFPR

Dr. Aurora Trinidad Ramirez Pozo
Department of Informatics, UFPR

Curitiba, the 1st of March 2013.

Dedication

To my dear grandmother Dirce Miró Vianna,
who has always been an example of strength and love.

Acknowledgements

This work would not be possible without the help of many. First of all, I thank God for making everything possible.

The woman that I love, Andréa Poletti Dall'Oglio, had to abdicate many of her wills on behalf of myself during the whole period in which I have developed this dissertation, so that I could conclude it. In this way she showed her great love for me, and for that I am deeply indebted to her.

I also owe my deepest gratitude to my parents, Eng. Júlio Xavier Vianna Júnior and Ana Íria Golin Vianna, for the boundless support they gave me through my whole life, and for providing me the most valuable gifts, i.e., love, education and faith. Because of them, today I can chase my dreams.

Special thanks goes to all my friends and family, who make my life a lot more joyful and interesting. To my sisters Juliana Golin Xavier Vianna and Paula Golin Xavier Vianna. To my colleagues and friends from the Institute of Technology for Development (LACTEC) and the Federal University of Paraná (UFPR), M.Sc. Luciano Fedalto, Eng. Eduardo Massashi Yamao, Eng. José Renato Taborda Ribas, Luis Gustavo Tomal Ribas, M.Sc. Arthur Fernando Bonelli, M.Sc. Rafael Bartnik Grebogi, and others.

I would like to express my gratitude to Dr. Leandro dos Santos Coelho, my supervisor, not only for the orientation and support on the present and previous works, but also for the friendship and for many personal advices.

I wish to thank the examining committee members, Ph.D. Alessandro Lameiras Koerich, Dr. Alexandre Rasi Aoki and Dr. Aurora Trinidad Ramirez Pozo, for their suggestions and contributions to this dissertation.

Many thanks to aeronautical engineers M.Sc. Gustavo Oliveira Violato and Odilon Antônio Camargo do Amarante, for sharing their knowledge on aerodynamics, which made this dissertation a much better work. To Rodrigo Canestraro Quadros and Diogo Rafael Labegalini, for the development of a macro to import the blade geometry to a Computer-Aided Design (CAD) software. To M.Sc. Helon Vicente Hultmann Ayala, for reviewing this document and suggesting many improvements to it, and also for the great friendship. To

M.Sc. Leonardo Trigueiro dos Santos and M.Sc. Daniel Cavalcanti Jeronymo, for helping me on LaTeX typesetting. To M.Sc. Luiz Alberto Jorge Procopiak, who is responsible for introducing me to the field of wind power. To Eng. Augusto Xavier Morando and M.Sc. Frederico Schneider, for the friendship, support and exchange of information about wind power in Brazil.

My thanks to the fellows of the Hydroelectric Company of the São Francisco (CHESF), Eng. Pedro Bezerra de Carvalho Neto, Eng. Ricardo Barreto Fellows, M.Sc. Paulo César de Souza Câmara, Dr. Alcides Codeceira Neto, and Dr. Eduardo Sodré.

I acknowledge the work of Andrew Platt and Danny C. Sale on Wind-Turbine Performance Predictor (WT_Perf) and Horizontal Axis Rotor Performance Optimization (HARP_Opt), respectively, and thank the National Renewable Energy Laboratory (NREL) of the United States of America for making these tools available. Without these tools, the present work would be in a much more incipient stage.

I am grateful to everyone else who directly or indirectly contributed to the present work.

This work was a part of the Research and Development (R&D) project named "*Aerogerador Brasileiro Classe Megawatt – Fase I – Projeto Conceitual*" (Brazilian Megawatt Class Wind Turbine – Phase I – Conceptual Design), from the R&D program of the National Agency of Electrical Energy (ANEEL), supported by CHESF and executed by LACTEC.

Epigraph

"Denn durch den Irrgarten kann dich
nur ein wirklicher Wunsch führen"
(For only a true wish can guide you through the maze)

Michael Ende [1]

Abstract

The application of Evolutionary Algorithms (EAs) to wind turbine blade design can be interesting, by reducing the number of aerodynamic-to-structural design loops in the conventional design process, hence reducing the design time and cost. Recent developments showed satisfactory results with this approach, mostly combining Genetic Algorithms (GAs) with the Blade Element Momentum (BEM) theory. The general objective of the present work is to define and evaluate a design methodology for the rotor blade geometry in order to maximize the energy production of wind turbines and minimize the mass of the blade itself, using for that purpose stochastic multi-objective optimization methods. Therefore, the multi-objective optimization problem and its constraints were formulated, and the vector representation of the optimization parameters was defined. An optimization benchmark problem was proposed, which represents the wind conditions and present wind turbine concepts found in Brazil. This problem was used as a test-bed for the performance comparison of several metaheuristics, and also for the validation of the defined design methodology. A variable speed pitch-controlled 2.5 MW Direct-Drive Synchronous Generator (DDSG) turbine with a rotor diameter of 120 m was chosen as concept. Five different Multi-objective Evolutionary Algorithms (MOEAs) were selected for evaluation in solving this benchmark problem: Non-dominated Sorting Genetic Algorithm version II (NSGA-II), Quantum-inspired Multi-objective Evolutionary Algorithm (QMEA), two approaches of the Multi-objective Evolutionary Algorithm Based on Decomposition (MOEA/D), and Multi-objective Optimization Differential Evolution Algorithm (MODE). The results have shown that the two best performing techniques in this type of problem are NSGA-II and MOEA/D, one having more spread and evenly spaced solutions, and the other having a better convergence in the region of interest. QMEA was the worst MOEA in convergence and MODE the worst one in solutions distribution. But the differences in overall performance were slight, because the algorithms have alternated their positions in the evaluation rank of each metric. This was also evident by the fact that the known Pareto Front (PF) consisted of solutions from several techniques, with each dominating a different region of the objective space. Detailed analysis of the best blade design showed that the output of the design methodology is feasible in practice, given that flow conditions and operational features of the rotor were as desired, and also that the blade geometry is very smooth and easy to manufacture. Moreover, this geometry is easily exported to a Computer-Aided Design (CAD) or Computer-Aided Engineering (CAE) software. In this way, the design methodology defined by the present work was validated.

Key-words: Wind turbine blade. Multi-objective optimization. Evolutionary algorithm. Metaheuristic. Aerodynamic design.

Resumo

O processo de projeto de uma pá de turbina eólica pode ser dividido em duas etapas: projeto aerodinâmico e projeto estrutural. O projeto aerodinâmico consiste na seleção da geometria ótima da superfície externa da pá (geometria da pá), que é definida pela família de aerofólios, ou também chamados perfis aerodinâmicos, e distribuições de corda, ângulo de torção e espessura. O projeto estrutural é definido pela seleção de materiais da pá e pela definição da seção transversal estrutural ou longarina dentro do envelope externo. Tanto o projeto aerodinâmico quanto o estrutural podem ser vistos como problemas de otimização contínuos e restritos. Os Algoritmos Evolutivos (AEs) têm se mostrado eficazes na resolução de problemas de otimização em muitos campos da engenharia, e possuem implementação simples e flexível. AEs podem lidar melhor com problemas complexos, como problemas multi-objetivo restritos com espaço objetivo não-diferenciável e um grande número de mínimos locais, do que algoritmos baseados em gradiente. A aplicação de AEs no projeto de pás de turbinas eólicas pode ser interessante, por reduzir o número de iterações entre projeto aerodinâmico e estrutural no processo convencional de projeto, reduzindo assim o tempo e o custo de projeto. Pesquisas recentes mostraram resultados satisfatórios com esta abordagem, principalmente combinando Algoritmos Genéticos (AGs) com a Teoria do Elemento de Pá (TEP). A maioria desses trabalhos, no entanto, apresentam algumas deficiências que podem comprometer a ampla aplicação de suas técnicas propostas, tais como: falta de uma investigação detalhada sobre o desempenho de AEs na tarefa de otimização de geometria da pá; conceitos obsoletos de turbinas eólicas utilizados na formulação do problema de otimização; representação incipiente da geometria da pá; e falta de análise estrutural integrada à otimização da geometria. Nesse contexto, o problema abordado pelo presente trabalho consiste em identificar se e como é possível melhorar a otimização evolutiva da geometria de pás de rotores eólicos e resolver as falhas de abordagens anteriores, mencionadas anteriormente. A hipótese da presente pesquisa é que a otimização evolutiva da geometria da pás é melhorada por uma abordagem em que são investigados tanto o desempenho de vários métodos de otimização como a formulação do problema de otimização multi-objetivo. Essa formulação incorpora análise aerodinâmica e estrutural, e uma representação da geometria de pás que proporciona uma liberdade adequada para as suas curvas e fornece geometrias suaves e viáveis. Dessa forma, essa abordagem fornece soluções realistas e de alta qualidade, com alta eficiência computacional. O objetivo geral do presente trabalho é definir e avaliar uma métodologia de projeto para a geometria de pás de rotores eólicos, a fim de maximizar a produção de energia de turbinas eólicas e minimizar a massa da pá, utilizando para o isso métodos estocásticos de otimização multi-objetivo. Para isso, o problema de otimização multi-objectivo e suas restrições foram formulados, e a representação vetorial dos parâmetros de otimização foi definida. Um problema de otimização foi proposto como estudo de caso, que representa as condições de vento e conceitos de turbinas eólicas atuais encontrados no Brasil. Este problema foi usado para avaliar e comparar o desempenho de várias metaheurísticas, assim como para validar a metodologia de projeto definida. O conceito de turbina escolhido

foi uma máquina de 2,5 MW com gerador síncrono e acoplamento direto, operação em velocidade variável, controlada por *pitch*, e com um diâmetro de rotor de 120 m. Cinco Algoritmos Evolutivos Multi-objetivo (AEMOs) diferentes foram selecionados para serem avaliados na resolução do problema do estudo de caso: Algoritmo Genético de Ordenação pela Não-dominância versão II (AGON-II), Algoritmo Evolutivo Multi-objetivo com Inspiração Quântica (AEMIQ), duas abordagens do Algoritmo Evolutivo Multi-objetivo baseado em Decomposição (AEMO/D), e Algoritmo de Otimização Multi-objetivo por Evolução Diferencial (MOED). Os resultados mostraram que as duas melhores técnicas para este tipo de problema são AGON-II e AEMO/D, uma tendo apresentado soluções mais amplas e uniformemente espaçadas, e a outra tendo uma melhor convergência na região de interesse. AEMIQ foi o pior AEMO em questão de convergência, e MOED o pior em distribuição de soluções. Mas as diferenças no desempenho geral foram sutis, pois os algoritmos alternaram suas posições no *ranking* de avaliação de cada métrica. Isto também foi evidenciado pelo fato de que a Fronteira de Pareto (FP) conhecida consistiu em soluções de várias técnicas, cada uma dominando uma região diferente do espaço objetivo. A análise detalhada do projeto da melhor pá mostra que a solução gerada pelo método de otimização é totalmente viável, uma vez que as condições de fluxo e as características de funcionamento do rotor ficaram de acordo com o que se deseja, e também que a geometria de pá obtida é muito suave e fácil de fabricar. Além disso, esta geometria é facilmente exportada para um *software* CAD (*Computer-Aided Design*) ou CAE (*Computer-Aided Engineering*). Deste modo, a metodologia de projeto definida pelo presente trabalho foi validada.

Palavras-chave: Pá de turbina eólica. Otimização multi-objetivo. Algoritmo evolutivo. Metaheurística. Projeto aerodinâmico.

List of Figures

List of Tables

List of Acronyms

AEP	Annual Energy Production
ANEEL	*Agência Nacional de Energia Elétrica* (National Agency of Electrical Energy)
BEM	Blade Element Momentum
BNDES	*Banco Nacional de Desenvolvimento Econômico e Social* (National Bank of Economic and Social Development)
CAD	Computer-Aided Design
CAE	Computer-Aided Engineering
CHESF	*Companhia Hidro Elétrica do São Francisco* (Hydroelectric Company of the São Francisco)
COE	Cost of Energy
DDSG	Direct-Drive Synchronous Generator
DE	Differential Evolution
DFIG	Doubly-Fed Induction Generator
DM	Decision Making
DUT	Delft University of Technology
EA	Evolutionary Algorithm
FX	Franz Xaver Wortmann
GA	Genetic Algorithm
GDE	Generalized Differential Evolution
GP	Genetic Programming
HARP_Opt	Horizontal Axis Rotor Performance Optimization
HAWT	Horizontal Axis Wind Turbine
IEC	International Electrotechnical Commission
LACTEC	*Instituto de Tecnologia para o Desenvolvimento* (Institute of Technology for

	Development)
LEN	*Leilão de Energia Nova* (New Energy Auction)
LER	*Leilão de Energia de Reserva* (Reserve Energy Auction)
LFA	*Leilão de Fontes Alternativas* (Alternative Sources Auction)
MATLAB	MATrix LABoratory
MODE	Multi-objective Optimization Differential Evolution Algorithm
MOEA	Multi-objective Evolutionary Algorithm
MOEA/D	Multi-objective Evolutionary Algorithm Based on Decomposition
MOP	Multi-objective Optimization Problem
MPPT	Maximum Power Point Tracking
NACA	National Advisory Committee for Aeronautics
NREL	National Renewable Energy Laboratory
NSGA	Non-dominated Sorting Genetic Algorithm
NSGA-II	Non-dominated Sorting Genetic Algorithm version II
ONVG	Overall Non-dominated Vector Generation
ORC	Optimal Regimes Characteristic
PDE 2020	*Plano Decenal de Expansão de Energia 2020* (Energy Expansion Ten-year Plan 2020)
PF	Pareto Front
PROINFA	*Programa de Incentivo às Fontes Alternativas de Energia Elétrica* (Incentive Program for Electric Energy Alternative Sources)
PS	Pareto Set
Q-bit	Quantum-inspired bit
QEA	Quantum-inspired Evolutionary Algorithm
QMEA	Quantum-inspired Multi-objective Evolutionary Algorithm
RAM	Random-Access Memory
R&D	Research and Development
SBX	Simulated Binary Crossover

SPI	Shape Preserving Interpolation
T-MOEA/D	MOEA/D in which the Tchebycheff approach is used
UFPR	*Universidade Federal do Paraná* (Federal University of Paraná)
VBA	Visual Basic for Applications
W-MOEA/D	MOEA/D in which the weighted sum approach is used
WT_Perf	Wind-Turbine Performance Predictor

List of Symbols

a	Axial induction factor
a'	Tangential induction factor
A	Rotor disc area; Set of decision vectors
a_c	Constant for the Glauert correction
A_{cross}	Cross section area of a blade
b_j^t	Best binary individual from $B(t)$ in QEA
B	Number of blades; Set of decision vectors
$B(t)$	Best binary individuals in QEA generated between iterations 0 and t
c	Airfoil chord length
C	Scale parameter of the Weibull probability density function; Coverage metric function
c_{CPi}	Ordinate of the i-th chord control point
c_{CRk}	Ordinate of the k-th chord circular root control point
C_D	Drag coefficient
C_L	Lift coefficient
C_n	Normal load coefficient
C_P	Rotor power coefficient
c_{root}	Chord at the root
C_t	Tangential load coefficient
C_T	Thrust coefficient
c_{tip}	Chord at the tip
d	Distance from the point of interest to the neutral axis, in strain calculations
$\overline{d}$	Mean of all d_i in a PF approximation set (A or B)
D	Drag

d_i	Distance of the i-th point to its closest neighbour, in a PF approximation set (A or B)
dr	Length of a blade element
E	Elastic modulus of the bulk material
F	Prandtl's tip loss factor; Objective vector in MOPs
F_C	Capacity factor
F_m	Mutation scale factor in DE
F_S	Safety factor
$F_1(x)$	Objective function number 1
$F_2(x)$	Objective function number 2
$f(V)$	Probability of occurrence of the wind speed V
h	Number generated randomly with uniform distribution in the range $[0, 1]$
h_{hub}	Hub height
h_{year}	Number of hours in the year, i.e., 8760 hours
k	Shape parameter of the Weibull probability density function; Number of solutions in a non-dominated set A
K	Penalty factor for maximum angle of attack constraint
K_{avl}	Availability of the turbine
K_{cr}	Crossover constant in DE
l	Lower limit vector
L	Lift
l_i	Lower limit for the i-th element of the solution vector x
m	Number of Q-bits in the individuals of QEA
M	Bending moment
m_b	Blade mass
n	Population size; Number of true airfoils; Number of decision vectors in a set (A or B)
N	Number of sub-problems in MOEA/D

n_{elm}	Number of blade elements
NF_i	Non-dominated front of level i
n_g	Number of groups in the update process of QMEA
n_p	Domination count, i.e., the number of solutions that dominate p
n_x	Number of decision variables
p_c	Crossover probability
P_{conv}	Power losses at the electronic converter
P_{fe}	Iron losses at the generator
P_{fri}	Frictional losses at bearings and bushings of the drive train
P_{gear}	Mechanical power losses at the gearbox
p_m	Mutation probability
P_m	Mechanical power at the shaft
P_{out}	Output power of the turbine
p_{rank}	Non-domination rank of the solution p, i.e., the level of the non-dominated front that p belongs
P_{rated}	Rated power of the turbine
P_{rot}	Copper losses at the rotor field winding
$P_r(t)$	Floating point representation of the classical population $P(t)$ in QEA at iteration t
P_{stat}	Copper losses at the stator winding
$P(t)$	Population of classical bits individuals in QEA at iteration t; Parent population at iteration t in NSGA-II
q_j^t	j-th Q-bits individual in QEA at iteration t
Q	Aerodynamic torque
$Q(t)$	Population of Q-bits individuals in QEA at iteration t; Offspring population at iteration t in NSGA-II
r	Radial position along the blade
R	Total rotor radius

Re	Reynolds number
r_{hub}	Hub radius
R^m	Objective space in MOPs
r_{rte}	Radius for the root transition end
r_{rts}	Radius for the root transition start
$R(t)$	Combined parent and offspring populations at iteration t in NSGA-II
r_{tts}	Radius for the tip transition start
S	Spacing metric function
S_p	Set of solutions dominated by p
t	Absolute or dimensional thickness
T	Aerodynamic thrust; Neighbourhood size in MOEA/D
t_{CPj}	Absolute thickness corresponding to the j-th relative thickness control point
t_{max}	Maximum number of iterations in QEA; Maximum shell thickness for the calculation procedure of A_{cross}
t_{min}	Initial shell thickness for the calculation procedure of A_{cross}
t_r	Relative thickness
t_{rCPj}	Ordinate of the j-th relative thickness control point
t_{shell}	Cross section shell thickness
u	Upper limit vector
u_i	Upper limit for the i-th element of the solution vector x
$U(\Delta\theta)$	Quantum rotation gate
V	Wind speed
V_{ave}	Average or mean wind speed
V_{in}	Cut-in wind speed
V_{out}	Cut-out wind speed
V_{rated}	Rated wind speed of the turbine
V_∞	Free stream air flow speed

x	Solution vector
$x_{distance}$	Crowding-distance of solution x
x^i	i-th solution vector or point of a set (A or B)
x_i	i-th element of the solution vector x
x_j^t	j-th binary individual in QEA at iteration t
α	Angle of attack; Probability amplitude of the quantum state $\|0\rangle$
α_{stall}	Stall angle of attack
β	Probability amplitude of the quantum state $\|1\rangle$
Γ	Gamma function
Δt	Thickness step for the calculation procedure of A_{cross}
ΔV	Wind speed discretization step for the power curve
$\Delta\alpha$	Margin for the angle of attack constraint
$\Delta\theta$	Rotation angle applied by the quantum gate
ε	Strain at a point of interest
ε_{allow}	Maximum allowable strain
η	Efficiency of the mechanical-electrical system
θ	Blade pitch angle
η_c	Distribution index for crossover operator
η_m	Distribution index for mutation operator
θ_{CPi}	Ordinate of the i-th twist control point
θ_{CR}	Ordinate of the twist circular root control point
θ_l	Blade local pitch angle
λ	Tip speed ratio
λ_{opt}	Optimum tip speed ratio of the rotor
ν_{air}	Kinematic viscosity of the air
ρ_{air}	Air density
ρ_{mat}	Density of the bulk isotropic material

σ	Rotor solidity
ϕ	Relative flow angle
$\|\psi\rangle$	State of a quantum bit using Dirac notation
Ω	Angular velocity of the rotor; Parameter space in MOPs
Ω_{min}	Minimum allowable angular velocity of the rotor
Ω_{rated}	Rated angular velocity of the rotor

Contents

1 Introduction

The Brazilian electricity matrix is based on large hydroelectric power plants, which represent over 65% of its total installed capacity (see Figure 1.1), according to the National Agency of Electrical Energy (ANEEL) [2]. But the country is recently experiencing a boom in the energy sector based on renewable sources like wind, solar and small hydro. This boom was initially driven by the Incentive Program for Electric Energy Alternative Sources (PROINFA) introduced in 2002, and recently by the regulated auctions that take place regularly since 2009. In this context, the wind energy market in Brazil is recently growing fast.

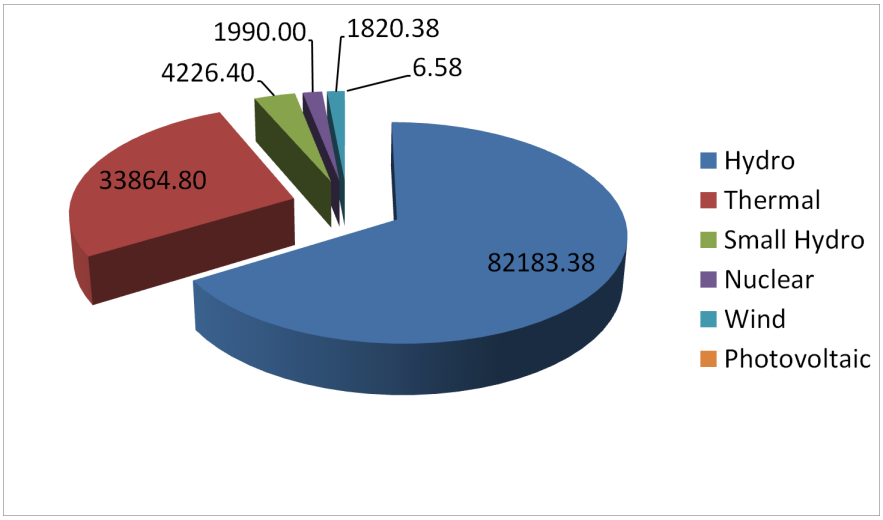

Figure 1.1: Brazilian current installed capacity per source (in MW), adapted from ANEEL [2].

Brazil has great wind resources, especially at coastal regions, where there are high annual average speeds with high direction and speed steadiness. The Brazilian wind atlas, published in 2001 [3], showed an estimated wind power potential of 143 GW at the height of 50 m, but new measurements recently made at 80 to 100 m high indicate that the actual potential can be more than 300 GW.

In 2010, a total of 326 MW of wind power were installed in Brazil, which represented

a growth of 64.1% in wind power installed capacity. In 2011, the growth was of 452 MW, or 54.4%. The mark of 2000 MW of wind power capacity was recently reached, in 2012, which represents about 1.6% of total generating capacity in the Brazilian power system. From 2009 to 2011, there were roughly 2000 MW per year contracted through the regulated auctions, meaning that there will be at least another 6000 MW to be installed until 2016. The Brazilian Energy Expansion Ten-year Plan 2020 (PDE 2020) [4] estimates that by 2020 there will be more than 11000 MW of wind power installed capacity (Figure 1.2).

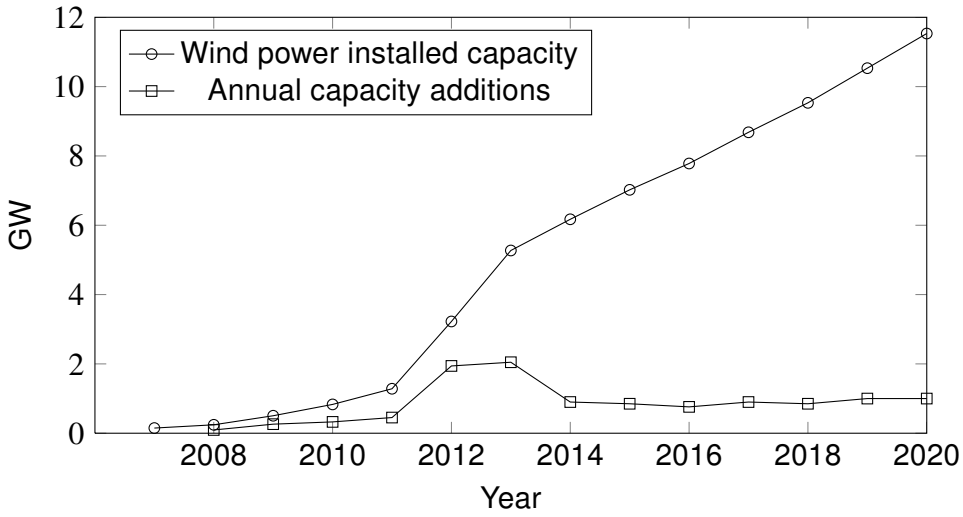

Figure 1.2: Annual wind power capacity additions in Brazil (past installations and prognosis), adapted from PDE 2020 [4].

Since 2002, the energy selling prices for wind power have been dropping from about R$300 / €112 per MWh (PROINFA prices) to less than R$90 / €34 per MWh — R$87.98 / €32.61 per MWh was the mean price for wind energy at the last auction of 2012 (Figure 1.3) [5]. The reason for this is both the wind resource, which causes high energy production (capacity factors around 50%), and the competition between a growing number of turbine manufacturers in the country. Today there are around 10 manufacturers in Brazil, including the ones that are operating, developing or still planning their production facilities.

Thereby, the Brazilian wind market is emerging, seeming to be soon one of the largest markets in the world. For the next years there will be opportunities in the country, as well as great challenges, since there will be a substantial increase in power installation, comparing to previous years. The main challenges are: solving the logistical problems of the supply chain; ensuring greater financial resources, since only one bank could not be enough to supply the demand; increasing the productive capacity of the wind industry; granting access to the grid, and also enhance the transmission lines between the northeast and the southeast regions of Brazil; and developing technology suited to Brazilian condi-

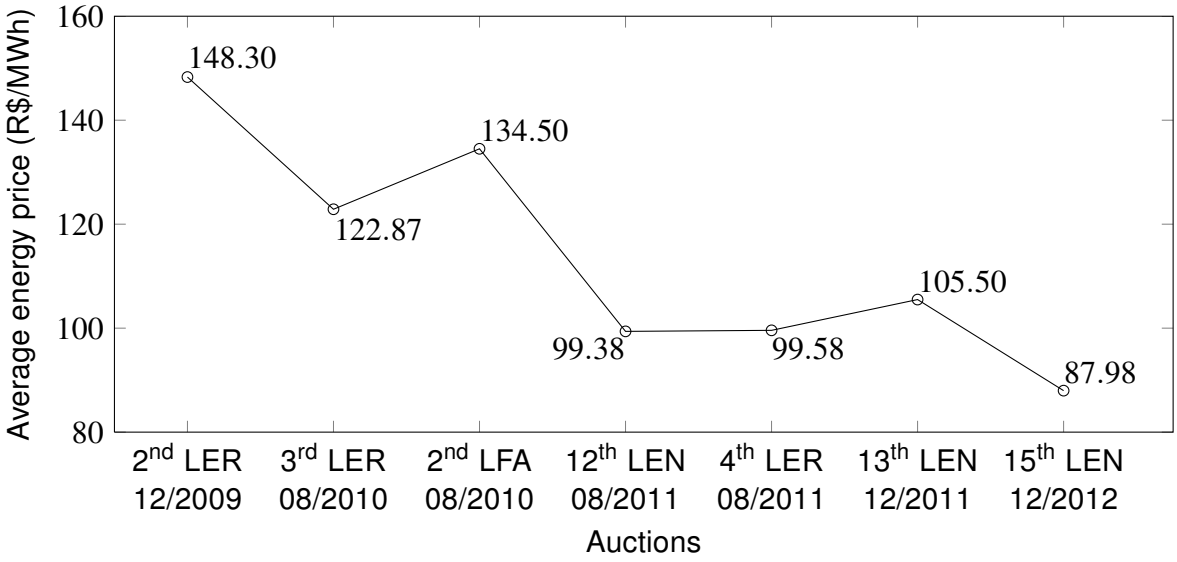

Figure 1.3: Average energy price development since the beginning of the auctions [5].

tions. This last challenge motivates and justifies the work reported by this dissertation.

The dropping energy prices in Brazil demand reductions on the Cost of Energy (COE) from wind turbines, in order to keep the economic feasibility of the wind farm projects, and also to make the wind energy a competitive source in the energy market. With regard to the rotor blade design, it must aim at achieving lighter blades, with higher rotor efficiency for the turbine to produce more energy. Reducing the blade mass will reduce its cost, and in this way will also reduce the initial capital cost of the wind farm project, since the cost of the blades represent almost 20% of the total cost of a wind turbine. Additionally, increasing the wind turbine Annual Energy Production (AEP) will increase the operating revenue of the wind farm project. Hence, the impact of both initial capital cost reduction and increase in operating revenue is the reduction on the COE. This is why the maximization of the AEP and the minimization of the blade mass are strong candidates for objective functions of the blade geometry optimization, as detailed further on.

The design process of a wind turbine blade can be divided into two steps: aerodynamic design and structural design. The aerodynamic design consists in the selection of optimal geometry of the blade external surface (blade geometry), which is defined by the airfoil family and the distributions of chord, twist angle and thickness. The structural design is defined by the blade materials selection and definition of the structural cross section or spar within the outer envelope [6]. Both the aerodynamic and structural designs can be seen as continuous constrained optimization problems.

The following sections of this chapter present, in this order: the state of the art of

the problem addressed by the present work; the definition of this problem; the hypothesis of the research; the general and specific objectives of this work; the main original contributions given by it; and at last the overall organization of this document.

1.1 State of the Art of the Problem

Evolutionary Algorithms (EAs) have shown to be effective in solving optimization problems in many engineering fields, whereas of easy and flexible implementation. EAs can better handle complex problems, such as multi-objective constrained problems with non-differentiable objective space and a large number of local minima, than gradient-based algorithms. The use of EAs in the wind energy field has been recently increasing. For example, a Genetic Algorithm (GA) has been recently used by Jureczko, Pawlak and Mezyk [7] to optimize the blade structural design. The application of such tools to the blade aerodynamic design can be interesting, allowing the optimization of the blade design parameters in order to, for example: maximize generated power under a given operating condition, maximize AEP for a specific wind speed distribution (site-specific optimization), minimize the amount of blade material and/or minimize the COE. Moreover, EAs can help to reduce the time and cost of the wind turbine blade design process, by integrating the blade aerodynamic and structural optimization.

Recent developments showed satisfactory results with this approach, mostly combining GAs with the Blade Element Momentum (BEM) theory, as reported by Selig and Coverstone-Carroll [8], Méndez and Greiner [9], Liu, Chen and Ye [10], Xuan et al. [11], Eke and Onyewudiala [12] and Sale [13]. In addition, Casás, Peña and Duro [14] developed an automatic design environment for the blade geometry through a macroevolutionary algorithm, using a combination of blade element theory and a panel method, applying neural networks and an integral boundary layer code to improve accuracy of the approach. Benini and Toffolo [15] proposed a multi-objective approach based on Genetic Programming (GP) and Pareto concepts to the blade aerodynamic design, aiming to both maximize AEP and minimize COE, also using the BEM theory. More recently, in 2012, the Cuckoo Search Algorithm and the Quantum-inspired Evolutionary Algorithm (QEA) have been applied to blade geometry design respectively by Ernst et al. [16] and Vianna Neto et al. [17], in mono-objective approaches.

Most of these works, however, present some shortfalls that may compromise the wide application of their proposed techniques. For instance, there is a lack of investigation

on the performance of the optimization methods applied in [8, 9, 11–13, 15, 17], which could be enhanced. Another problem that arises is the use of outdated wind turbine concepts, such as stall-controlled turbines, in the optimization problem, which happens in [8–10, 15]. The blade geometry representation could be better exploited in some of theses works, e.g. in [9, 12, 14], in order to give more freedom to the geometry curves or to enable more realistic solutions. Furthermore, the integration of some kind of structural analysis to the geometry optimization could bring better results to the following works [9, 10, 14, 16, 17].

1.2 Problem Definition

In this context, the problem to be addressed by the present work consists in identifying if and how it is possible to enhance the evolutionary optimization of wind turbine blade geometry and solve the previously mentioned shortfalls of previous approaches, namely:

- Lack of detailed investigation on the performance of evolutionary algorithms in the task of blade geometry optimization;
- Outdated wind turbine concepts utilized in the simulation test-bed;
- Incipient blade geometry representation;
- Lack of structural analysis integrated to the geometry optimization.

1.3 Hypothesis

The hypothesis of the present research is that the rotor blade geometry evolutionary optimization is enhanced by an approach in which both the performance of several optimization methods and the Multi-objective Optimization Problem (MOP) formulation are assessed. This MOP formulation incorporates aerodynamic and structural analysis, and a blade geometry representation that gives a proper freedom to its curves and provides smooth and feasible geometries. In this way, this approach provides high quality and realistic solutions with high computational efficiency.

1.4 Objectives

The objectives of this research were broken into general and specific, which are summarized as follows.

The general objective is to define and evaluate a design methodology for the rotor blade geometry in order to maximize the energy production of wind turbines and minimize the mass of the blade itself, using for that purpose stochastic multi-objective optimization methods.

In order to achieve the general objective, the following specific objectives were outlined:

- Based on the Horizontal Axis Rotor Performance Optimization (HARP_Opt) code of Sale [18], formulate the multi-objective optimization problem, proposing a modified blade geometry representation and three novel constraints;
- Propose an original benchmark problem, based on the wind conditions and present wind turbine concepts found in Brazil, to be used as a test-bed for the design methodology;
- Evaluate and compare the performance of selected metaheuristics, namely Non-dominated Sorting Genetic Algorithm version II (NSGA-II), Quantum-inspired Multi-objective Evolutionary Algorithm (QMEA), two approaches of Multi-objective Evolutionary Algorithm Based on Decomposition (MOEA/D), and Multi-objective Optimization Differential Evolution Algorithm (MODE), in solving the benchmark problem, and also evaluate the solutions obtained by the defined design methodology.

1.5 Main Contributions

The author found that the approach that best suits the problem defined in Section 1.2 is the HARP_Opt of Sale [13]. The HARP_Opt is a code implemented in MATrix LABoratory (MATLAB), which uses the Wind-Turbine Performance Predictor (WT_Perf) code [19] as the BEM model in the evaluation of solutions and the multi-objective GA function from the MATLAB Global Optimization Toolbox as the Multi-objective Evolutionary Algorithm (MOEA). Furthermore, a simple structural model is applied in the HARP_Opt geometry optimization, which provides a preliminary aerodynamic design that already balances the

loads and stresses through the blade span, avoiding stress concentration points. This can reduce the number of aerodynamic-to-structural design loops in the conventional process of blade design, thus reducing the design time and cost. The blade geometry representation in HARP_Opt is performed through the use of Bézier curve parametrization, described by Farin [20], which provides smooth curves for the distributions of chord and twist. For these reasons, the HARP_Opt was chosen as a baseline to the development of the present work.

In this way, most of the original contributions of this work regard modifications and new features to the HARP_Opt approach. These contributions are summarized below:

- Application of the mechanical-electrical system efficiency (η) curve, combined with the rotor performance curve (C_P versus λ), in the determination of the optimal rotational speed of the rotor in relation to the wind speed. This procedure is explained in Subsection 2.1.2. Thereby, the steady state operation of the Maximum Power Point Tracking (MPPT) strategy is modelled more accurately, and the evolutionary search will tend towards rotors with higher optimum tip speed ratios (λ_{opt}). In HARP_Opt only the C_P versus λ curve is used for this process.

- Modification to the circular root transition feature, by the inclusion of a circular root control point at the twist curve, in order to remove discontinuities in this curve. This is shown in Subsection 4.2.3.

- Development of a tip transition feature (described in Subsection 4.2.4), since in most of the blade designs a chord value close to zero is adopted at the tip. Through this feature the chord goes smoothly from its optimal value before the tip to the zero value at the tip.

- Modification to full-cosine spacing of the chord and twist control points radial positions (mentioned in Subsection 4.2.1), instead of half-cosine in HARP_Opt. This gives a higher control point density towards the root and the tip of the blade, giving more freedom to the curves in these regions. In HARP_Opt, with half-cosine spacing, the curves are too restricted in the tip region. The tip region needs flexibility because of the tip transition feature.

- Modification of the thickness interpolation, with the use of monotone piecewise cubic interpolation, as described by Fritsch and Carlson [21], instead of piecewise constant or piecewise linear interpolation. The interpolation process in the root transition region was integrated with the whole blade, simplifying the original HARP_Opt interpolation

process, which was broken in multiple regions. In addition, the iterative process used to determine the root chord was removed. The modified thickness interpolation process is presented in Subsection 4.2.2.

- Modification of the monotonicity constraint, which in HARP_Opt was applied to the control points, and here it is applied to the properties at the blade element centers. The chord, twist and thickness curves are indeed required to be monotonically decreasing, from the root to the tip of the blade, but not the control points. In Section 4.2, the Figure 4.2 shows a typical example of twist and chord curves that are monotonically decreasing, but the control points are not. If the control points are required to be monotonically decreasing, the freedom of the geometrical curves is compromised. The modified monotonicity constraint is described in Subsection 4.3.2.

- Inclusion of a constraint to the maximum chord location, which is proposed in Subsection 4.3.3, in order to avoid infeasible blade geometries. This constraint is specially needed when the control points are not required to be monotonically decreasing, because in this case the probability that the location of the maximum chord ends up too far from the root is much higher.

- Proposition of a maximum angle of attack constraint, in order to ensure that the design angle of attack throughout the blade span keep a safe margin from the stall angle of attack. This constraint is defined in Subsection 4.3.4.

The HARP_Opt was published as an open source code [18] with a corresponding user's guide [13], and thereby no formal mathematical description was made from the MOP of this approach. Consequently, another original contribution of the present work is the unprecedented formulation of this MOP, including its objective functions, constraints and the vector representation of decision variables. In addition, the original benchmark problem proposed in Section 4.4 is expected to give its own contribution for future performance assessments of different optimization methods, for this is the only problem found in the literature which is based on wind conditions and present wind turbine concepts found in Brazil.

Finally, while the most of the EAs applied to the blade design are genetic based algorithms, the present work evaluates the performance of several EA frameworks in solving the multi-objective optimization of the wind turbine blade geometry. In this way, the performance of NSGA-II, QMEA, two approaches of the MOEA/D, and MODE are compared against each other, using for that purpose the proposed benchmark problem as a test-bed.

As for the problem of blade design no previous application of the last three techniques was found in the literature, their performance assessment in this problem is also an original contribution of the present work.

1.6 Overall Structure of the Dissertation

The remainder of this dissertation is organized as follows. Chapter 2 describes the wind energy concepts required to formulate the multi-objective optimization problem of the blade geometry design, including the technology of wind turbines, the characteristics of wind resources, the AEP estimation and blade design aspects. Concepts as the MPPT, power control by active pitch and the BEM theory are also presented in this chapter.

The concepts of evolutionary optimization are discussed in Chapter 3. Initially in this chapter, MOP is mathematically described, and the Pareto dominance and optimality are presented. Recent MOEA applications are reviewed, as well as indicators to measure their performance. Then the metaheuristics that are evaluated in the present work, including NSGA-II, QMEA, MOEA/D and MODE, are briefly described.

Chapter 4 defines the formulation of the objective functions and constraints of the MOP addressed in this research. The approach adopted in the present work for the blade geometry representation is also detailed in this chapter. In addition, a benchmark problem is proposed, based on current turbine concepts and wind conditions in Brazil, to be used in the performance evaluation of the optimization algorithms.

The results obtained with the design methodology developed are presented and analysed in Chapter 5. But first the materials and methods applied in the experiments are described. Then, then performance of different stochastic optimization algorithms applied to the proposed benchmark problem are compared, considering several runs for each of them. The obtained Pareto Front (PF) and Pareto Set (PS) are analysed, and also the resulting blade designs of some solutions picked from the obtained PS. At last in this chapter, the best blade design found is detailed.

Finally, Chapter 6 gives the conclusions and final remarks, and outlines some topics for future research on the subject of this dissertation.

2 Wind Power

This chapter discusses about the wind energy concepts required to develop this dissertation. First a brief motivation is given, by an introduction about the situation of the wind power in Brazil. Secondly, a description about the technology of wind turbines is made, focusing on the operational and design aspects that have an impact on the blade design. Then the characteristics of wind resources and how to estimate from them the AEP of wind turbines are detailed. At last, the aspects of the blade design are presented.

2.1 Wind Turbines

Modern wind turbines use the lift force generated by the blades to move the rotor and generate electricity. Nowadays, the most common design of wind turbine is the Horizontal Axis Wind Turbine (HAWT), which is the focus of this dissertation. A typical HAWT consists of the following subsystems [22], that are also shown in Figure 2.1:

- Rotor, which corresponds to the blades, the pitch system and the hub that supports them;
- Drive train, i.e., the turbine rotating parts (except the rotor), represented by the shafts, gearbox (except on direct-drive machines), coupling, mechanical brake and generator;
- Nacelle and mainframe, including the baseplate and yaw system;
- Tower and foundation;
- Control systems;
- Electrical system components, such as cables, switches, transformers, power electronic converters and capacitors.

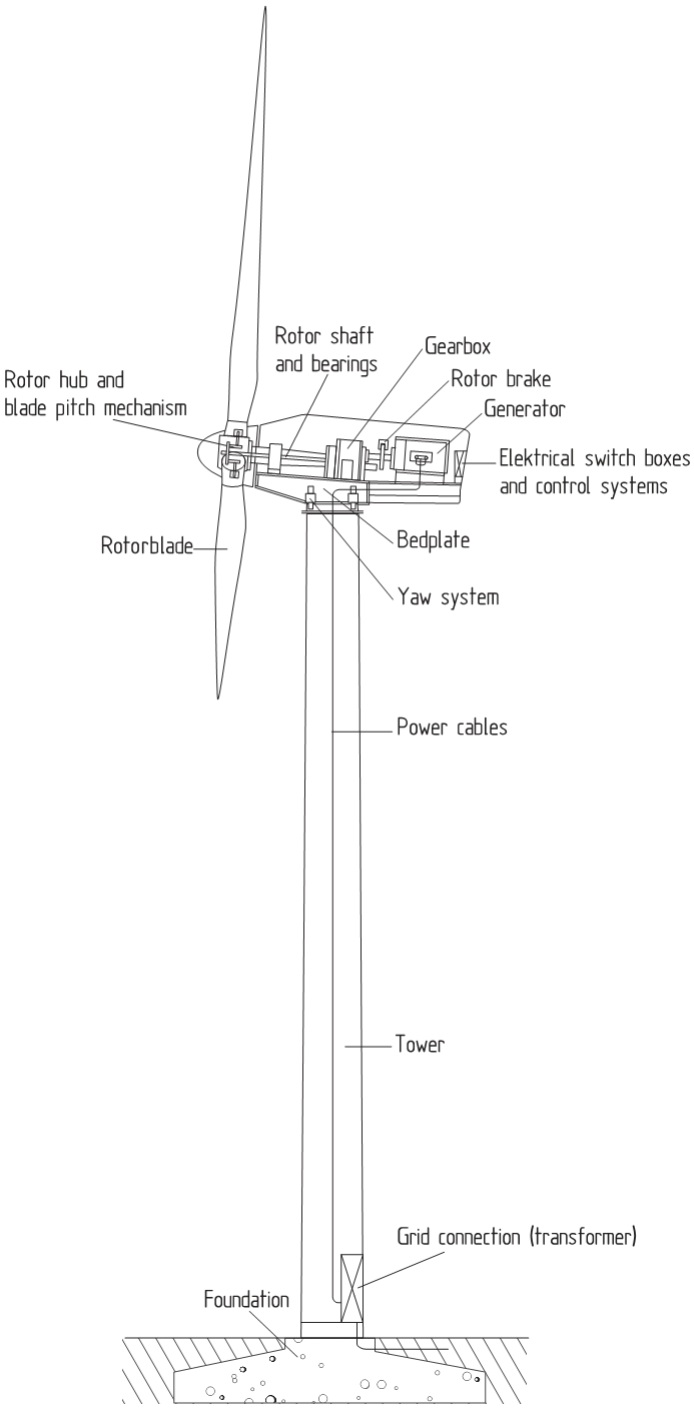

Figure 2.1: Components of a HAWT, reproduced from Hau [23].

As the present dissertation focuses on the rotor blade geometry design, the stratification of this component is also mentioned here. Thereby, the blade is comprised of the following elements:

- External panels, or shells, which gives the aerodynamic shape and is responsible for withstanding part of the bending load;
- Internal longitudinal spars and shear webs, that resist to the shear load and a part of the bending load, restrict the deformation of the cross section and prevents the buckling of the panels;
- Inserts and bushings, which transfer the loads from panels and spars to the hub;
- Lightning protection, that transfers the energy of the lightning strikes from the tip to the root of the blade.

Many options of design configuration of HAWTs were tried during the evolving process of the technology, but nowadays the large scale wind turbines that are being produced seem to agree on most of this options, which are listed below:

- Rotor with 3 blades;
- Upwind position of the rotor, with respect to the tower;
- Variable speed operation;
- Power control by active pitch;
- Driven yaw control.

This configuration of HAWT is adopted for the studies reported by this dissertation. The main design options that are still varying between the manufactures are: direct-drive or geared drive train; and synchronous generator or Doubly-Fed Induction Generator (DFIG). When necessary, this work focuses on Direct-Drive Synchronous Generator (DDSG) wind turbines.

Table 2.1 shows typical relative component costs of DDSG turbines, computed for a 2.5 MW machine using the cost and scaling model from the National Renewable Energy Laboratory (NREL) of the United States [24]. Through this table, it can be seen that the generator, the tower and the blades are the most economically representative components

Table 2.1: Relative component costs of a 2.5 MW DDSG wind turbine.

Component	Relative cost (%)	Component	Relative cost (%)
Blades	18.57	Mainframe	2.10
Hub	3.37	Nacelle cover	1.00
Main shaft	0.46	Electrical connections	5.07
Generator	24.51	Pitch system	6.51
Mechanical brake and coupling	0.15	Power electronic converters	7.50
Yaw system	4.18	Control, safety and condition monitoring systems	1.25
Hydraulic and cooling systems	1.18	Tower	24.16

of such a type of HAWT. Together, they represent over 67% of the total cost of a DDSG wind turbine. It must be noticed that the wind turbine cost represent about 70% or more of the initial capital cost of a wind farm project.

The next subsections describe the definition of the power curve of wind turbines, and the control aspects that impact the blade design methodology developed within this dissertation, i.e., the maximum power point tracking and power control by active pitch.

2.1.1 Power Curve

The power curve from a wind turbine indicates the power that will be delivered to the electrical grid (output power) in relation to the wind speed. A typical power curve from a modern wind turbine is shown in Figure 2.2. The turbine starts delivering power from a minimum wind speed (cut-in wind speed), so that it can overcome the internal power losses and consumptions. Increasing the wind speed from that point on will increase the output power in a cubic relation, until it reaches the rated power of the turbine, at rated wind speed. At higher wind speeds than this, the output power will be held constant. However, there is a maximum wind speed for turbine to operate safely (cut-out wind speed), and if the wind exceeds this speed, the turbine will shut off.

At wind speeds between the cut-in and rated speeds, the wind turbine operates at its maximum efficiency. The pitch of the blade is kept constant at the design value, and the rotational speed of the rotor is controlled according to the MPPT strategy (which is described

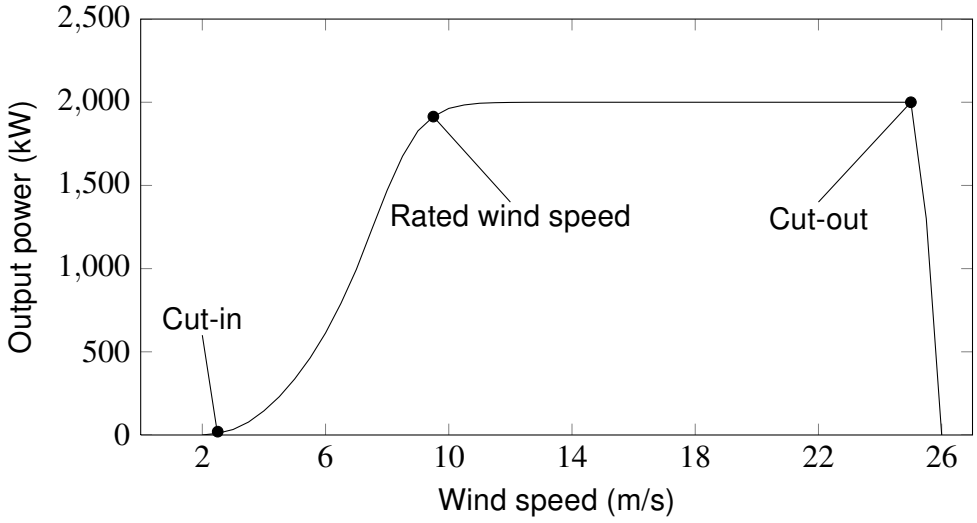

Figure 2.2: Typical power curve from a modern HAWT.

in Subsection 2.1.2), using the generator torque as the control variable. Furthermore, if the wind speed is over the rated speed, then the rotational speed is kept constant at its rated value and the mechanical power from the shaft is limited by pitching the blades (details of this technique are given in Subsection 2.1.3).

The output power is given by the available wind kinetic power multiplied by the general efficiency of the wind energy conversion system. At first, the aerodynamic efficiency of the rotor is to be defined, through its power coefficient (C_P):

$$C_P = \frac{P_m}{\frac{1}{2} \cdot \rho_{air} V_\infty^3 \cdot A} , \tag{2.1}$$

where P_m is the mechanical power converted to the shaft, ρ_{air} is the air density, V_∞ is the free stream flow speed, and A is rotor disc area. The efficiency of the mechanical-electrical system (η), i.e., the drive train and power electronic converters, is then given by:

$$\eta = 1 - \frac{P_{gear} + P_{fri} + P_{fe} + P_{stat} + P_{conv} + P_{rot}}{P_m} . \tag{2.2}$$

In Equation 2.2, P_{gear}, P_{fri}, P_{fe}, P_{stat}, P_{conv} and P_{rot} are, respectively: mechanical power losses at the gearbox (if any); frictional losses at bearings and bushings of the drive train; iron losses at the generator (eddy current and hysteresis losses); copper losses at the stator winding of the generator; switching and conduction losses at the power electronic converter; and copper losses caused by the excitation current at the rotor field winding (except in case of permanent magnet excitation). Since the focus of this dissertation is on

the design of the blades, no mathematical description of these power losses are given here. The reader is referred to Polinder et al. [25] and Polinder and Slootweg [26] for details on the formulation of these variables.

To give some level of detail about these variables, the drive train model of Polinder et al. [25] was used to compute the power losses and efficiency of the electrical systems of a DDSG wind turbine. The Figure 2.3 shows the results of the computations, relating the efficiency and power losses to the wind speed at which the HAWT operates. It is clearly seen that largest part of the losses on this kind of wind turbine is due to the copper losses at the stator winding. On the other hand, on DFIG wind turbines most part of the losses are located at the gearbox, what was shown by Polinder et al. [25].

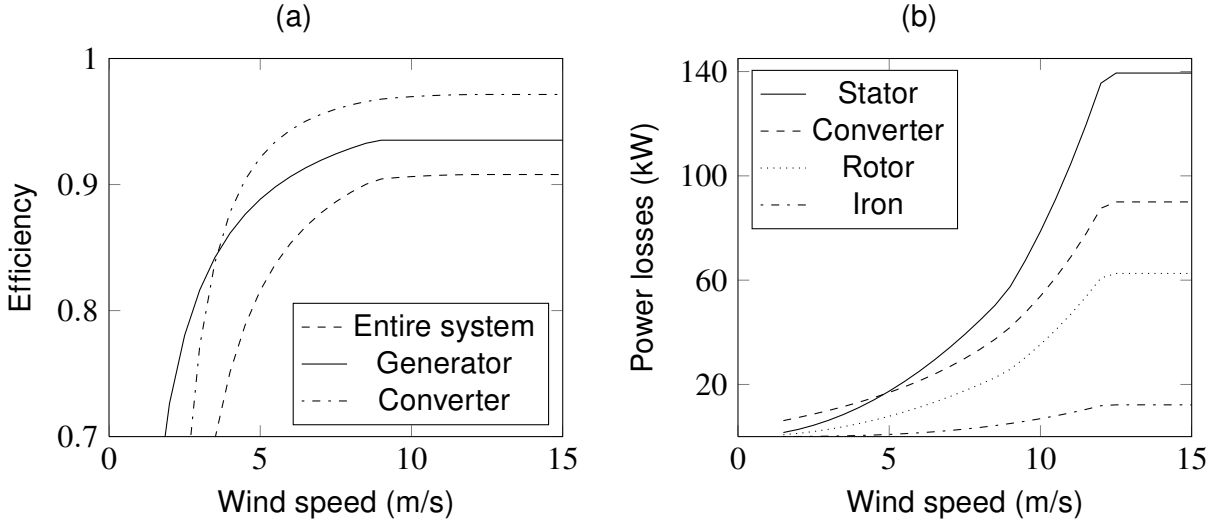

Figure 2.3: Efficiency of the electrical systems of a DDSG wind turbine (a) and their respective losses (b), adapted from [25].

At last, the output power of the turbine (P_{out}) is mathematically defined by:

$$P_{out} = \frac{1}{2} \cdot \rho_{air} \cdot V_{\infty}^{3} \cdot A \cdot C_P(\lambda, \theta) \cdot \eta(P_m, \Omega) \,, \tag{2.3}$$

where λ is tip speed ratio, which is defined in Section 2.4, θ is the blade pitch angle and Ω is the angular velocity of the rotor. As one can see, the power coefficient of the rotor depends on the state of the tip speed ratio and the blade pitch angle, and the efficiency of the mechanical-electrical system depends on the state of the mechanical power on the shaft and the angular velocity of the rotor of the generator (same as angular velocity of the wind turbine rotor in case of direct-drive turbine). Details on the power coefficient of the rotor are described in Section 2.4. An example of variation of the electrical system efficiency, with respect to the shaft power and angular velocity of the rotor, is illustrated at the Figure 2.4

(a) for an electrically excited DDSG machine, and the same for a machine with permanent magnet excitation at Figure 2.4 (b).

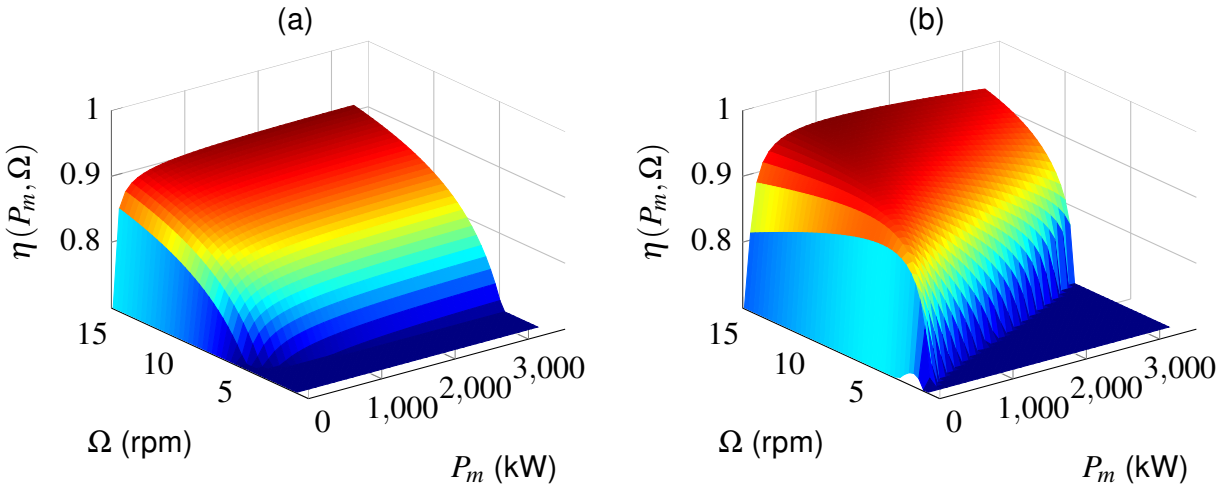

Figure 2.4: Electrical system efficiency, with respect to the shaft power and angular velocity of the rotor, for generators with electrical (a) and permanent magnet (b) excitation.

2.1.2 Maximum Power Point Tracking

As already mentioned, in the partial load regime, the wind turbine operates with maximum efficiency, and this condition is referred to as the Optimal Regimes Characteristic (ORC). For each wind speed, there is a corresponding rotational speed of the rotor (the same of the generator, in case of direct-drive) that maximizes the output power of the turbine. Usually, for the turbine to operate at the ORC, the MPPT strategy sets the reference of the rotational speed control loop. The MPPT is a very reliable and robust control method, and basically consists of a hill-climbing method [27] for dynamically driving the operating point to the ORC, with minimal information from the system. The power characteristics of the rotor are completely unknown, and the shaft rotational speed and active power of the generator are the only required measurements from the system. Some searching (probe) signal is used to obtain gradient estimations of these measured variables [28].

For the present work, the interest in this subject is the steady-state modelling of the MPPT, for the computation of the power curve of the turbine. This is much more simple than the dynamic modelling of MPPT, and therefore this subject is not extensively described here. If the reader is interested, several aspects and details of the MPPT are presented by Munteanu et al. [28].

As Equation 2.3 shows, the rotational speed of the rotor (Ω) affects both C_P and η. Therefore, the rotational speed that brings the turbine to the ORC, given a wind speed,

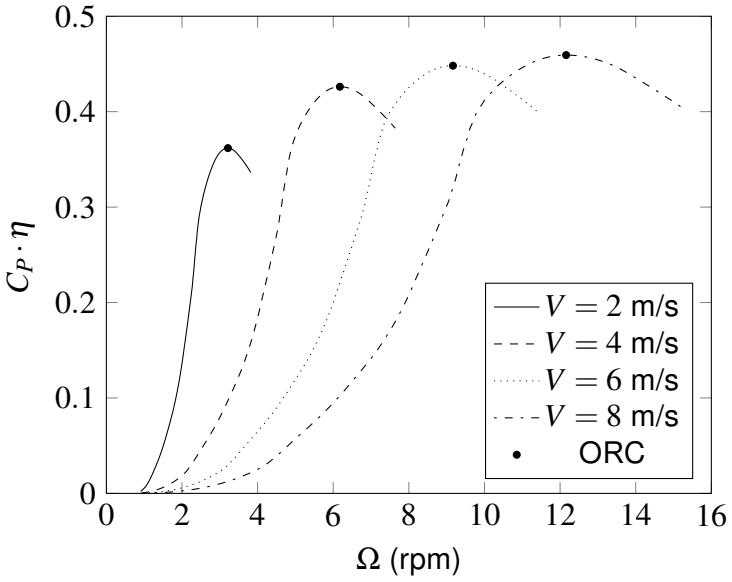

Figure 2.5: Optimal regimes characteristic for several wind speeds.

is the one that maximizes $C_P \cdot \eta$. Figure 2.5 illustrates this approach, by pointing the ORC for several wind speeds in combined rotor performance and mechanical-electrical system efficiency curves, i.e., $C_P \cdot \eta$ versus Ω curves. In the present work, this is how the optimal rotational speed is determined, with respect to the wind speed. One must remind, though, that the rotational speed is limited to its rated value Ω_{rated}.

2.1.3 Power Control by Active Pitch

When the turbine operates at the full load regime, i.e., when the wind speed is above rated, the rotor power (P_m) must be aerodynamically limited. Otherwise the generator or the whole turbine would be damaged by overload, because the available power from the wind varies with the wind speed cubed (see Equation 2.21). This is carried out by increasing the blade pitch angle (θ), i.e., turning the blade into the wind, what decreases the angle of attack and also the lift throughout the blade, consequently reducing the rotor power coefficient. This action is known as the active pitch control.

Once again, at this dissertation the interest in the pitch control is the steady-state modelling for purposes of power curve computation. For this reason only a brief description of this topic is given here. Figure 2.6 shows how the pitch angle must change with the wind speed for the output power to remain constant. This contour plot of the output power was computed through a BEM model, considering a rotor with 120 m diameter.

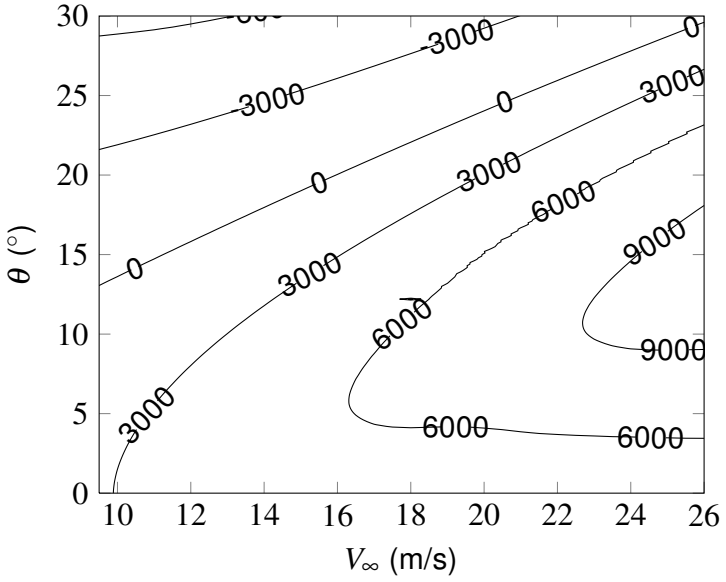

Figure 2.6: Contour plot of the output power (in kW) with regard to wind speed and blade pitch angle, for a rotor with 120 m diameter.

2.2 Characteristics of Wind Resources

The wind is a complex resource, and many statistical functions and parameters are used to analyse and represent it, each with a different purpose. The main ones and the feature that they represent are summarized as follows:

- Annual mean wind speed — represents the average of wind speeds through the year, and is calculated from measurement data. It is used in the AEP estimates.
- Extreme wind speed — is the highest speed that occur within some specific recurrence time, for example 50 years. It is of particular concern of in the structural design of turbines, because they must withstand the loads under this condition.
- Probability density function — used to represent the frequency of occurrence of the wind speeds. It is very important to the AEP estimation.
- Wind rose — corresponds to the probability distribution function of the wind direction variation in time. It is of great interest when positioning the turbines in wind farms.
- Wind shear profile function — stands for the atmospheric boundary layer, which is important to the rotor load estimations and to the conversion of wind speeds from one hight to another in the site assessment process. This function uses the terrain roughness parameter as input.

- Turbulence intensity — represents the wind turbulence, and it is of particular interest in the calculation of turbine wakes and its impact on downwind turbines. The turbulence also causes fluctuating loads at the rotor blades, and must be considered when performing their structural design.

In the work reported by this dissertation, a vertical wind shear profile was considered, i.e., no vertical speed variation. And also no turbulence was taken into account, because these effects have not a great impact on the rotor performance optimization. In this way, as in the approach showed here the blade geometry is optimized for the maximum AEP under a specific wind speed distribution, the most important statistical function for this work is the probability density function. Therefore, this is the only item from the list above that is detailed here, as follows.

The wind speed is usually measured using anemometers located in met masts, and the information provided by it is recorded by data-loggers, in the form of 10-minute mean speed and standard deviation. The Weibull probability density function [29] fits well to the 10-minute mean speed distribution from most of the sites. This function is expressed as follows:

$$f(V) = \frac{k}{C} \cdot \left(\frac{V}{C}\right)^{k-1} \cdot e^{-(V/C)^k}, \tag{2.4}$$

where $f(V)$ is the probability of occurrence of the wind speed V, C is the scale parameter, and k is the shape parameter. Figure 2.7 shows the plot of the Weibull distribution for some values of C and k. The impact of C in the flow speed probability distribution is that for higher values of this parameter, higher wind speeds will have a higher probability, thus increasing the mean wind speed. As for the shape parameter, a higher value of k will cause a sharper peak in the curve, which means that there is less wind speed variation, i.e., the standard deviation is lower.

The international standard IEC 61400-1 [30], from the International Electrotechnical Commission (IEC), describes how to calculate the mean wind speed (V_{ave}) from the Weibull function as

$$V_{ave} = C \cdot \Gamma\left(1 + \frac{1}{k}\right), \text{ where} \tag{2.5}$$

$$\Gamma(z) = \int_0^\infty e^{-t} \cdot t^{z-1}\, dt \tag{2.6}$$

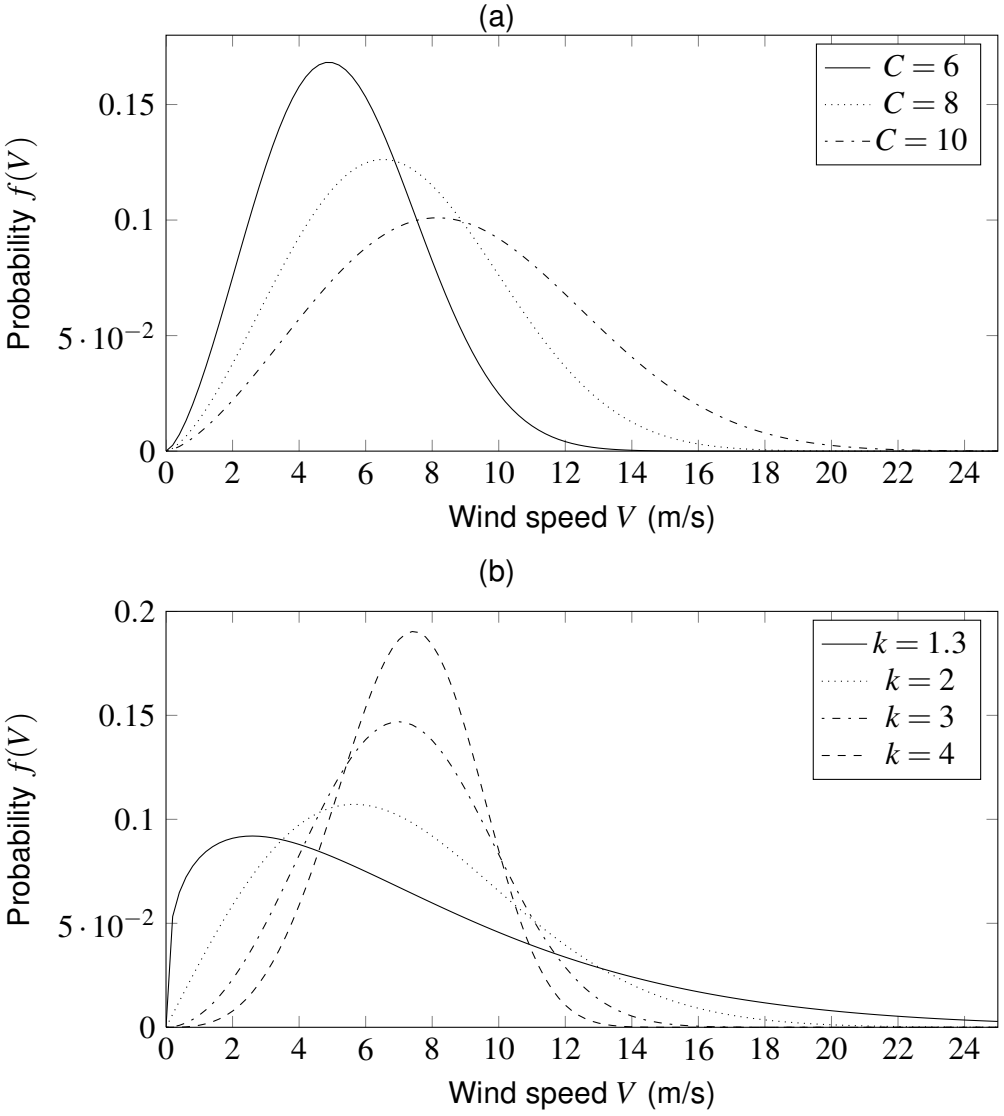

Figure 2.7: Effect of the variation of C in the Weibull distribution, with $k = 2.5$ (a), and of the variation of k, with $C = 8$ (b).

is the gamma function.

2.3 Annual Energy Production

The AEP can be estimated from the power curve of a wind turbine together with the wind speed probability distribution, which were both described in previous sections. It is mathematically expressed as

$$AEP = h_{year} \cdot \int_{V=V_{in}}^{V_{out}} P_{out}(V) \cdot f(V)\, dV \cdot K_{avl}\ , \tag{2.7}$$

where h_{year} is the number of hours in the year, i.e., 8760 hours, V_{in} and V_{out} are the cut-in and cut-out wind speeds, and K_{avl} is the availability of the turbine, that is the average fraction of the time in which the turbine is ready to generate electricity.

The capacity factor (F_C) can now be defined: it is the ratio of the actual mean power computed over a period of time by the rated power of the turbine (P_{rated}), which is expressed as

$$F_C = \frac{AEP}{h_{year} \cdot P_{rated}} \,. \tag{2.8}$$

2.4 Wind Turbine Blade Design

The first element to be addressed in the rotor design is the blade, which is its most essential element. The blade is the device that converts the kinetic energy of the wind into torque to generate useful power. A successful blade design must satisfy a whole range of requirements and objectives, some of which are in conflict. These requirements and objectives can be summarized as follows:

- Maximize the AEP for the specified wind speeds distribution;
- Minimize weight and cost;
- Resist the static and dynamic loads applied to the blade during its life cycle;
- Reduce noise generation;
- Restrict deflections of the blade tip to avoid collisions to the tower;
- Avoid resonances;
- Define pitch angle values for wind speeds above rated, in order to limit the output power to its rated value;
- Ease the manufacturing process;
- Ease the materials recycling after the life cycle of the blade;
- Preserve the health and safety of the workers.

As already described, the design process of a blade can be divided into two steps: aerodynamic design and structural design. The aerodynamic design consists in defining the optimal geometry of the outer surface of the blade (blade geometry), which is defined by the selection and positioning of the airfoils, and the determination of chord, twist and thickness radial distributions. The structural design is defined by the blade material selection and by the definition of the structural cross section or spar inside the outer envelope [6].

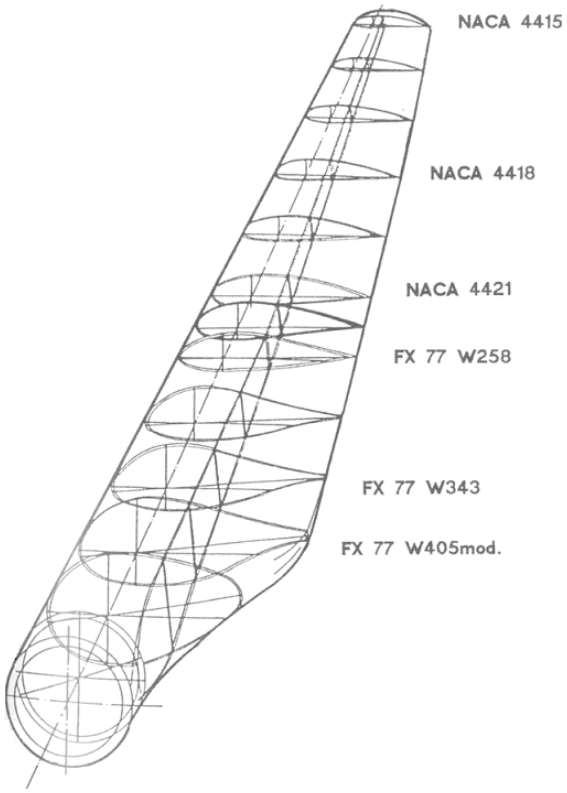

Figure 2.8: Positioning of airfoils along the blade span, reproduced from Gasch and Twele [31].

The HAWTs are developed using modern families of airfoils, so that the blade tip region is designed with a thin airfoil, for a high lift-to-drag ratio (L/D), and the root region is designed with a thicker airfoil with similar characteristics, to increase the moment of inertia. Figure 2.8 shows the positioning of airfoils along the length of the blade. It can be seen that the airfoils thickness increase towards the root, for ease of the blade coupling to the pitch bearing.

There are several ways to determine the spanwise distributions of chord, twist and thickness. The most fundamental ones are the analytical solutions of Betz [32] and Schmitz [33] theories. The latter consists in a complement of the former, by taking into account rotational wake effects. These analytical solutions provide the chord and twist values relative

to rotor radius, given the design tip speed ratio, the airfoils spanwise positioning and the specified angle of attack. But the BEM [34] is a more accurate theory for predicting rotor performance, that considers a finite number of blades and hub- and tip-losses, yet by this theory there is no analytical solution for the optimum values of chord and twist. Therefore, one way of solving this problem is to optimize these parameters by hand at selected radial stations, with the aid of contour plots from the rotor power coefficient and angle of attack in relation to chord and twist angle. These contour plots are generated by computing a BEM model several times, for each combination of chord and twist discrete values. This process result in a more aerodynamically efficient blade geometry, but it requires more time and it is more susceptible to the designer's experience. Additionally, this also requires the previous positioning of airfoils.

All of the techniques mentioned in the previous paragraph aim at maximizing the aerodynamic efficiency under specified conditions of wind speed and tip speed ratio. This means that the optimum performance out of this condition is not guaranteed. Besides, the interaction of the blade geometry to its structure is not verified, what means that this geometry will probably have to be revised after the structural design of the blade. Recently, numerical optimization algorithms have been applied to define the blade geometry [35–39], most of which are gradient-based algorithms. This allows site-specific optimization, i.e., maximizing the AEP for a given wind speed distribution, what provides a better performance under different operating conditions. In most of these cases, a complex design platform was developed, which integrates the setting of chord, twist and thickness distributions into a holistic design process (with aerodynamic analysis, aeroelastic load calculation, structural design, turbine controller tuning, noise prediction and/or cost estimation). The geometry problem then becomes much more complex, as a multi-objective, -disciplinary, -variable, and -constrained problem. This is why MOEAs become more attractive for this task.

On the other hand, the structural design starts with the material selection that will be used on the blade. The materials most commonly used in wind turbine blades are fiber-reinforced plastics (composites), which have interesting characteristics for this application, such as low density and high strength. Most of the composites reinforcements used consist of carbon or glass fibers, while the polyester, vinylester and epoxy are the most used resins. Figure 2.9 illustrates the application of several materials to the blade structural design.

After the selection and configuration of materials is determined, then the calculation of all loads that will be applied to the blade, during the life cycle of the turbine, is performed. This is usually done by a computer code based on an aeroelastic model [40]. This model

must dynamically represent the wind field, the aerodynamics of the rotor, the wind turbine structure, and its control system. Normally a geometrically non-linear finite element or a modified modal analysis approach is applied [40].

The rotor of a wind turbine must operate not only under conditions of static loads, but also periodically and stochastically varying loads. Such dynamic loads occur on a high number of cycles, and thus fatigue is a primary concern. The cyclic stresses should be reduced as possible, and the materials selected for construction must withstand these stresses for as many cycles as possible. For the rest of the turbine, the rotor behaves as a generator of cyclic load, especially for the drive train [22].

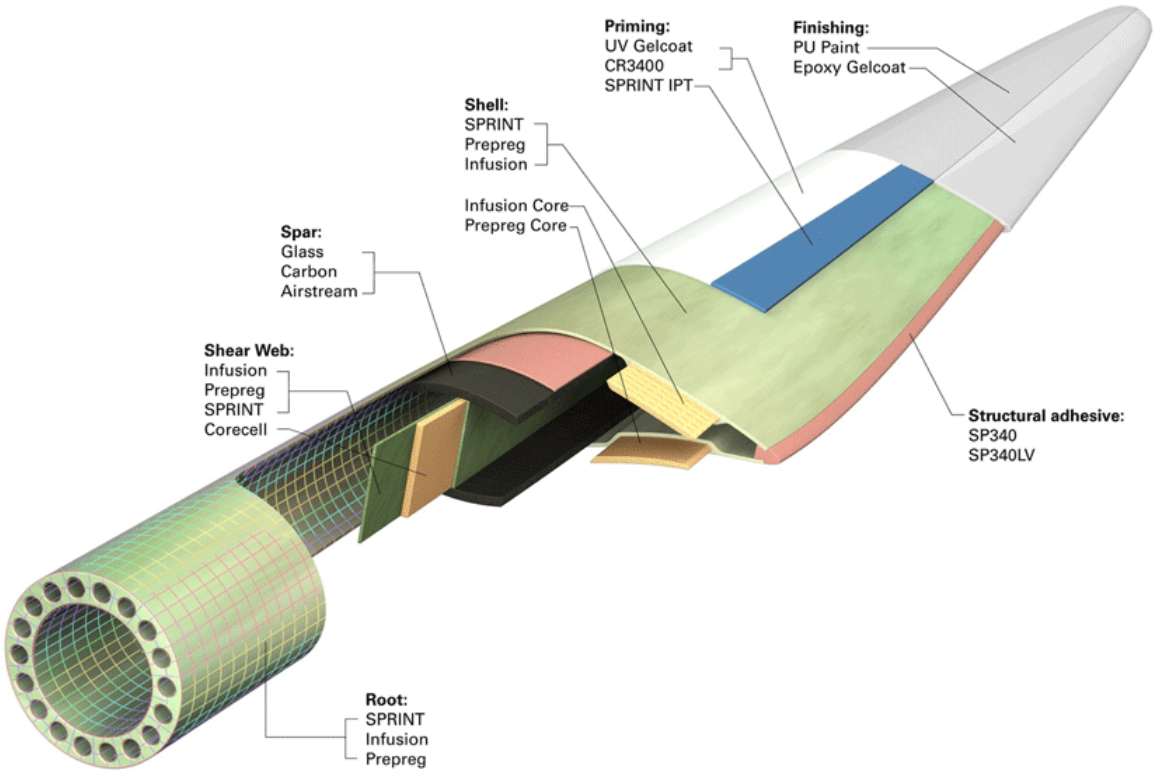

Figure 2.9: Several materials applied on a blade structural design.

Usually the design process of a blade is done iteratively, due to the fact that aerodynamic and structural characteristics have an impact on each other. The process starts with a preliminary blade geometry definition, followed by a preliminary structural design and an aeroelastic analysis. It then returns to the previous step, and tunes the aerodynamic design, going afterwards again to the structural analysis. This loop repeats itself until the desired blade design is reached.

A common practice in the industry is to have one engineering team for the aerodynamic design and another for the structural design of the blade, because these tasks involve different backgrounds and therefore require different engineer profiles. This causes the blade design process to be segmented, becoming more time-consuming and making harder to find a trade-off between aerodynamic and structural efficiency. A more integrated approach, as the one of Fuglsang [37], could address this issues and reduce the number of aerodynamic-to-structural design loops in the process of blade design, hence reducing the design time and cost.

This dissertation focuses on the aerodynamic design optimization, and therefore it does not describe the detailed structural modelling of wind turbine blades. But if the reader is interested, this information is found in the literature [6, 22, 23, 40–42]. The next subsection then describes the BEM model, which is used for the rotor aerodynamic performance analysis.

2.4.1 Blade Element Momentum Theory

A widely used and accurate method for estimating the performance of propellers and helicopter rotors is assuming that the flow on the rotor occurs in circular stream tubes that do not interact with each other. This method, used together with the induced velocities has been called by many names, including BEM Theory, Vortex Theory, Strip Theory, among others, and is frequently applied in wind turbine study. BEM theory, which can be seen as a two-dimensional flow on each radial section of the blade, considering that the air is slowed in the axial direction and accelerated in the tangential direction, is described by Wilson and Lissaman [34].

From the BEM theory is possible to estimate static loads on a wind turbine and the generated power under different conditions of wind, rotational speed and pitch angle. Therefore it is assumed that the blade geometry has been previously defined, i.e., the distributions of chord length (c) and local pitch angle (θ_l) along rotor radius (r) are known, as well as the performance data of the airfoils used. For determinate values of wind speed (V_∞) and angular velocity of the rotor (Ω), the local conditions of flow for a given section dr can be obtained by the following procedure (including the Prandtl tip loss factor [43]):

- Step 1: Define the initial value of the axial and tangential induction factors, respectively a and a' ($a = a' = 0$ is an option to start the iterations);
- Step 2: Compute the relative flow angle ϕ, by Equation 2.9;

$$\phi = \arctan\left(\frac{(1-a)\cdot V_\infty}{(1+a')\cdot\Omega\cdot r}\right) \tag{2.9}$$

- Step 3: Compute Prandtl's tip loss factor (F), using the Equations 2.10 and 2.11, where R is the total rotor radius and B is the number of blades;

$$F = \frac{2}{\pi}\arccos\left(e^{-f}\right) \tag{2.10}$$

$$f = \frac{B(R-r)}{2\cdot r\cdot\sin(\phi)} \tag{2.11}$$

- Step 4: Compute the local angle of attack α by Equation 2.12;

$$\alpha = \phi - \theta_l \tag{2.12}$$

- Step 5: Find the lift and drag coefficients to the angle of attack α previously computed, respectively $C_L(\alpha)$ and $C_D(\alpha)$, from the properties of the airfoil section in r;

- Step 6: Compute the normal (C_n) and tangential (C_t) load coefficients, by Equations 2.13 and 2.14;

$$C_n = C_L\cos(\phi) + C_D\sin(\phi) \tag{2.13}$$

$$C_t = C_L\sin(\phi) - C_D\cos(\phi) \tag{2.14}$$

- Step 7: Compute the solidity (σ), defined as the fraction of the ring area in the control volume that is covered by the blades, through the Equation 2.15, given by

$$\sigma(r) = \frac{c(r)\cdot B}{2\cdot\pi\cdot r} \tag{2.15}$$

- Step 8: Compute a and a', by Equations 2.16 and 2.17;

$$a = \frac{1}{\frac{4\cdot F\sin^2(\phi)}{\sigma\cdot C_n} + 1} \tag{2.16}$$

$$a' = \frac{1}{\frac{4 \cdot F \sin(\phi)\cos(\phi)}{\sigma \cdot C_t} - 1} \tag{2.17}$$

- Step 9: Compute the error between the iteration values for a and a';
- Step 10: If the error is greater than a tolerance parameter, return to Step 2 and repeat the procedure, or else finish.

With the obtained data is possible to compute the elementary axial force dT generated in a ring element with thickness dr, by Equation 2.18 as follows, where ρ_{air} is the air density.

$$dT = 4 \cdot \pi \cdot r \cdot \rho_{air} \cdot V_\infty^2 \cdot a(1-a)F \cdot dr \tag{2.18}$$

Similarly, the torque dQ developed by the blade element in a stream tube (annular element) is obtained, as follows:

$$dQ = 4 \cdot \pi \cdot r^3 \cdot \rho_{air} \cdot V_\infty \cdot \Omega \cdot a'(1-a)F \cdot dr \tag{2.19}$$

And the power dP_m generated by the blade element is given by:

$$dP_m = \Omega \cdot dQ \tag{2.20}$$

Numerically integrating the Equations 2.18 to 2.20, one can obtain the total axial force, or thrust (T), the total torque (Q) and the total power (P_m) generated by aerodynamic forces acting on the rotor. The rotor power coefficient (C_P) can be computed by dividing the total generated power on the rotor by the total wind kinetic power on the rotor plane, as shown by Equation 2.21:

$$C_P = \frac{P_m}{\frac{1}{2} \cdot \rho_{air} \cdot \pi \cdot R^2 \cdot V_\infty^3} \tag{2.21}$$

However, when the axial induction factor becomes greater than approximately 0.4, the BEM theory fails (Figure 2.10). To compensate this effect, Glauert [45] proposed a correction to the thrust coefficient (C_T), based in experimental data of the helicopter rotor with high induced speed. According to the empirical relation found in [41], which is derived

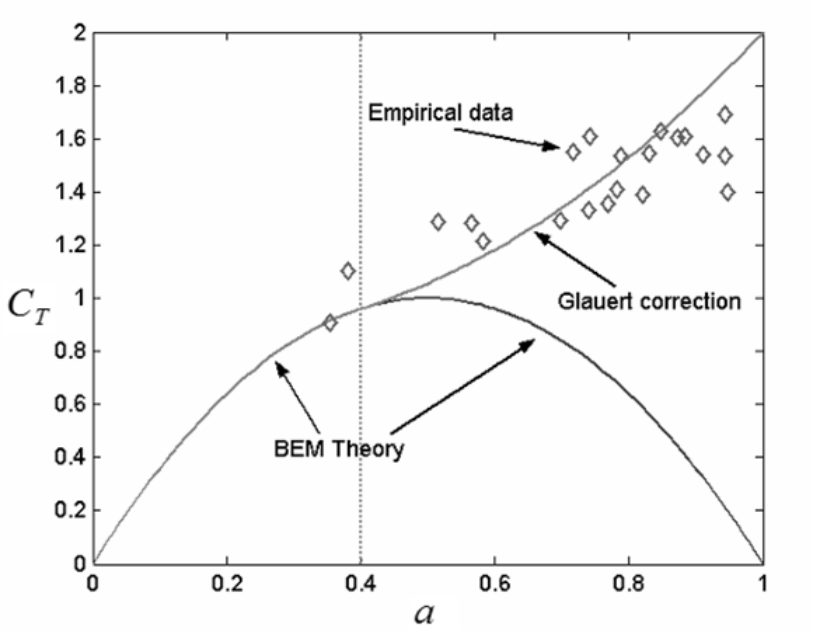

Figure 2.10: Different expressions for the thrust coefficient by the axial induction factor, reproduced from Moriarty and Hansen [44].

from the Glauert correction, when a is greater than a_c, a_c being approximately 0.2, the Equation 2.16 should be replaced by Equations 2.22 and 2.23 as follows:

$$a = \frac{1}{2}\left[2 + K(1 - 2 \cdot a_c) - \sqrt{(K(1 - 2 \cdot a_c) + 2)^2 + 4(K \cdot a_c^2 - 1)}\right] \tag{2.22}$$

$$K = \frac{4 \cdot F \sin^2(\phi)}{\sigma \cdot C_n} \tag{2.23}$$

Further details about the BEM theory formulation and the concepts involved can be found in [42].

3 Evolutionary Optimization Algorithms

This chapter presents the stochastic optimization methods, also known as meta-heuristics or EAs, that were chosen to be evaluated in solving the optimization problem of blade geometry design. First, in Section 3.1, a brief introduction to the multi-objective evolutionary optimization is given, reviewing some basic concepts as Pareto domination and Pareto optimality. Still in this section, brief reviews of recent MOEA applications and performance metrics are given. Then the GA, QEA, MOEA/D and Differential Evolution (DE) approaches are described, respectively in Sections 3.2, 3.3, 3.4 and 3.5.

3.1 Multi-objective Evolutionary Optimization

MOPs, as the name suggests, consist in minimizing (or maximizing) multiple objective functions, which are often in conflict with each other. This is mathematically described by

$$\begin{aligned} &\min\ F(x) = (F_1(x), \cdots, F_m(x))^T \\ &\text{subject to } x \in \Omega\ . \end{aligned} \tag{3.1}$$

In the Equation 3.1, x is the solution vector (also referred to as decision vector), and Ω is the parameter space (or decision space). $F : \Omega \rightarrow R^m$ is the objective vector and R^m is the objective space. Since there is no single solution that simultaneously minimizes all objective functions, the aim of multi-objective optimization is to find the solutions that yield the best trade-off between the objectives. These solutions are called Pareto optimal solutions.

To define the concept of Pareto optimality, one must first define the Pareto dominance concept. One vector $u \in R^m$ is said to dominate another vector $v \in R^m$ (denoted as $u \prec v$) if and only if $\forall i \in \{1, \cdots, m\} : u_i \leq v_i$, and $\exists j \in \{1, \cdots, m\} : u_j < v_j$. Now, a solution vector $x \in \Omega$ is a Pareto optimal solution to the problem of Equation 3.1 if $\nexists y \in \Omega : F(y) \prec F(x)$.

The PS is the set of all the Pareto optimal solution vectors and the PF is the image of the PS in the objective space [46, 47].

Because of the population-based nature of EAs, they are able to approximate the entire PF of a MOP in a single run. EAs must address two issues when solving MOPs: the convergence to the true PF, and the diversity of the solutions in the non-dominated front. The interest in applying EAs to handle MOPs, which are referred to as MOEAs, has been growing since Schaffer's seminal work [48]. For the last 20 years, a lot of research has been done on MOEAs, being one of the most explored research areas in the evolutionary computation field [47].

In 2011, Zhou et al. [47] have made a survey of the development of MOEAs mainly during the previous eight years, covering algorithmic frameworks, selection and offspring reproduction operators, MOEAs with specific search methods, MOEAs for multimodal problems, constraint handling in MOEAs, computationally expensive MOPs, dynamic MOPs, noisy MOPs, combinatorial and discrete MOPs, benchmark problems, performance indicators, and applications.

The main algorithm frameworks and their first propositions are, as pointed out by Zhou et al. [47]: Pareto domination based MOEAs, as the NSGA-II of Deb et al. [49]; MOEA based on decomposition, by Zhang and Li [46]; MOEA based on decision maker's preference, by Fonseca and Fleming [50] and Tanino et al. [51]; indicator-based MOEAs, by Zitzler and Künzli [52]; hybrid MOEAs, as the ones by Elhossini, Areibi and Dony [53], Li and Wang [54], and Yang, Jiao and Gong [55]; memetic MOEAs, by Ishibuchi and Murata [56]; and MOEAs based on co-evolution, such as the one by Deb, Mohan and Mishra [57].

Recent MOEA applications are briefly reviewed in Subsection 3.1.1, focusing on the four algorithms that are evaluated in the present work, namely NSGA-II, QMEA, MOEA/D and MODE. Then, in Subsection 3.1.2, the performance measures used in this work for the performance assessment of these MOEAs are also reviewed.

3.1.1 Recent MOEA Applications

Only one case has been found in the literature that reports the use of NSGA-II to wind turbine blade geometry optimization [58], but in other optimization fields this algorithm is widely applied. Still in the field of renewable energy, Thiaux et al. [59], in 2010, have optimized stand-alone photovoltaic systems through NSGA-II, with the aim of quantifying the gross energy requirement reduction by minimizing the storage capacity. Examples of

recent NSGA-II applications in other fields and the year they were published are: decision thresholds for distributed detection in wireless sensor networks (circuits and communications) [60] in 2010, eradication of persistent pathogens (life sciences) [61] in 2010, web page recommendation (pattern classification) [62] in 2010, and electric motor speed control (control systems) [63] in 2011.

As for QMEA, MOEA/D and MODE, no previous records of wind turbine blade geometry optimization using these metaheuristics were found in the literature. QMEA and similar approaches, however, have been recently applied to: flow-shop scheduling problems [64] in 2007, hardware-software co-synthesis problems in embedded systems [65] in 2008, fuzzy path planning in mobile robot soccer systems [66, 67] in 2009 and 2012, optimal control of two-link inverted pendulum [68] in 2010, footstep planning for humanoid robots [69] in 2011, optimal posture control of humanoid robots (modelled by a four-link inverted pendulum) [70] in 2012, and multi-task agent coalition formation problem [71] also in 2012.

Recent applications of MOEA/D were reported to: flow-shop scheduling problems [72] in 2008, multi-topology sizing of analog integrated circuits [73] in 2009, passive vehicle suspension optimization [74], optimization of degree distributions in Luby Transform codes (communication applications) [75], mobile agent-based wireless sensor network routing [76] and classification rule mining [77] in 2010, and route planning over an unstructured environment [78] in 2011.

On the other hand, in recent years MODE approaches were used on: optimal power flow problem (electrical power systems) [79] and numeric association rules mining [80] in 2008, no-wait flow-shop scheduling [81], design optimization of robot grippers [82], optimization of capacitive voltage divider [83] and micro-array data fuzzy clustering [84] in 2009, and linear antenna array design (electromagnetic optimization) [85] in 2010.

3.1.2 Performance Measures

Over the past few decades, many indicators, or also called metrics, have been proposed for the quantitative comparison of the performance of different MOEAs. A summary of these metrics and their respective original references are listed in Table 3.1. As the output of MOEAs is normally an approximation of the PS, mainly two features of this output are measured by these performance metrics: the convergence to the true PF; and the distribution of approximated solutions [47].

Four performance indicators are used in this dissertation, the two set coverage, the

Table 3.1: Performance metrics and their references, adapted from Zhou et al. [47].

Metric name	Reference
R indicator	[86]
Hypervolume	[87]
Enclosing hypercube	[88]
Objective vector	[88]
ε-indicator	[88]
Number of Pareto points contained	[88]
Average best weight combination	[89]
Distance from reference set	[90]
Fraction of PF covered	[91]
Error ratio	[92]
Overall Non-dominated Vector Generation (ONVG)	[92]
Generational distance	[93]
Maximum PF error	[92]
Chi-square-like deviation	[94]
Spacing	[95]
Maximum spread	[96]
Minimum distance between two solutions	[97]
Coverage error	[97]
Two set coverage	[87]
Deviation from uniform distribution	[98]
Pareto spread	[99]
Accuracy	[99]
Number of distinct choices	[99]
Cluster	[99]

hypervolume, the spacing and the ONVG. These indicators have been chosen partly due to the fact that they do not require the true PF in their computation, since the true PF to the problem handled in this dissertation is not known. The two set coverage, as defined by Zitzler and Thiele [87], corresponds to the share of the solutions in B that are dominated by at least one solution in A, A and B being two sets of decision vectors. This metric is defined by the function

$$C(A,B) = \frac{|\{u \in B; \exists v \in A : v \text{ dominates } u\}|}{|B|} , \tag{3.2}$$

which maps the ordered pair (A,B) to the interval $[0,1]$. If all the solutions in B are dominated by at least one in A, then $C(A,B) = 1$, yet if no solution in B is dominated by the solutions of A, then $C(A,B) = 0$. But $C(A,B)$ is not necessarily equal to $1 - C(B,A)$. From this point on this function is referred to as the coverage metric.

That same authors also define the hypervolume metric [87], as the volume enclosed by the union of the polytopes formed by the intersections of hyperplanes perpendicular to each axis and passing through each point of the set of objective vectors. In the two-dimensional case, the hypervolume represents the area covered by a given approximation of the PF of a two-objective MOP, with respect to the objective space. This could be seen as the sum of the rectangular areas limited by a reference point and the points in the PF approximation set, as illustrated by Figure 3.1 for a minimization MOP. For this metric, scaling and normalization of the objective space is necessary, for the different objectives to contribute approximately equally to the metric value [100].

The distribution of the points in the PF approximation set is represented by the spacing metric, proposed by Schott [95], which is computed by the variance of the distance of each point to its closest neighbour. This is given by the function

$$S(A) = \sqrt{\frac{1}{|A|-1} \sum_{i=1}^{|A|} (\overline{d} - d_i)^2} , \tag{3.3}$$

where

$$d_i = \min(|F_1(x^i) - F_1(x^j)| + |F_2(x^i) - F_2(x^j)|) . \tag{3.4}$$

In this function, x^i is i-th decision vector or point in A, $i, j = 1, 2, \cdots, n$, n being the number of points in A, and $\overline{d}$ is the mean of all d_i. F_1 and F_2 are the objective functions. If

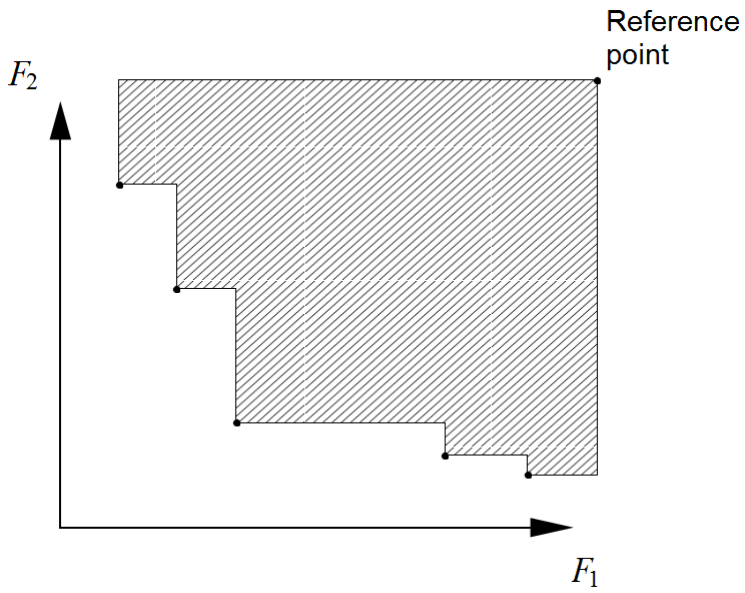

Figure 3.1: Hypervolume metric represented by the hatched area, adapted from Knowles and Nakayama [101].

$S(A) = 0$, it means that all the points in A are evenly spaced from one another. This metric also requires the scaling and normalization of the objective space.

The ONVG metric was first characterized by Van Veldhuizen [92], and indicates the total number of non-dominated solutions in a set of decision vectors (A). The ONVG is mathematically described as

$$\text{ONVG} = |A| \,. \tag{3.5}$$

3.2 Genetic Algorithm

GA was proposed by Holland in 1975 [102], and simulates the theory of biological evolution (natural selection) to solve optimization problems. This algorithm works with populations of individuals, which are represented by chromosomes, i.e., strings of binary or real parameters (representing genes). Each individual represents, through its parametric string, a possible solution to the optimization problem.

The population undergoes an evolutionary process, through which the GA performs the search for better solutions. At each iteration of the algorithm, each individual of the current generation of the population is evaluated to define its fitness value, by the computation

of the objective function. Then the best individuals are selected to create the offspring generation of the population, through genetic manipulation, using therefore operators of crossover and mutation.

The crossover operator is inspired on the process of reproduction, and is responsible for combining the chromosomes of the individuals chosen as parents in the selection process, thereby generating the chromosomes of the offspring individuals. Moreover, the mutation operator is inspired on the process of biological mutation, randomly shifting certain genes of the chromosomes, and its function in the GA is to maintain the diversity of the solutions, thus escaping from local optima. The NSGA-II, a multi-objective version of GA, is briefly reviewed in the next subsection.

3.2.1 Non-dominated Sorting Genetic Algorithm version II

One of the most successful multi-objective versions of GA, the NSGA-II, was proposed by Deb et al. [49, 103] in 2000 as an improved version of the original Non-dominated Sorting Genetic Algorithm (NSGA) of Srinivas and Deb [94], solving some shortfalls of this first version. In this metaheuristic, multiple objectives are reduced to a single fitness measure: the sorting rank based on non-domination level and crowding-distance. This makes NSGA-II a fast and efficient MOEA, being currently applied in most MOEA performance comparisons.

This non-dominated sort procedure assigns a rank to each solution, that corresponds to the level of the non-dominated front that it belongs. The non-dominated sort is better understood by interpretation of Figure 3.2(a), of a minimization MOP. Each individual is assigned a rank according to the level of the non-dominated front that it belongs. The selection operator in NSGA-II is the usual binary tournament, but the selection criterion is based on the crowded-comparison operator, which, as defined by Deb et al. [49, 103], requires primarily the non-domination rank, and in case of draw it then uses the crowding-distance.

The diversity preservation, or niching, is conducted by NSGA-II through a crowding-comparison approach. This metaheuristic promotes the individuals with higher crowding-distance values in the selection and population reduction phases. This keeps the spread of solutions and helps NSGA-II to explore the fitness landscape. The crowding-distance of a solution is calculated as half of the cuboid perimeter formed by its neighbour solutions, with a normalized objective space. As a matter of clarity, this cuboid is shown as a dashed box

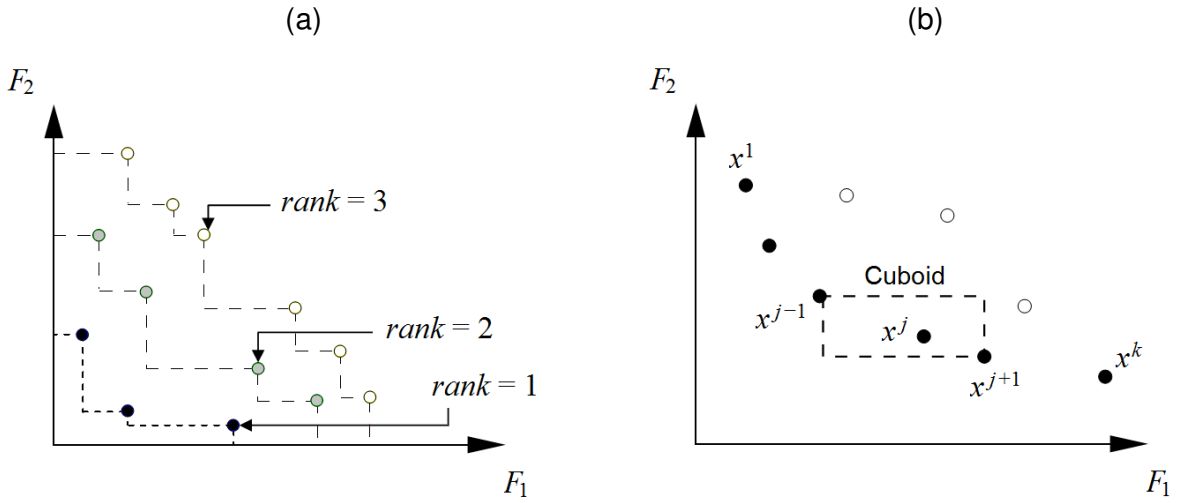

Figure 3.2: Non-domination rank (a) and crowding-distance calculation (b), adapted from Salazar, Rocco and Galván [104] and Deb et al. [103].

in Figure 3.2(b). Details of the NSGA-II are presented in Appendix A.

3.3 Quantum-inspired Evolutionary Algorithm

Han and Kim [105] proposed QEA in 2002. QEA is based on the concepts and principles of quantum computation, such as quantum bits and superposition of states. Like other EAs, QEA is also characterized by the representation of the individual, the evaluation function and the population dynamics. However, instead of binary, numeric or symbolic representation, QEA uses Quantum-inspired bits (Q-bits) for a probabilistic representation. The Q-bit is defined by Han and Kim [105] as the smallest unit of information for representing individuals, and means quantum-inspired bit, which is inspired on the qubit or quantum bit. Unlike the classical bit, the Q-bit does not represent only the value 0 or 1 but a superposition of the two. A Q-bit-coded individual probabilistically represents all the states in the search space.

The Q-gate was introduced by Han and Kim [105] as a Q-bit variation operator, which is used to update the individuals and achieve the evolutionary search. A suitable Q-gate is adopted in compliance with the optimization problem, usually comprising of a rotation gate. Figure 3.3 depicts the polar plot of the rotation gate for Q-bit individuals. In this dissertation, the angle parameters and lookup table used for the rotation gate of QEA were the same as the ones adopted in [105]. The magnitude of the rotation angle has an effect on the speed of convergence, but if it is too big, the solutions may diverge or converge prematurely to a local optimum. The sign of the angle determines the direction

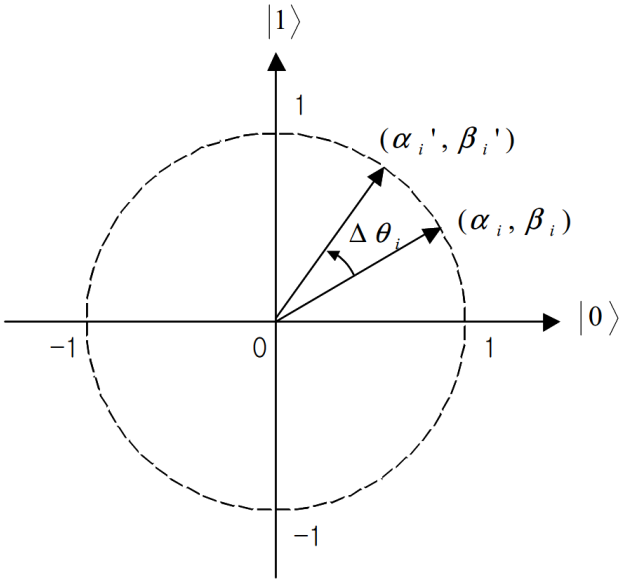

Figure 3.3: Polar plot of the rotation gate for Q-bit individuals, reproduced from Han and Kim [105].

of convergence [105]. A migration process is also applied to induce a variation of the probabilities of a Q-bit individual.

Recently, some QEAs have been proposed for some combinatorial [105–107] and continuous [108–110] optimization problems. An improved version of QEA was proposed by Vianna Neto, Bernert and Coelho in 2011 [111]. QEA is detailed in Appendix B, and the next subsection briefly describes the QMEA.

3.3.1 Quantum-inspired Multi-objective Evolutionary Algorithm

The multi-objective version of QEA, the QMEA, was proposed by Kim, Kim and Han in 2006 [112]. It consists in fitting the original QEA into a MOEA framework, by using the fast non-dominated sorting and crowding distance assignment procedures from the NSGA-II.

In QEA, when Q-bit individuals are updated by a rotation gate, the update operation refers to bits of the best solution [112]. In QMEA, there is no single best solution, since a non-dominated set of solutions is sought. Therefore, the population is classified into several groups $(G_1, G_2, \cdots G_n)$, according to non-domination level and crowding-distance, G_1 being the best group and G_n the worst. Then, the Q-bit individuals in G_1 are used as the reference to the update process of the individuals in the other groups. In this way, the individuals in G_i refer to the i-th individual in G_1. Figure 3.4 illustrates this procedure. Elitism is ensured

by retaining the individuals of the best group.

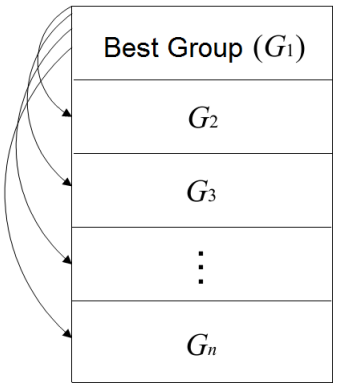

Figure 3.4: Group update procedure in QMEA, reproduced from Kim, Kim and Han [112].

3.4 Multi-objective Evolutionary Algorithm Based on Decomposition

The MOEA/D, one of the most recent MOEA frameworks, was introduced by Zhang and Li in 2007 [46]. This algorithm decomposes the MOP into several scalar optimization sub-problems, by aggregating all the original individual objectives with respect to a set of weight vectors, and simultaneously optimizes these sub-problems. There are several methods in the literature for MOP decomposition [113], which in theory could be applied in MOEA/D, and the weighted sum and Tchebycheff approaches are the most popular ones. Both MOEA/D in which the weighted sum approach is used (W-MOEA/D) and MOEA/D in which the Tchebycheff approach is used (T-MOEA/D) are applied in the present work.

Based on the euclidean distance of the weight vectors, neighbouring relations are established between the sub-problems. In the optimization process, each sub-problem uses information of only its neighbouring sub-problems. The diversity of the weighted vectors naturally leads to diversity of the solutions in the objective space, and therefore no crowding distance assignment is needed in MOEA/D. Another feature of MOEA/D is that it takes advantage of scalar optimization methods, since each solution is associated with a scalar optimization problem.

Two populations are kept by MOEA/D during the evolutionary process, one consisting of the best solution found so far for each sub-problem, and the other is an external population formed by the non-dominated solutions found until the moment. Genetic operators are used to generate offspring individuals for each sub-problem, selecting as parents only

individuals from neighbouring sub-problems of the former. The number of sub-problems and neighbourhood size are considered inputs to MOEA/D.

3.5 Differential Evolution

The DE was introduced by Storn and Price in 1995 [114], as a population-based heuristic for minimization of non-linear and non-differentiable continuous space functions. Like GAs, this algorithm also incorporates genetic operators, such as mutation, crossover and selection, but in a different approach. Mutation is carried out by use of scaled differences of randomly selected and distinct population members. Through crossover operation, a target vector (parent individual) exchanges elements with its corresponding mutant vector, in order to form a trial vector (offspring individual), and in this way DE increases population diversity. Two methods are used for crossover in the original DE algorithms [115]: exponential (also known as two point modulo), or binomial (also referred to as uniform). By the selection operation, if the trial vector yields a lower or equal objective function value compared to the corresponding target vector, the former replaces the latter in the next generation. Only three parameters need to be set by the user in DE: the population size, the mutation scale factor, and the crossover constant.

A total of ten different DE schemes were suggested by Storn and Price [115, 116], and the $DE/x/y/z$ notation was introduced by them to classify these variants. x represents a string that specifies the vector to be mutated, either $rand$ for a randomly selected vector or $best$ for the vector with the highest fitness. y is the number of difference vectors used for mutation. At last, z is a string that stands for the crossover method used, either bin for binomial or exp for exponential. The most popular of these ten schemes is the $DE/rand/1/bin$. Over the past years, several variants of the original DE schemes have been proposed by many researchers, and the main ones were outlined by Das and Suganthan in 2011 [117], in a survey of the state-of-the-art on DE.

Also many DE multi-objective approaches (MODEs) have been proposed, which were surveyed by Das and Suganthan [117] as well. Pareto dominance is used by most of these approaches, mainly in the selection operation, as reported in [118–124]. Many of the cases also apply distance metrics, that are mostly based on the crowding distance of NSGA-II, to improve the distribution of solutions in the non-dominated front, e.g. in [118, 120–125]. In [126], an uniform distribution of the solutions in a multi-objective DE algorithm is obtained by means of the ε-dominance concept [127]. Other DE multi-objective

approaches skip non-dominated sorting and crowding distance assignment by use of MOP decomposition concepts [128–130]. Additionally, self-adaptive DE concepts have been proposed for solving MOPs [131–133].

4 Formulation of the Optimization Problem

The optimization problem dealt by this dissertation consists in defining the distributions of chord, twist and thickness throughout the blade span that maximize the AEP and minimize the blade mass. The model applied for the optimization is based on the HARP_Opt code, from the NREL of the United States of America [18], but with some enhanced features. The next sections of this chapter describe the objective functions and constraints of the optimization problem, the representation of the blade geometry, and the benchmark problem used to evaluate the performance of the optimization algorithms.

4.1 Objective Functions

The next subsections give the details of the two objective functions involved in the design methodology developed for this dissertation, that are the maximization of the AEP and the minimization of the total blade mass. As previously mentioned, reducing the blade mass will reduce its cost, and in this way will also reduce the initial capital cost of the wind farm project. Additionally, increasing the wind turbine AEP will increase the operating revenue of the wind farm project. Hence, the impact of both initial capital cost reduction and increase in operating revenue is the reduction on the COE, which is needed to keep the economic feasibility of the wind farm projects in Brazil, and also to make the wind energy a competitive source in the energy market.

4.1.1 Maximization of the Annual Energy Production

The first objective function applied to the blade geometry optimization is to maximize the AEP of a turbine that operates under a specific wind speed probability distribution. The formulation of the AEP was already presented in Section 2.3, but it is still going to be redisplayed here. Hence, this objective function is expressed as

$$\max\ F_1(x) = AEP(x) = h_{year} \cdot \int_{V=V_{in}}^{V_{out}} P_{out}(V,x) \cdot f(V)\, dV \cdot K_{avl}\ . \tag{4.1}$$

To compute the power curve function $P_{out}(V,x)$, the following procedure is applied:

- First the blade geometry represented by the solution vector x is used as an input to a BEM model to generate the performance curve of the rotor, i.e., the C_P versus λ curve.
- Then the C_P versus λ curve is combined with the efficiency curve of the mechanical-electrical system (η versus Ω) to determine the optimal rotational speed of the rotor with respect to the wind speed V, according to the MPPT strategy. The MPPT strategy is briefly described in Subsection 2.1.2. The rotational speed is limited to its rated value Ω_{rated}.
- Afterwards, again with a BEM model, the output power is calculated to the whole range of wind speeds, from V_{in} to V_{out}, using the previously defined values of rotational speed. The output power is also limited to its rated value P_{rated}.

The wind speed probability density function $f(V)$ is computed through the scale and shape parameters of the Weibull function [29], as displayed in Section 2.2.

4.1.2 Minimization of the Blade Mass

The second objective function considered at the multi-objective optimization problem formulated here is to minimize the total blade mass, while satisfying a maximum allowable strain when subjected to the maximum aerodynamic loads. For that purpose, a simple structural model was used, which represents the blade as a simple beam with bulk isotropic material properties. The blade cross section is modelled as thin shell, without any shear web [13]. This model does not represent the actual blade structural design, but it can well reproduce the interaction of the aerodynamic design with the structural one.

The result of the multi-objective optimization of the blade geometry using this structural model is a preliminary aerodynamic design that already balances the loads and stresses through the blade span, avoiding stress concentration points. This can reduce the number of aerodynamic-to-structural design loops in the conventional process of blade design, described in Section 2.4, hence reducing the design time and cost.

The second objective function is then expressed by

$$\min\ F_2(x) = m_b(x) = \rho_{mat} \int_{r=r_{hub}}^{R} A_{cross}(x)\, dr\,, \tag{4.2}$$

where $m_b(x)$ is the mass of the blade with geometry represented by x, $A_{cross}(x)$ is the area of this blade's cross section at r, ρ_{mat} is the density of the bulk isotropic material, and r_{hub} is the hub radius.

Pseudocode 1 Computation of the blade mass

Begin procedure
  Find the flow speed, from the range of V_{in} to V_{out}, that generates the maximum root bending moment
  Use L and D from that flow speed to calculate the spanwise bending moments at the center of the blade elements, normal and tangent to the chord
  for $i = n_{elm} \rightarrow 1$ **do**
    $t_{shell} \leftarrow t_{min}$
    while $t_{shell} < t_{max}$ **do**
      Calculate the centroid and area moments of inertia of the i-th element shell geometry
      Calculate $\varepsilon(r)$ at the four extreme points of the i-th element shell geometry
      if $\max[\varepsilon(r)] < \varepsilon_{allow}$ **then**
        break while
      end if
      $t_{shell} \leftarrow t_{shell} + \Delta t$
    end while
    Calculate A_{cross} from t_{shell}
    $t_{min} \leftarrow t_{shell}$
  end for
End procedure

The calculation of $A_{cross}(x)$ is not very straightforward, because it must be performed iteratively for each of the n_{elm} blade elements. Pseudocode 1 illustrates this procedure. For a specific element, the strain $\varepsilon(r)$ is calculated at the four extreme points of the element shell geometry, as demonstrated in Figure 4.1. This starts with an initial shell thickness value (t_{min}), which is increased by Δt at each iteration of the procedure, until the strain at all four points are lower than the maximum allowable strain (ε_{allow}), or until the maximum shell thickness (t_{max}) is reached. t_{max} corresponds to half of the dimensional thickness t of the airfoil at the current blade element. At this point, the value of the shell thickness (t_{shell}) for the current element is definitive, and the $A_{cross}(x)$ for this element can be calculated. The shell thickness must be monotonically increasing from the tip to the hub.

The strain in a point of interest is calculated by

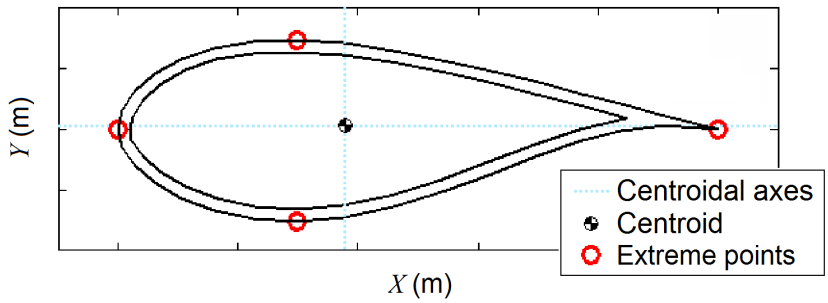

Figure 4.1: Cross section of the blade as modelled in the optimization problem, and the location of the four extreme points for the strain calculations, adapted from Sale [13].

$$\varepsilon(r) = \frac{F_S \cdot M(r) \cdot d(r)}{E \cdot I(r)} \,, \tag{4.3}$$

where F_S is a safety factor, $M(r)$ is the bending moment applied to the element with center in r, $I(r)$ is the area moment of inertia of the cross section of this element, $d(r)$ is the distance from the point of interest to the neutral axis, and E is the elastic modulus of the bulk material.

In order to compute the maximum spanwise bending moments at the center of the blade elements ($M(r)$), first the wind speed speed, from the range of V_{in} to V_{out}, for which the maximum root bending moment occurs must be determined. This is done through the analysis of the results of the BEM model computations. The spanwise bending moments, normal and tangent to the chord, are then calculated using the lift and drag (L and D) generated at the elements under that wind speed.

4.2 Blade Geometry Representation

The representation of the blade geometry in the solution vector (x) of the optimization algorithms is done through the use of control points, which are shown as the squares in Figure 4.2. The solution vector is formed by the ordinates of five control points for the twist distribution and five for the chord, and by the radial position of n control points for the relative thickness (t_r), where n is the number of true airfoils used, as shown by:

$$x = [\theta_{CP1},\ \theta_{CP2},\ \theta_{CP3},\ \theta_{CP4},\ \theta_{CP5},\ c_{CP1},\ c_{CP2},\ c_{CP3},\ c_{CP4},\ c_{CP5},\ r(t_{rCP1}), \cdots, r(t_{rCPn})] \,, \tag{4.4}$$

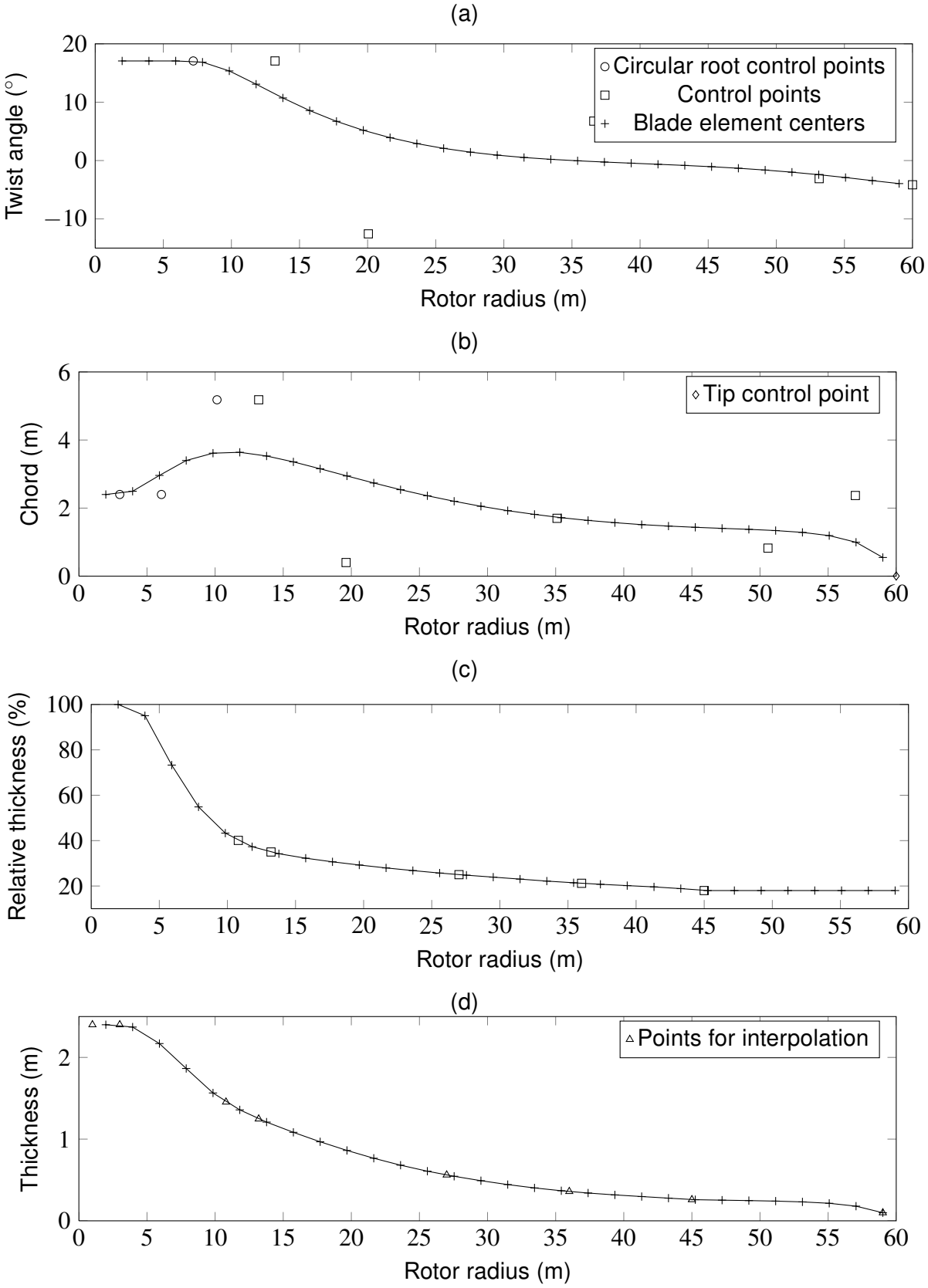

Figure 4.2: Blade geometry representation: twist angle (a), chord(b), relative thickness (c) and absolute thickness (d).

where θ_{CPi}, $i = 1,2,\cdots,5$, is the ordinate of the i-th twist control point, c_{CPi} is the ordinate of the i-th chord control point, and $r(t_{rCPj})$, $j = 1,2,\cdots,n$, is the abscissa of the j-th relative thickness control point. The relative thickness is defined as the thickness-to-chord ratio:

$$t_r = \frac{t}{c} \tag{4.5}$$

where t is the absolute or dimensional thickness.

The next subsections describe the degrees of freedom of the control points, the calculation of the property values at the blade element centers, and the circular root and tip transitions.

4.2.1 Degrees of Freedom of the Control Points

The abscissae values (radial positions) for the twist and chord control points are kept fixed during the iterations of the optimization algorithms. This means that these control points are allowed to move only vertically. Their radial positions are defined by cosine spacing, and in this way there is a higher density towards the root and the tip of the blade, giving more flexibility for the curves in these regions. This flexibility is needed in the root region, because the optimum twist and chord curves drop rapidly towards the center of the blade, and in the tip region because of the transition of the optimum chord curve to a zero chord value at the tip.

Yet for the thickness control points, the ordinates values are the ones held fixed, meaning that they can move only horizontally. Their ordinates are given by the relative thickness of the true airfoils used. The relative thickness control points represent the spanwise placement of these airfoils.

4.2.2 Properties at the Blade Element Centers

The Bézier curve parametrization, described by Farin [20], is used to determine the twist and chord values at the blade element centers, with the control points as inputs. The blade element centers values are represented by the crosses in Figure 4.2.

In order to determine the absolute and relative thicknesses at the blade elements, the monotone piecewise cubic interpolation, as described by Fritsch and Carlson [21], is used. Since the absolute thickness curve, rather than the relative, is the one that must be

smooth, the interpolation is performed on this curve. Initially, the relative thickness control points, together with the root and tip points, are converted to absolute thickness points. These converted points are shown by the triangles in Figure 4.2. This is done by multiplying the relative thickness values by the corresponding chord values at the same radial position, as in

$$t_{CPj} = t_{rCPj} \cdot c(r(t_{rCPj})) \ , \tag{4.6}$$

where t_{CPj} is the absolute thickness value that corresponds to the j-th relative thickness control point, t_{rCPj} is the relative thickness value of the same control point, and $c(r(t_{rCPj}))$ is the chord value interpolated at the radial position of this control point.

The interpolation at the blade elements centers is then performed using these converted points. Now, to get the relative thickness values at the blade element centers, the inverse procedure is done: the dimensional thickness values at the blade element centers are divided by the corresponding chord values.

4.2.3 Circular Root Transition

The root is modelled with a circular cross section, and therefore the transition from the root to the optimum curves is done through the use of extra control points, shown by the circles in Figure 4.2. At the twist curve, the circular root control point has always the same ordinate as θ_{CP1}, i.e., it moves vertically together with θ_{CP1}. The same happen for c_{CP1} and the chord circular root control point close to it. At the chord curve, the ordinates of the first two circular root control points, from the root to the center, remain fixed at the value specified for the diameter of the circular root.

Two input parameters define the radial positions of the circular root control points: r_{rts} and r_{rte}, respectively the radius for the root transition start and for the root transition end. The radial positions of the circular root control points are then given by:

$$r(\theta_{CR}) = r_{rte} - \Delta_r \ , \tag{4.7}$$

$$r(c_{CR1}) = r_{rts} \ , \tag{4.8}$$

$$r(c_{CR2}) = r_{rts} + 0.3 \cdot (r_{rte} - r_{rts}) \text{ , and} \tag{4.9}$$

$$r(c_{CR3}) = r_{rte} - 0.3 \cdot (r_{rte} - r_{rts}) \text{ ,} \tag{4.10}$$

where $r(\theta_{CR})$ is the radial position of the twist circular root control point, $r(c_{CRk})$, $k = 1,2,3$, is the radial position of the k-th chord circular root control point, and $\Delta_r = 0.1 \cdot R$.

By the use of this circular root transition method, the blade geometry curves remain very smooth close to the root, thus avoiding load concentration points, while satisfying the requirements of the connection to the hub.

4.2.4 Tip Transition

In most of the blade designs, a chord value close to zero is adopted at the tip. Hence, a tip transition method was developed, through which the chord goes from its optimal value before the tip to the zero value at the tip. The radial position of the last moving chord control point (c_{CP5}) is placed within a certain distance form the tip, and a fixed chord control point is added at tip of the blade with the desired tip chord value, which is shown in Figure 4.2 as a diamond. The radial position of c_{CP5} is given by the input parameter r_{tts} (radial value for the tip transition start).

With this tip transition method, the chord curve remains also very smooth close to the tip, while satisfying the zero chord tip requirement.

4.3 Constraints

There are four constraints that are considered for optimization problem defined here, which are detailed in the next subsections. First, there is the upper and lower limits of the solution vector. The second one is the monotonicity constraint that applies to the distribution curves. Then there is a constraint for the location of the maximum chord value, and the last one is a constraint to maximum angle of attack.

4.3.1 Upper and Lower Bounds

Each value of the solution vector must be subjected to upper and lower limits, or bounds, in order to restrict the search space. This is represented by the following equation:

$$l_i \leq x_i \leq u_i \,, \tag{4.11}$$

where $x_i,\ i = 1, 2, \cdots, (10+n)$, is the i-th parameter of the solution vector, and l_i and u_i are respectively its lower and upper bounds. Every possible solution generated during the iterations of the optimization algorithm will lie in between these limits.

The upper and lower bounds are given as input parameters for the optimization algorithm, and their values will impact directly on the performance of the algorithm. If the search space is too wide, the algorithm may take too long to converge, or may even not converge to the optimal solution at all. On the other hand, if the search space is too narrow, the optimal solution might be outside its limits, and will never be found. The definition of the bound vectors is an empirical and iterative task.

Another function of the upper and lower bounds is to limit the optimization parameters for some specific purpose. For example, one may wish that the blade chord does not be greater than a certain value (usually about 4 or 5 meters, for large onshore turbines), because otherwise it would be very difficult to transport it.

Furthermore, the appropriate selection of the upper and lower bounds can also reduce the death rate at the optimization algorithms, caused by violations of the constraint of the maximum chord location and monotonicity constraint, described in the following subsections.

4.3.2 Monotonicity

The twist and thickness (both relative and absolute) values at the center of the blade elements are required to be monotonically decreasing, from the root to the tip of the blade. In this way

$$\theta_l(r - dr) \geq \theta_l(r) \,, \tag{4.12}$$

$$t(r-dr) \geq t(r) \text{ , and} \tag{4.13}$$

$$t_r(r-dr) \geq t_r(r) \text{ ,} \tag{4.14}$$

with r varying from the center of the second blade element to the center of the last. For the chord distribution, the monotonicity constraint applies only at blade elements that are located closer to the tip than the location of the maximum chord, that is

$$c(r-dr) \geq c(r), \; \forall r > r(\max(c)) \text{ .} \tag{4.15}$$

If any of the monotonicity constraints are violated, a death penalty is applied. One must notice that, despite the monotonicity constraint is applied to the values at the blade element centers, there is nothing that obligates the control points to be monotonically decreasing as well.

4.3.3 Location of the Maximum Chord

The location of the maximum chord is desired to be close to the radial position of the root transition end (r_{rte}). Depending on the configuration of the upper and lower bounds, sometimes this can fail, and location of the maximum chord will end up far from the r_{rte}. To prevent the optimization algorithm to get into this situation, a constraint is applied to the location of the maximum chord, which is described by

$$r(\max(c)) < r_{rte} + 0.08 \cdot R \text{ .} \tag{4.16}$$

And also if this constraint is violated, a death penalty is applied.

4.3.4 Maximum Angle of Attack

The performance of an airfoil becomes very uncertain when the operational angle of attack gets close to the stall angle of attack. Therefore, it is necessary that the design angle of attack throughout the blade span keep a certain distance from the stall angle of attack. For this reason another constraint is employed at the optimization problem:

$$\alpha(r) < \alpha_{stall}(r) - \Delta_{\alpha},\ \forall r > \max(r(t_{rCP1}), r(\max(c)))\ , \tag{4.17}$$

where $\alpha_{stall}(r)$ is the stall angle of attack for the airfoil at the blade element with center at r, and $\Delta\alpha$ is the margin for the angle of attack constraint, which is an input parameter (circa 2°). This constraint applies for elements that are located further in radius than the location of the maximum chord, or the location of the first true airfoil used, whichever happens last.

An additive penalty function is used for the AEP objective function if the maximum angle of attack constraint in violated. It is represented by

$$F_1(x) = AEP - K^2 \cdot 10^4\ , \text{ where} \tag{4.18}$$

$$K = \int_{r=max(r(t_{rCP1}),r(\max(c)))}^{R} \max(\alpha(r) - \alpha_{stall}(r) + \Delta\alpha, 0)\, dr\ . \tag{4.19}$$

4.4 Benchmark Problem

A benchmark problem was set, based on the wind conditions and present wind turbine concepts found in Brazil, in order to evaluate the defined design methodology and the performance of the selected metaheuristics. It consists in optimizing the blade geometry of a variable speed pitch-controlled 2.5 MW DDSG HAWT with a rotor diameter of 120 m. Table 4.1 demonstrates the parameters used in this benchmark problem. In this table, h_{hub} is the hub height, Ω_{min} is the minimum allowable rotor speed, v_{air} is the kinematic viscosity of the air, ΔV is the wind speed discretization step for the power curve, and c_{root} and c_{tip} are the chord values at the root and at the tip, respectively.

The DU-airfoils were chosen for this benchmark. This airfoil family was developed in the Delft University of Technology (DUT) for over a decade, beginning from the early nineties, by a number of projects funded by European Union, the Netherlands Agency for Energy and the Environment, and various European blade manufacturers [134–136].

In this context, the selected airfoils were, namely: DU 00-W-401; DU 00-W-350; DU 97-W-300; DU 91-W2-250; DU 00-W-212; and DU 96-W-180. The relative thickness (t_r) of these airfoils are, respectively, 40.1%, 35.0%, 30.0%, 25.0%, 21.2% and 18.0%. The wind tunnel data from the airfoils is used as input to the BEM model, and the their coordinates are used in the blade mass computation.

Table 4.1: Parameters of the benchmark optimization problem.

Parameter	Value	Parameter	Value
P_{rated}	2500 kW	C	9.5
B	3	k	3.6
R	60 m	E	27.6 GPa
r_{hub}	0.995 m	ρ_{mat}	1800 kg/m^3
n_{elm}	30	ε_{allow}	$4 \cdot 10^{-3}$
h_{hub}	120 m	F_S	1.2
Ω_{min}	2 rpm	t_{min}	0.02 m
Ω_{rated}	13.5 rpm	Δt	$2 \cdot 10^{-4}$ m
ρ_{air}	1.225 kg/m^3	c_{root}	2.4 m
ν_{air}	$1.464 \cdot 10^{-5}$ m^2/s	c_{tip}	$5 \cdot 10^{-3}$ m
V_{in}	2 m/s	r_{rts}	0.05 (r/R)
V_{out}	26 m/s	r_{rte}	0.22 (r/R)
ΔV	0.5 m/s	r_{tts}	0.95 (r/R)
K_{avl}	100%	$\Delta\alpha$	2°

The upper and lower bound vectors for x, respectively u and l, are described in Table 4.2. In this table, the elements that represent radial locations at the blade span (u_{11} to u_{16} and l_{11} to l_{16}) are in expressed as dimensionless r/R units. In this benchmark problem, the efficiency of the mechanical-electrical system is considered a function only of the rotational speed Ω, and its plot is shown at Figure 4.3.

Table 4.2: Upper and lower bound vectors.

Element	Value	Element	Value
l_1	5°	u_1	35°
l_2	-20°	u_2	15°
l_3	-15°	u_3	15°
l_4	-15°	u_4	15°
l_5	-10°	u_5	10°
l_6	4.9 m	u_6	5.7 m
l_7	0.1 m	u_7	5.5 m
l_8	0.1 m	u_8	4.0 m
l_9	0.1 m	u_9	4.0 m
l_{10}	0.1 m	u_{10}	6.0 m
l_{11}	$0.14\ (r/R)$	u_{11}	$0.15\ (r/R)$
l_{12}	$0.16\ (r/R)$	u_{12}	$0.17\ (r/R)$
l_{13}	$0.19\ (r/R)$	u_{13}	$0.21\ (r/R)$
l_{14}	$0.27\ (r/R)$	u_{14}	$0.36\ (r/R)$
l_{15}	$0.50\ (r/R)$	u_{15}	$0.65\ (r/R)$
l_{16}	$0.70\ (r/R)$	u_{16}	$0.85\ (r/R)$

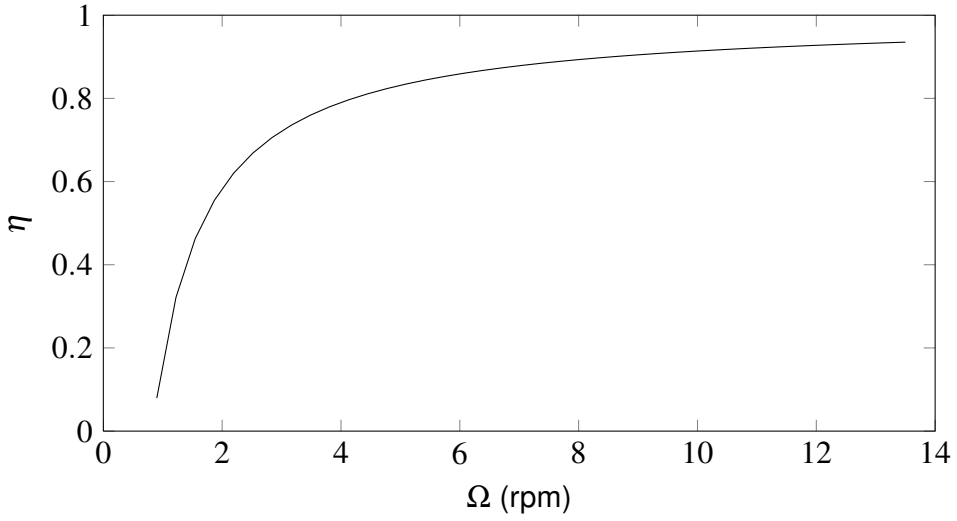

Figure 4.3: Efficiency curve of the benchmark mechanical-electrical system, with respect to the rotational speed Ω.

5 Experimental Results

This chapter presents and analyses the results obtained with the design methodology developed, which was applied to the benchmark problem described in Section 4.4. In Section 5.1, the materials and methods applied in the present work are presented, including hardware configuration, codes and parameter setting of the selected metaheuristics and of the BEM model. Several runs of each metaheuristic were performed, in order to reduce the uncertainty involved in the performance comparison of different stochastic optimization algorithms. The results from these runs are described in Section 5.2. The obtained PF and PS are analysed in Section 5.3. The blade element data and other details of the optimized blade designs are given in Section 5.4.

5.1 Materials and Methods

Since the experiments conducted for the present work were strictly computational, the materials and methods used to obtain the results of this research can be described by hardware and software configurations. The metaheuristics codes were implemented in the MATLAB programming environment version R2011a, and all experiments were run in the same computer, which has an Intel® Xeon® Processor W3690 (12 MB Cache, 3.47 GHz, 6 cores) and 6 GB Random-Access Memory (RAM) (1333 MHz, DDR3).

The next subsections present the MOEAs and BEM codes used in the experiments carried out for this research. MOEAs parameter setting is summarized in Table 5.1, and also described in detail in the following subsections. Since no parameter tuning was carried out in the present work, the parameters were set according to the original references of their corresponding algorithms and codes.

Table 5.1: MOEAs parameter setting.

MOEA	Parameter	Value
NSGA-II	n	100
	p_c	0.9
	p_m	$1/n_x$
	η_c	20
	η_m	20
QMEA	m	$16 \cdot n_x$
	n	100
	n_g	10
	$\Delta\theta$	0.01π
MOEA/D	N	100
	T	20
MODE	n	100
	F_m	0.5
	K_{cr}	0.2

5.1.1 NSGA-II

The real-coded NSGA-II MATLAB code from Seshadri [137] was applied in this research. The population size used for NSGA-II was 100 individuals. Tournament selection was used as the selection operator, with a mating pool size of half the population size, and with size of the tournament being 2, which corresponds to the binary tournament selection. The Simulated Binary Crossover (SBX) operator [138] was used with a crossover probability of $p_c = 0.9$, as well as a polynomial mutation operator [138] with a mutation probability of $p_m = 1/n_x$, n_x being the number of decision variables. The distribution indexes [138] for crossover and mutation operators were $\eta_c = 20$ and $\eta_m = 20$, respectively. All these parameter values correspond to the same ones reported by Deb et al. [49].

5.1.2 QMEA

Table 5.1 describes the parameter values employed in QMEA for the experiments. The binary resolution used in QMEA was 16 bits, and in this way the total number of Q-bits were $m = 16 \cdot n_x$. The population size n was again set to 100 individuals. The number of groups in the update process of QMEA was $n_g = 10$. And at last, the rotation angle $\Delta\theta$ applied was 0.01π. These parameter values correspond to the ones set by Kim, Kim and Han in the original description of QMEA [112]. The QMEA MATLAB code which was run in the experiments was developed by the author of this dissertation himself.

5.1.3 MOEA/D

For the experimental tests with MOEA/D, the MATLAB code written by Zhang [139] was applied to the benchmark problem described in Section 4.4. The only two parameters of this metaheuristic are the number of sub-problems N and the neighbourhood size T, which were set respectively as 100 and 20. These parameter values were the same as in [139]. The decomposition method must also be provided to MOEA/D, and here both the weighted sum and the Tchebycheff were used, what corresponds to W-MOEA/D and T-MOEA/D.

5.1.4 MODE

The MODE MATLAB code developed by Reynoso-Meza [140] was used to evaluate the performance of this metaheuristic. This implementation of MODE corresponds to the $DE/rand/1/bin$ scheme with a modified selection operation, in which the trial vector replaces the target vector if the former dominates or equals the latter. This is equivalent to the first version of the Generalized Differential Evolution (GDE) of Kukkonen and Lampinen [119, 141], and as a basic MODE it does not incorporate any distance metric. As in the other metaheuristics, the population size was specified as 100. The mutation scale factor F_m in the DE algorithm was set to 0.5, and the crossover constant K_{cr} to 0.2, the same way as in [140].

5.1.5 Performance Metrics

As previously mentioned, four performance metrics were applied in this dissertation: the two set coverage, the hypervolume, the spacing, and the ONVG. The MATLAB code developed by Kruisselbrink [142] was used for the hypervolume metric computation. As for the other three metrics, the MATLAB code used in their computation was written by the author of the present work, according to their definitions in Subsection 3.1.2.

5.1.6 BEM Model

The BEM model used for the aerodynamic analysis is implemented as the WT_Perf code [19]. This code was set to take account of the Prandtl tip- and hub-loss algorithms, of the rotational wake effects, of the drag term in the axial and tangential induction calculation, and to use the advanced brake-state model. The maximum number of iterations for the

induction factors was set to 1000, and the error tolerance for the induction iteration to 10^{-6}. No stall delay models were used.

The airfoil performance data, i.e., C_L and C_D versus α, for a given blade element were interpolated from the wind tunnel data of the two true airfoils that surround this element, using the Shape Preserving Interpolation (SPI) as described by Sale [13]. The relative thickness t_r is used as the input to balance the interpolation more to one of the true airfoils or to the other. The airfoil coordinates at this blade element were also interpolated in a similar way.

5.2 Performance Analysis of the Metaheuristics

For the analysis of performance of NSGA-II, QMEA, MOEA/D and MODE in solving the proposed benchmark problem, 30 experiments with each metaheuristic were run. The stopping criterion was the maximum number of objective functions evaluations, defined as 15000. After each run of an experiment, a non-dominated front is obtained. Combining the fronts of the 30 runs into a global non-dominated front gives a solution that is less influenced by the stochastic aspect of the metaheuristics, and in this way better for performance comparisons. These non-dominated fronts obtained over the 30 runs of each evaluated metaheuristic are given in Figure 5.1.

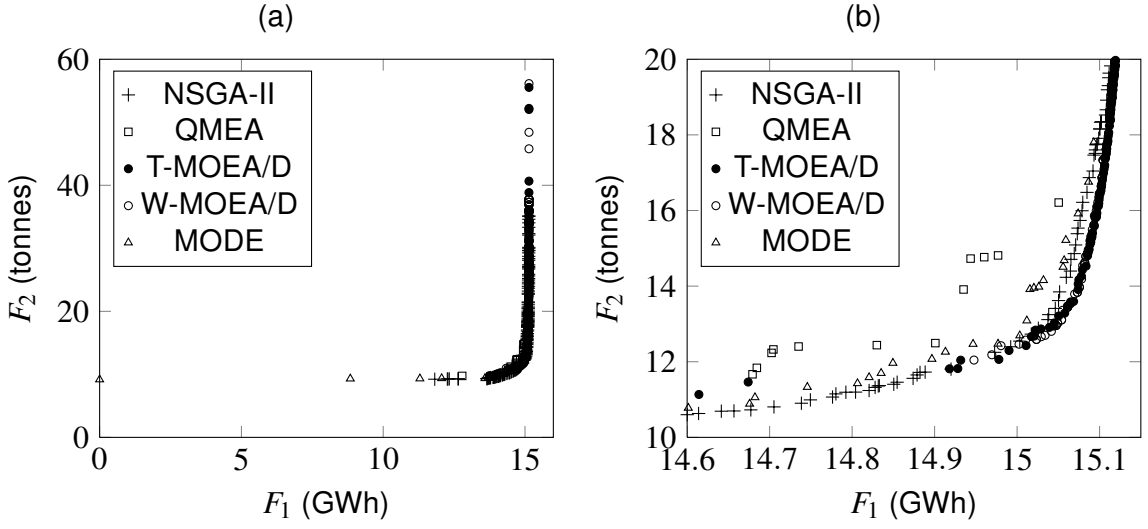

Figure 5.1: Non-dominated fronts obtained over the 30 runs of each evaluated metaheuristic, general view (a) and zoomed view (b).

There is a point of maximum curvature at the non-dominated fronts between the values 15 and 15.1 of F_1, which breaks the fronts in two segments, one below and one

above this point. At the segment below the point of maximum curvature, a small decrease in blade mass (F_2) causes a large decrease in AEP (F_1). The solutions of rotor design contained in this segment are characterized by low efficiency (C_P), and therefore low loads and low blade mass. Here the solutions provided by NSGA-II dominates most of the other solutions.

At the other segment, the one above the point of maximum curvature, a small increase in AEP causes a large increase in blade mass. In this segment, the solutions of both T-MOEA/D and W-MOEA/D dominate most of the solutions found by the other metaheuristics. Now the solutions here are characterized by high efficiency, high loads and high blade mass.

As both AEP and blade mass have an impact on the COE, one has to find a trade-off between these two objectives in order to come up with a reasonable blade design. A cost model, as the one of Fingersh, Hand and Laxson [24], can help on this task, in order to find the solution with the minimum COE. Another way to perform this task is to identify market trends and use them as references. With regard to blade mass, Fingersh, Hand and Laxson [24] report the mass scaling relationship for the 2006 blade designs from the manufacturer LM Wind Power (formerly LM Glasfiber), which yields a blade mass of 15.6 tonnes for a rotor radius of 60 m. One could expect a reduction of mass for current designs, say to around 14 tonnes, as a result of the blade technology evolution.

On the other hand, peak efficiency ($\max(C_P \cdot \eta)$) of commercial wind turbines (e.g. Enercon turbines [143]) are ranging from around 46% to 50%. For the benchmark problem of Section 4.4, this would yield a minimum AEP of 15 GWh. In this way, desired values for this benchmark case are around 15.1 GWh and 14 tonnes. In this region, the solutions of T-MOEA/D and W-MOEA/D dominate the ones of NSGA-II, QMEA and MODE, which is a good indication that MOEA/D performs better in this problem.

The coverage metric can be applied to the non-dominated fronts obtained over 30 runs of each metaheuristic, with the aim of measuring their dominance. Table 5.2 presents the results of this metric, which was used for every ordered pair of the five metaheuristics. The last column of the table displays the averages of each line, and the last line informs the averages of each column. In this way, one element of the last column represents the average fraction of the corresponding MOEA's solution set that is dominated by the solutions of other MOEAs. Likewise, an element of the last line stands for the average share of the solution sets of other MOEAs that is dominated by the solutions from the MOEA of the corresponding column.

Table 5.2: Coverage metric of non-dominated fronts obtained over 30 runs.

$B \backslash A$	NSGA-II	QMEA	T-MOEA/D	W-MOEA/D	MODE	Average
NSGA-II		0	0.520	0.507	0	0.257
QMEA	1.000		0.737	0.579	0.895	0.803
T-MOEA/D	0.039	0.008		0.241	0.024	0.078
W-MOEA/D	0.012	0.003	0.422		0.009	0.111
MODE	0.936	0.043	0.425	0.383		0.447
Average	0.497	0.013	0.526	0.427	0.232	

This table shows that T-MOEA/D has the largest dominance, dominating on average 52.6% of the solutions of other algorithms, with only 7.8% of its solutions being dominated by that of other metaheuristics. On average, the NSGA-II solution set dominates more than the set of W-MOEA/D, 49.7% against 42.7%, but it is also much more dominated by other algorithms solutions than W-MOEA/D, 25.7% against 11.1%. When analysing the coverage of these two algorithms, the non-dominated front of W-MOEA/D covers 50.7% of the NSGA-II front, while the opposite covers only 1.2%. Therefore W-MOEA/D takes the second place on this metric. The worst evaluated metaheuristic with regard to the coverage metric is the QMEA, which is on average dominated by 80.3% and dominates only 1.3% of the other fronts.

Table 5.3 shows the results of other performance metrics averaged over the 30 runs of the algorithms. For the hypervolume and spacing metrics calculation, the F_1 axis was reversed and normalized, and the F_2 axis was also normalized. The reference point for the hypervolume metric was then $(1, 1)$, which correspond to the maximum normalized F_1 and F_2 values, considering a minimization problem of both objective functions. The ONVG metric was computed over the non-dominated fronts of Figure 5.1, i.e., the 5 global non-dominated fronts of 30 runs each. The runtime was accounted for each run of an algorithm, and shown in Table 5.3 are the mean runtime values over the 30 runs.

Figures 5.2(a) and 5.2(b) details respectively the obtained hypervolume and spacing metrics for all runs, by drawing the box plot of the data. Through the hypervolume metric, NSGA-II and MODE are the best evaluated techniques. But Figure 5.1 shows that MODE has a better convergence at the region of low AEP (front segment below the point of maximum curvature), and its convergence in the region of interest, as previously mentioned around 15.1 GWh and 14 tonnes, is not very satisfying. The hypervolume rates are higher for the algorithms that can balance the convergence between the two front segments, that

Table 5.3: Average performance metrics over 30 runs.

Metric	NSGA-II	QMEA	T-MOEA/D	W-MOEA/D	MODE
Hypervolume	0.983	0.960	0.970	0.935	0.982
Spacing ($\cdot 10^{-2}$)	0.34	4.62	1.60	0.65	12.20
ONVG	148	19	253	346	47
Runtime (hours)	5.30	3.28	10.84	13.80	5.00

is, which reach a more widely converged front. As the W-MOEA/D front is the least converged at the segment below the point of maximum curvature, its hypervolume rate is much lower than that of the other metaheuristics. The NSGA-II has the highest hypervolume rate, because its front is well balanced. Furthermore, its converge in the region of interest is better than that of MODE. T-MOEA/D is also well evaluated by this metric.

The spacing metric values show that NSGA-II has in average the fronts with the most evenly spaced solutions. T-MOEA/D and W-MOEA/D fronts also have well spaced solutions, but the same is not true for QMEA and MODE, which got much higher rates for this metric. These assumptions are confirmed by the visual inspection of the fronts in Figure 5.1. As the MODE scheme used in the present work does not incorporate any distance metric, the distribution of solution points in the non-dominated front is really an issue with this approach.

The W-MOEA/D global front is the most populated of all, given that it presents the highest ONVG metric value, and the front of QMEA is on the other hand the least populated. The runtime values follow the same order of the ONVG values. That is mostly because if an algorithm generates more feasible solutions, the objective functions evaluations takes longer to run. When a solution is evaluated, first the geometrical constraints (monotonicity and location of maximum chord) are checked, and if any of them is violated, the BEM algorithm do not run, which explains the above assumption. The average time for evaluating an infeasible solution (a solution that violates at least one geometrical constraint) is 2.1 ms, whereas for the feasible counterpart this time is 2.75 s, i.e., more than a thousand times slower. As mentioned earlier, the stopping criterion was 15000 objective functions evaluations. In average, it would take more than 11 hours to evaluate this amount of feasible solutions, and only about 30 s if all of them were infeasible.

With all the results analysed in this section, the decision of which of the five metaheuristics performs best for the problem dealt with here is not a straightforward task. One

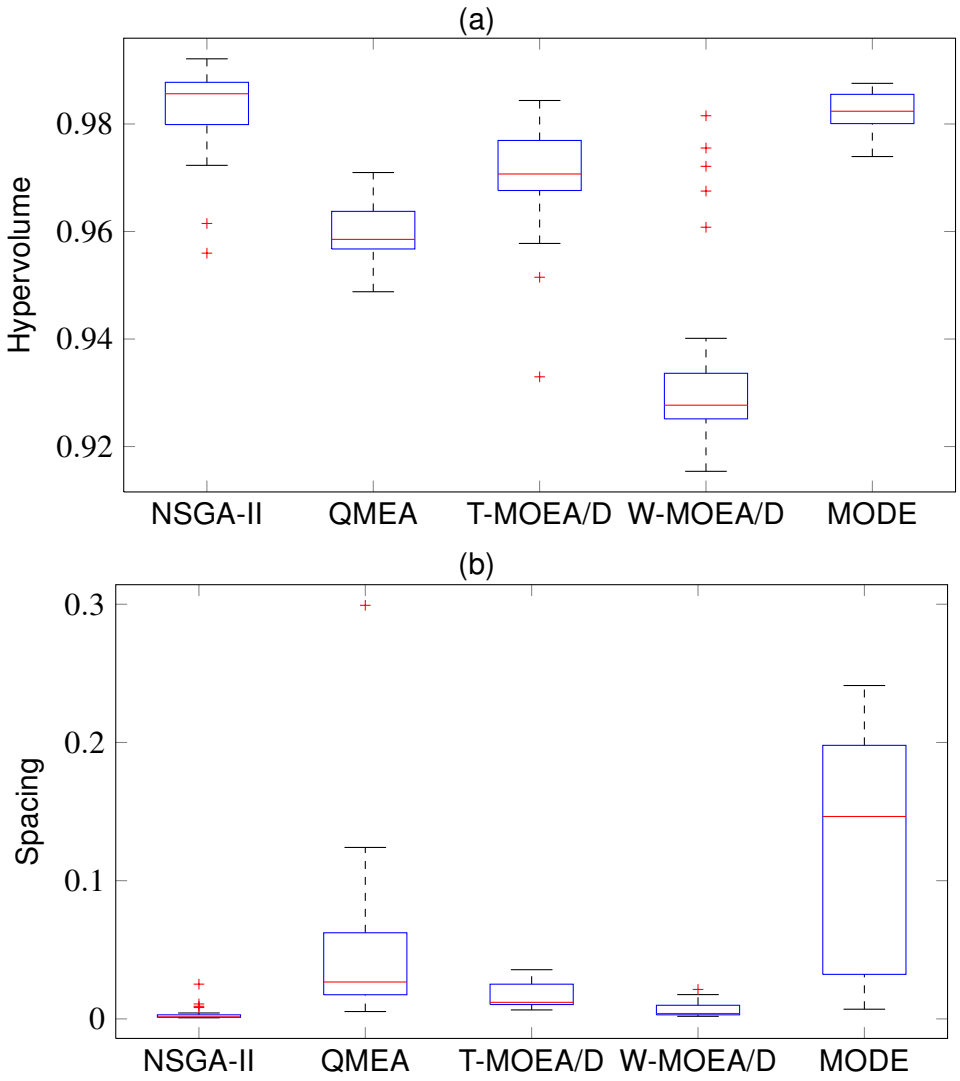

Figure 5.2: Box plot of the hypervolume (a) and spacing (b) metrics for 30 runs.

can see that the techniques evaluated are complementary, as they have alternated their positions in the rank of different performance metrics evaluations. Nonetheless, the results indicate that NSGA-II and T-MOEA/D have better performance than the other three algorithms, with T-MOEA/D performing better on the region of interest and NSGA-II on the overall front. The best result could be achieved with a combination of these two techniques.

5.3 Analysis of the Pareto Front and Set

The true PF to the benchmark problem proposed in Section 4.4 is not known, since it is a real-world application problem, and the known PF is considered here to be the non-dominated front of the solutions found by all five metaheuristics over all runs. This known PF is shown in Figure 5.3, that also details by which algorithm each solution was found.

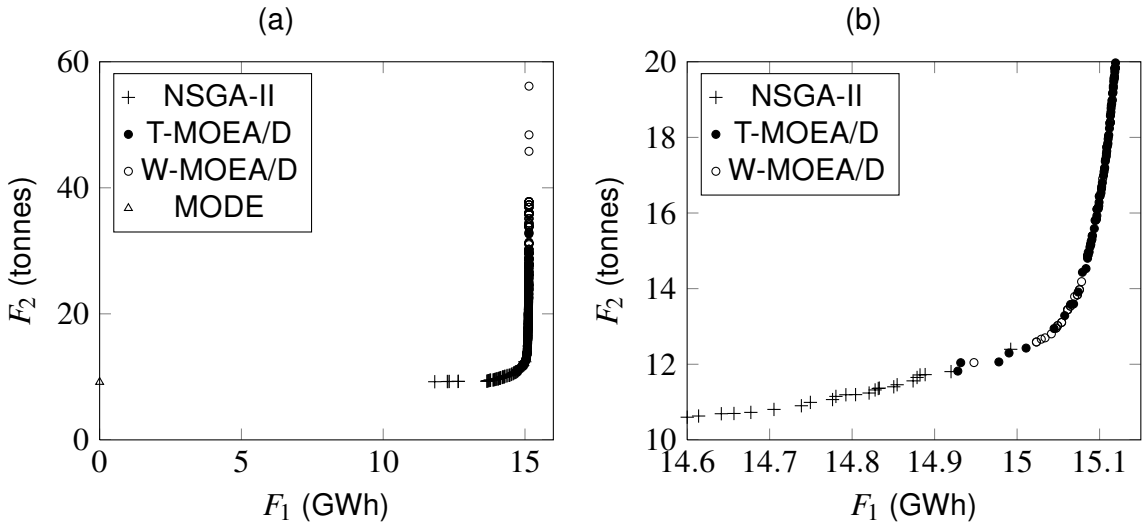

Figure 5.3: Known Pareto Front of the benchmark problem, general view (a) and zoomed view (b).

Finding the PF and PS does not completely solve a MOP. A single solution still have to be chosen out of the set by the decision maker, which is not a trivial process [144]. This process is known as Decision Making (DM). As previously mentioned, a good strategy for the DM at this specific problem could be finding the solution with the minimum COE, with the help of a cost model. But the application of such a model is left as future work, and here more simple and general DM strategies were adopted. The maximum harmonic mean of the normalized objective functions values provides a reasonable trade-off between the objectives, and this DM technique was successfully applied previously, e.g. by Ayala and Coelho in 2008 [145]. Another approach could be the human DM, which corresponds to manually choosing a desired solution out of the set, by using the personal knowledge of the problem.

Hence, these last two techniques, maximum harmonic mean and human DM, were applied to the known PF of the problem handled here. The selected solutions are illustrated at the PF by Figure 5.4, numbered from 1 to 4. Solution 2 is the result of the maximum harmonic mean, while solution 3 was chosen by human DM. The extreme solutions, numbers 1 and 4, were also selected for future analysis. The solutions 1 to 4 were found respectively by MODE, NSGA-II, T-MOEA/D and W-MOEA/D.

The human DM was based on the personal experience of the author, which tells that F_2 has a higher priority than F_1, because the former has a higher impact on the COE than the latter. In this way, the blade mass must be reduced as much as possible without causing a significant reduction in the AEP. Hence, the solution 3 was selected out of the lower part of the PF segment above the point of maximum curvature (this segment was

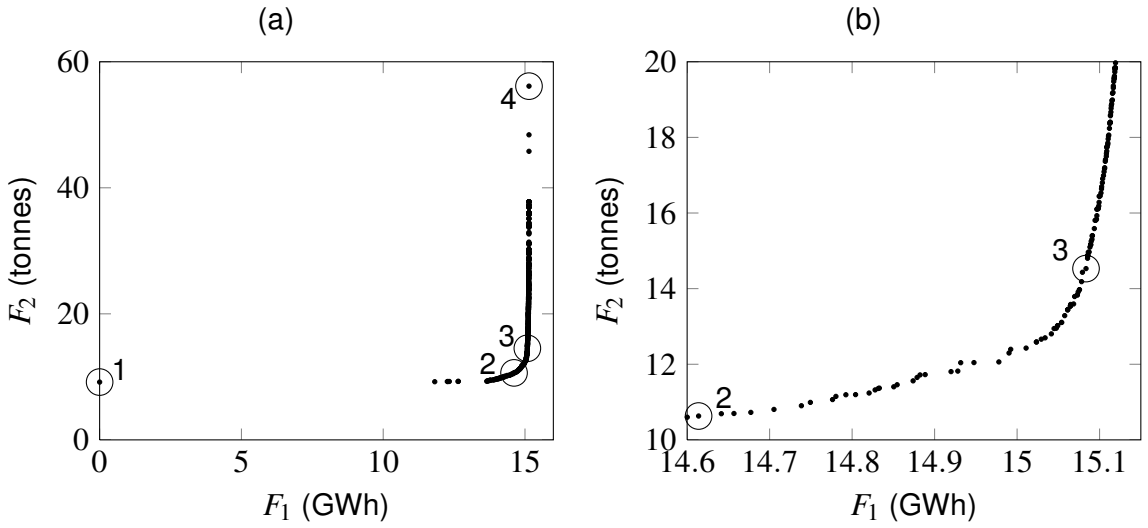

Figure 5.4: Selected solutions at the Pareto Front, general view (a) and zoomed view (b).

defined in Section 5.2). The values of AEP and blade mass from solution 3 are closer to the market trends than those of other solutions.

Recalling, market trends for AEP and blade mass considering the proposed benchmark problem are around 15.1 GWh and 14 tonnes, respectively. As previously described, Fingersh, Hand and Laxson [24] report the mass scaling relationship for the 2006 blade designs from the manufacturer LM Wind Power (formerly LM Glasfiber), which yields a blade mass of 15.6 tonnes for a rotor radius of 60 m. One could expect a reduction of mass for current designs, say to around 14 tonnes, as a result of the blade technology evolution. On the other hand, peak efficiency ($\max(C_P \cdot \eta)$) of commercial wind turbines (e.g. Enercon turbines [143]) are ranging from around 46% to 50%. For the benchmark problem of Section 4.4, this would yield a minimum AEP of 15 GWh.

Now for the analysis of the corresponding PS, a histogram of each element x_i of the solution vectors in the known PS is plotted in Figures 5.5 and 5.6. These histograms show that the domain of the search space for the specific problem dealt with here could be reduced, because the optimal values of some elements lie in just a segment of this domain, thus speeding up the convergence of the MOEAs. For example, the upper and lower bounds of x_1 are respectively 5 and 35 (see Table 4.2), but virtually all of the PS values for this element are between 10 and 18. From this analysis, the domain of the following elements could be reduced: x_1 to x_5, x_9 and x_{10}. One must be very careful, though, when restricting the search domain, because a reduction on the twist domain can affect the optimum location of the chord, and vice versa. Furthermore, the optimum domain of the elements for a problem with a unknown PF cannot be known a priori, i.e., before

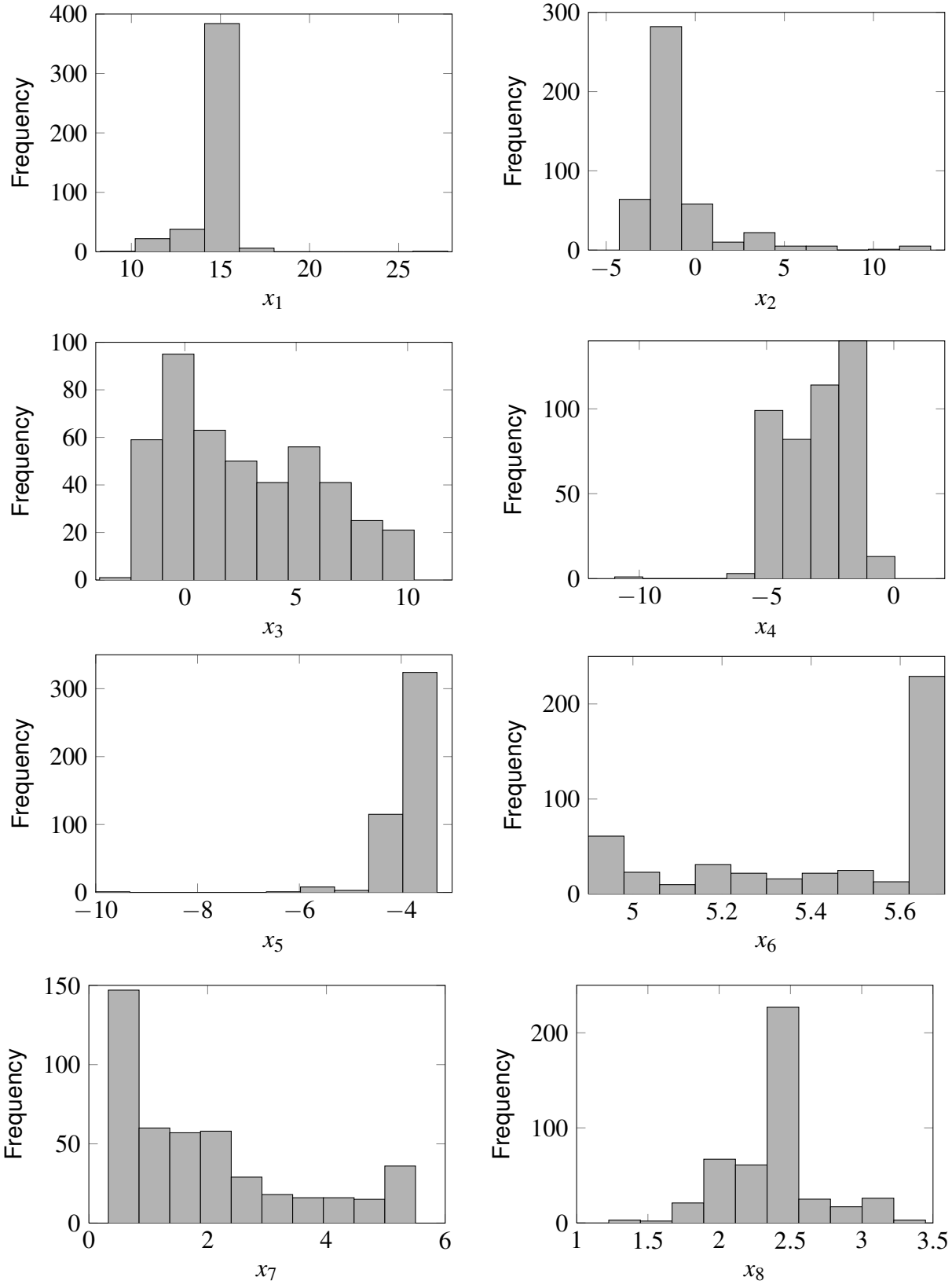

Figure 5.5: Histograms of the vectors elements in the Pareto Set, from x_1 to x_8.

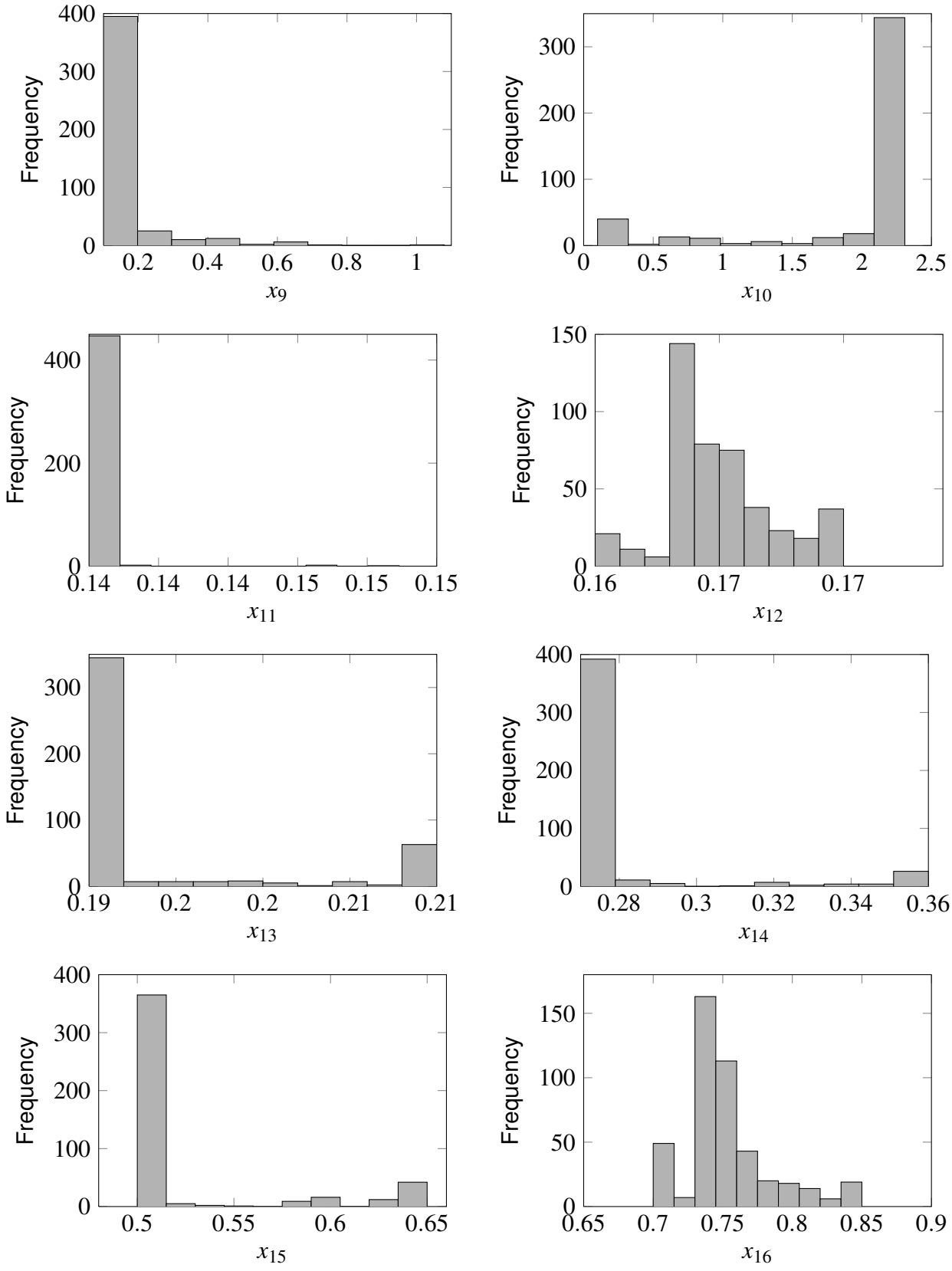

Figure 5.6: Histograms of the vectors elements in the Pareto Set, from x_9 to x_{16}.

running the MOEA.

5.4 Analysis of the Blade Designs

In order to evaluate and compare each of the selected solutions, and also to validate the defined blade geometry design methodology, detailed information about the corresponding blade designs is analysed in this section. At first, the twist, chord and thickness distributions are plotted in Figure 5.7. Solution 3 has the highest chord values, which makes its dimensional thickness also to be the highest. Higher blade thickness causes higher area moment of inertia, thus reducing strains and in this way improving the structure of the blade, which explains why solution 3 has a much lower blade mass than solution 4, still having similar efficiency. This Figure also shows a shortfall in the blade thickness representation: some bumps appear in the dimensional thickness distributions, between radius of 7 and 15 m. This is caused by the positioning of two true airfoils close to one another in the region of maximum chord. This could be solved in the future with an improved thickness representation, with similar features as the chord and twist representation.

The performance of designed rotors in the whole range of operation are compared in Figure 5.8, through the power coefficient (C_P) versus tip speed ratio (λ) curves. Solution 4 presents the highest C_P at the optimum tip speed ratio (λ_{opt}), but it has the sharpest performance curve, with faster decrease in C_P (efficiency degradation) for operation out of λ_{opt}. All the other solutions present equivalent wide performance curves, with solution 3 also showing high efficiency at λ_{opt}, comparable to solution 4.

Power and efficiency curves over the main range of wind speeds are presented in Figure 5.9(a) and (b), respectively. No difference can be noted in the power curve of solutions 3 and 4, but solution 2 presents a lower power curve than these two, reaching rated power (P_{rated}) at a bit higher rated wind speed (V_{rated}). Solution 1 does not show an acceptable power curve. Through the efficiency curve the differences in solutions 2 to 4 are more evident, with solution 4 being the most efficient.

Features of the objective function F_2, namely shell thickness (t_{shell}) and maximum strain ($\max[\varepsilon(r)]$), are plotted as a function of the rotor radius in Figure 5.10(a), (b) and (c). The $\max[\varepsilon(r)]$ is referred to as the maximum absolute strain at the four extreme points of the shell geometry (described in Subsection 4.1.2) as a function of the radial position. Solution 4 has by far the most thick shell, what makes this blade to be so heavy. This solution would be the one expected as the output of a mono-objective optimization method, considering

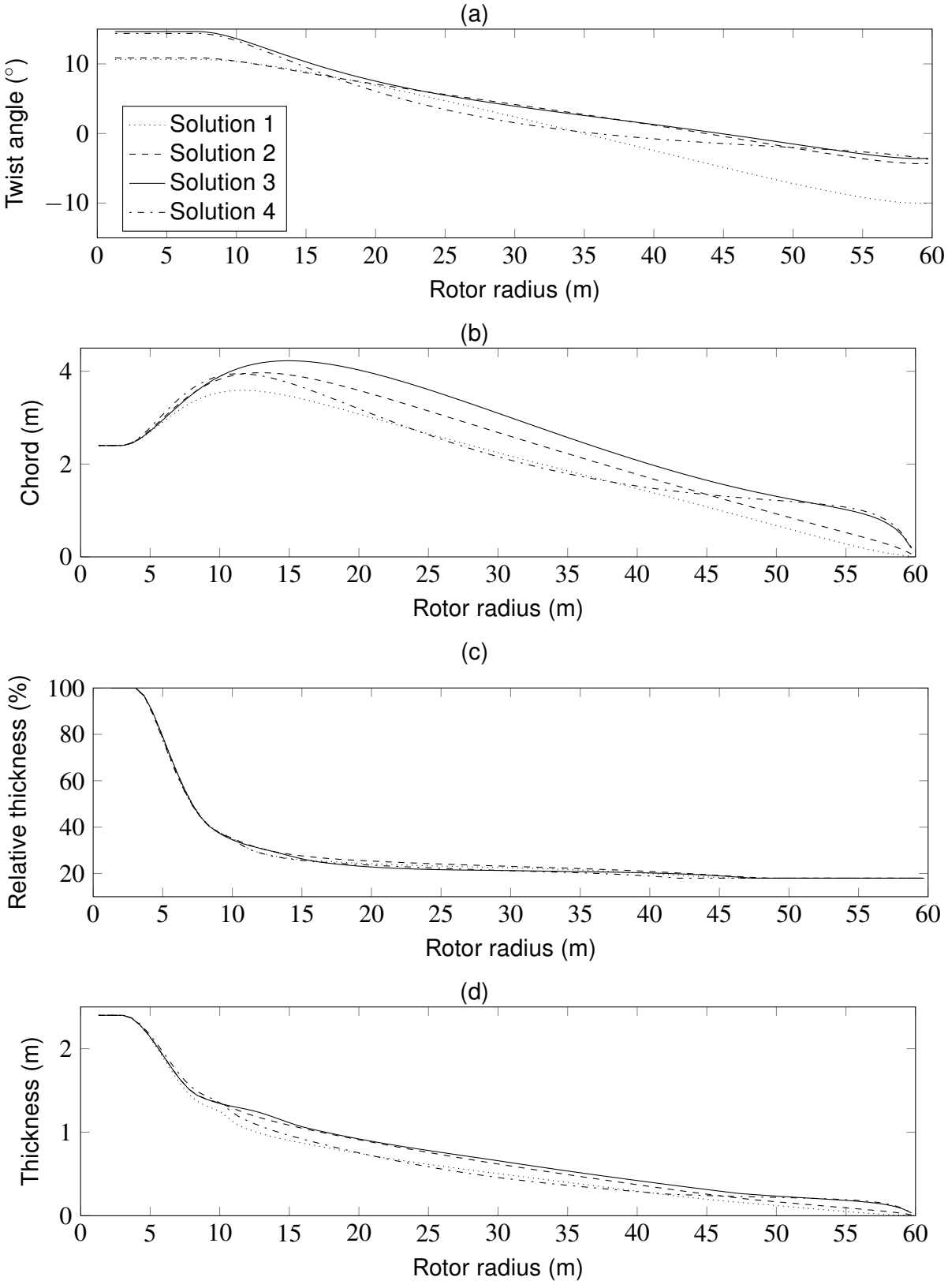

Figure 5.7: Blade geometry of selected solutions: twist angle (a), chord (b), relative thickness (c) and absolute thickness (d).

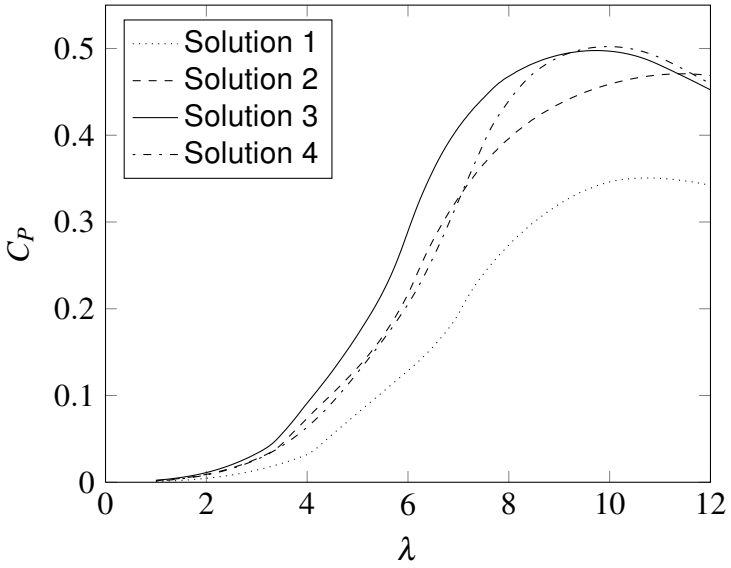

Figure 5.8: Rotor performance curve, C_P versus λ, of selected solutions.

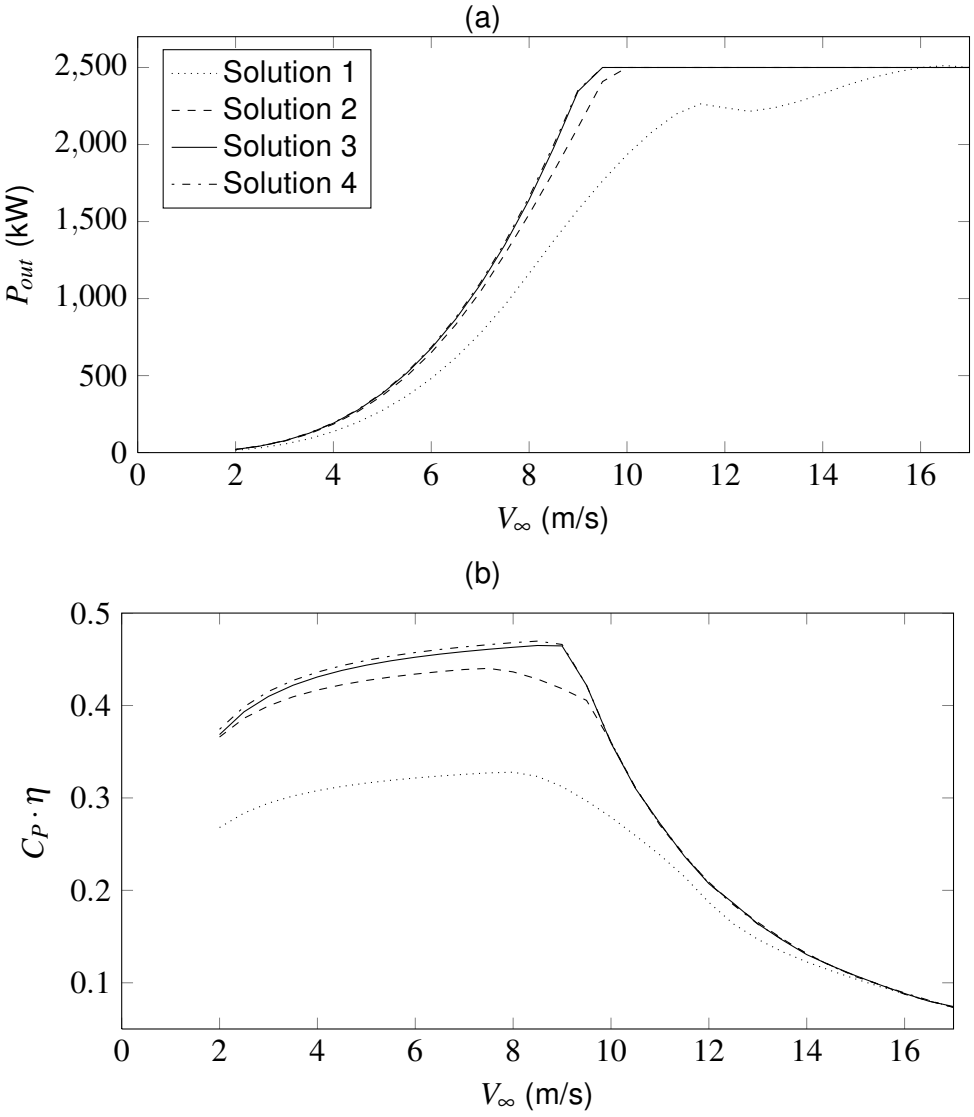

Figure 5.9: Power (a) and efficiency (b) curves of selected solutions.

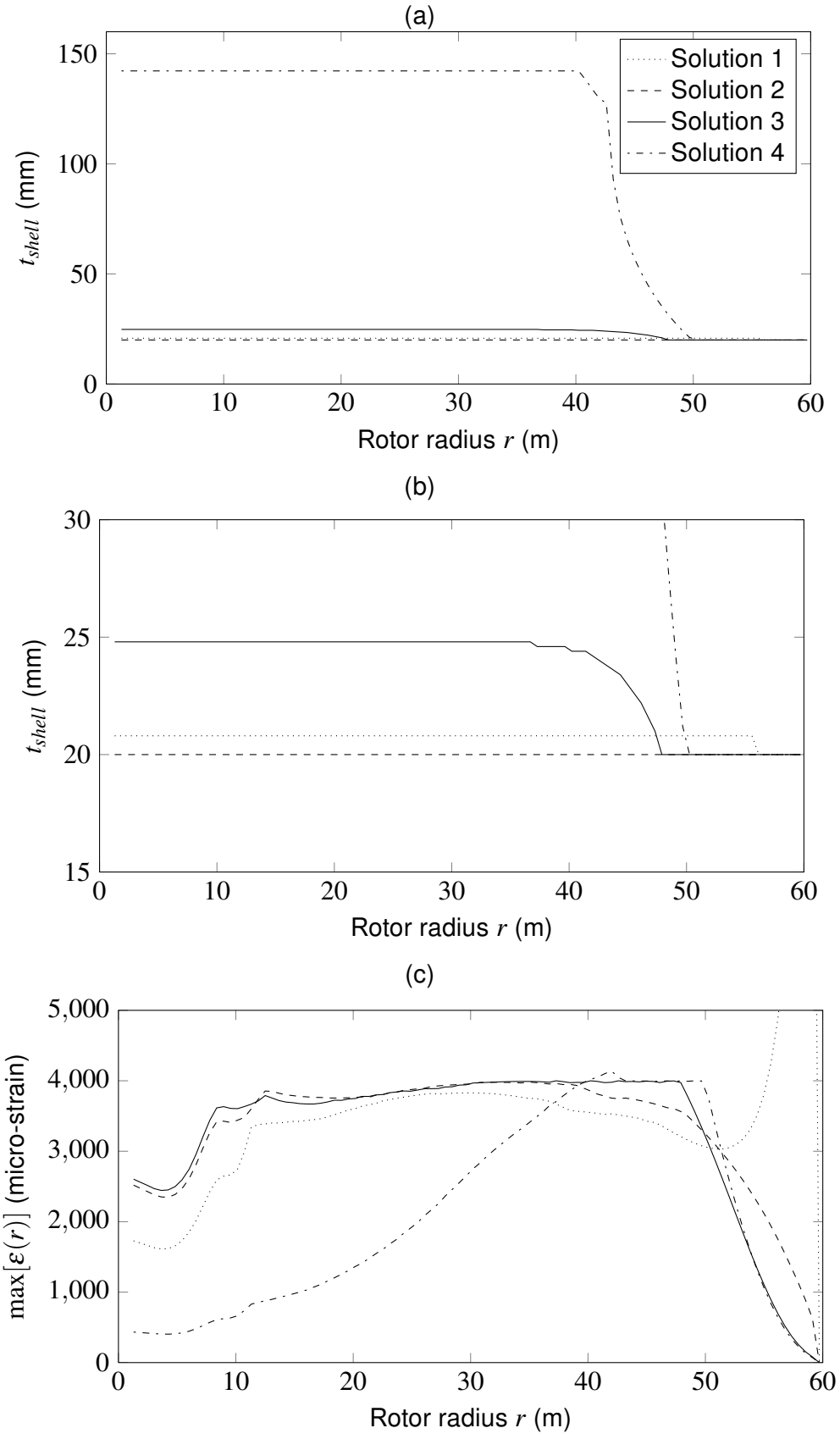

Figure 5.10: Spanwise shell thickness, general view (a) and zoomed view (b), and maximum strain (c) of selected solutions.

only AEP maximization. For this blade, the strains, and consequently the stresses, are concentrated in the region of 40 to 50 m radius. Solutions 2 and 3 can better balance the strains and stresses over the rotor radius. Furthermore, the maximum strain of solutions 1 and 4 overcomes the maximum allowable strain (ε_{allow}), which was set as 4000 micro-strains.

Table 5.4 summarizes some performance parameters of the selected rotor solutions. AEP and blade mass are increasing from solution 1 to solution 4, as already expected. The penalty factor K for the maximum angle of attack constraint is decreasing from solutions 1 to 4, with acceptable values for solutions 3 and 4. But none of the solutions completely satisfies the maximum angle of attack constraint, as $K \neq 0$ for all solutions. In this table, $\max(\varepsilon)$ corresponds to $\max[\varepsilon(r)]$ for all values of r. As already mentioned, maximum strains of solutions 1 and 4 exceeds ε_{allow}, solution 4 in just 139 micro-strains and solution 1 in 9381, which is over two times ε_{allow}. C_P for solutions 3 and 4 are, as desired, around 50%. λ_{opt}, F_C and V_{rated} values between these two solutions are very close, which suggests similar aerodynamic performance.

Table 5.4: Rotor performance parameters for selected solutions.

Parameter	Solution 1	Solution 2	Solution 3	Solution 4
AEP (GWh)	11.731	14.605	15.055	15.118
m_b (tonnes)	9.17	10.63	14.53	56.13
K	75.9	2.45	0.208	0.044
$\max(\varepsilon)$ (micro-strain)	13381	3982	4000	4139
C_P	0.350	0.471	0.498	0.502
λ_{opt}	10.75	11.45	9.75	10.0
F_C (%)	53.57	66.69	68.74	69.03
V_{rated} (m/s)	17.0	10.0	9.5	9.5

At last, with the aim of tracking record, the four solution vectors corresponding to the selected blade designs are presented in Table 5.5. Recalling, the search domain for these solution vectors is given by Table 4.2. With all the rotor performance data analysed until now, one concludes that solution 3 represents the best blade design, provided that it has an equivalent aerodynamic performance when compared to solution 4 (the one with highest AEP), and equivalent or superior structural performance compared to all other solutions. This solution is further analysed in Subsection 5.4.1, for the validation of the design methodology defined in this dissertation.

Table 5.5: Selected solution vectors (search domain is given by Table 4.2).

Element	Solution 1	Solution 2	Solution 3	Solution 4
x_1	10.6439	10.8597	14.6509	14.3824
x_2	6.7521	3.7000	−1.4410	−1.4309
x_3	0.7110	6.0846	7.8685	−1.4703
x_4	−10.9645	−5.3517	−4.8878	−1.1984
x_5	−10.0000	−4.2766	−3.5132	−3.7997
x_6	4.9000	5.2481	4.9863	5.7000
x_7	0.7700	2.3749	5.3049	0.4609
x_8	3.4472	3.0023	1.7253	2.2288
x_9	0.1000	0.2806	0.1000	0.1000
x_{10}	0.1000	0.6580	2.1238	2.3088
x_{11}	0.1408	0.1400	0.1400	0.1400
x_{12}	0.1678	0.1679	0.1639	0.1654
x_{13}	0.1900	0.2092	0.2100	0.1900
x_{14}	0.2915	0.3547	0.2701	0.2702
x_{15}	0.6050	0.6484	0.5113	0.5000
x_{16}	0.7733	0.8054	0.7877	0.7000

5.4.1 Detailing of Best Blade Design

The final results of the best blade design (solution 3) are given in this subsection. Flow conditions along the rotor radius are presented in Figure 5.11(a) and (b). Reynolds numbers (Re) are ranging from 2 to 9 million, which is compatible with the conditions of the wind tunnel tests carried out with the DU-airfoils (3 million). The angle of attack at the whole blade is within a secure distance of the stall angle of attack. The maximum angle of attack constraint is violated by a bit only very close to the tip (less than one meter from the tip), which is totally acceptable. Aerodynamic efficiency, L/D, is high from about 10 m radius, but low closer to the root, because of the circular root transition. C_P is also high, more than 50% from 10 m up to 55 m radius, but low at the tip because of the tip losses.

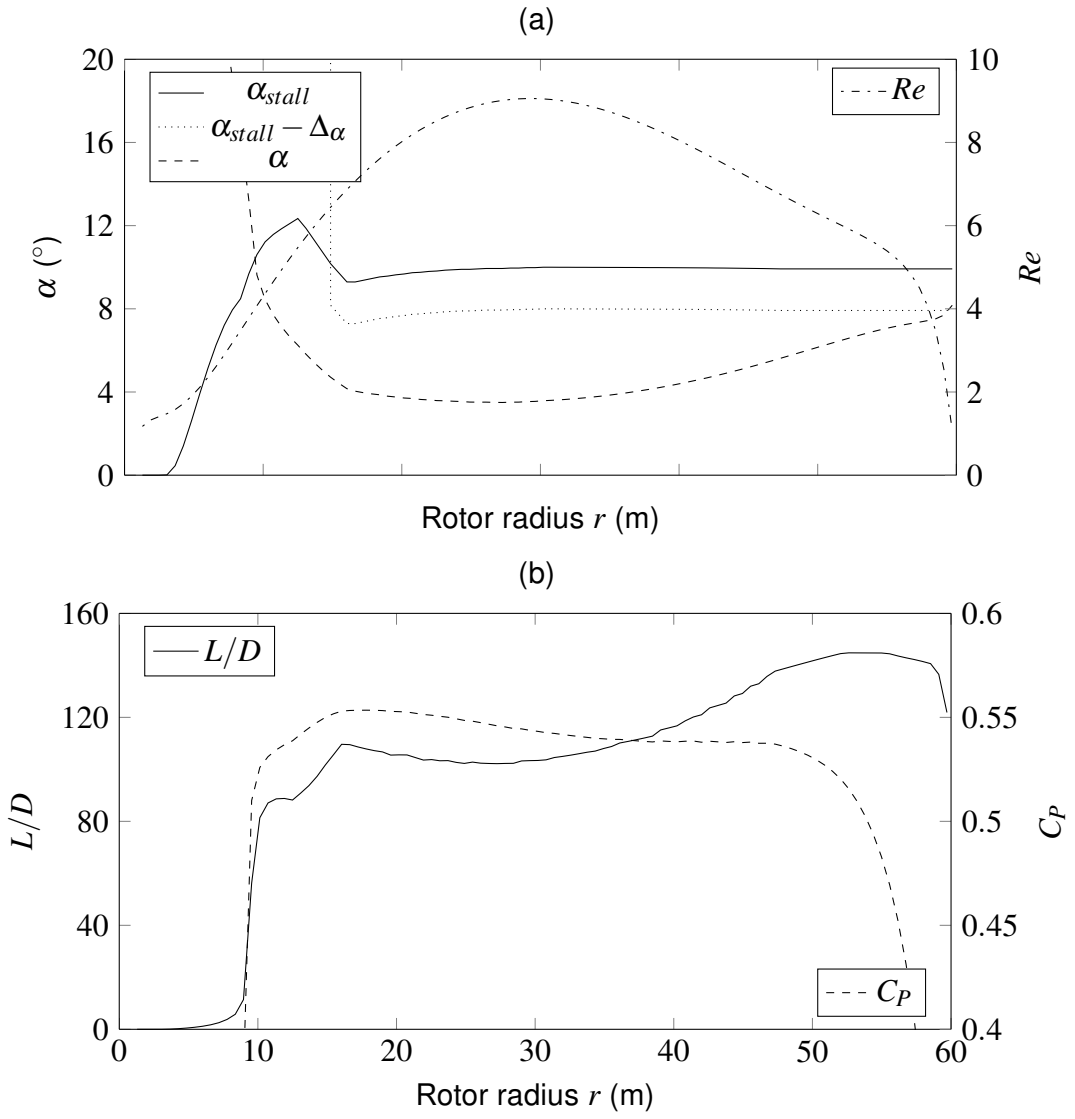

Figure 5.11: Flow conditions along the blade: α and Re (a), L/D and C_P (b).

The steady state operation of rotor speed and blade twist controllers for a turbine

with this blade should result in the curves presented in Figure 5.12(a). Because of the efficiency characteristics of the mechanical-electrical system, the MPPT strategy causes the λ to be a bit higher then λ_{opt}, at wind speeds lower than but close to V_{rated}, and even higher for wind speeds close to V_{in}. Moreover, for purposes of future micro-siting and structural design of tower, foundation and other components, the thrust characteristics, both T and C_P, at the range of wind speeds are plotted in Figure 5.12(b). Through this Figure, one can note the correlation of C_T with λ. The maximum thrust is around 450 kN.

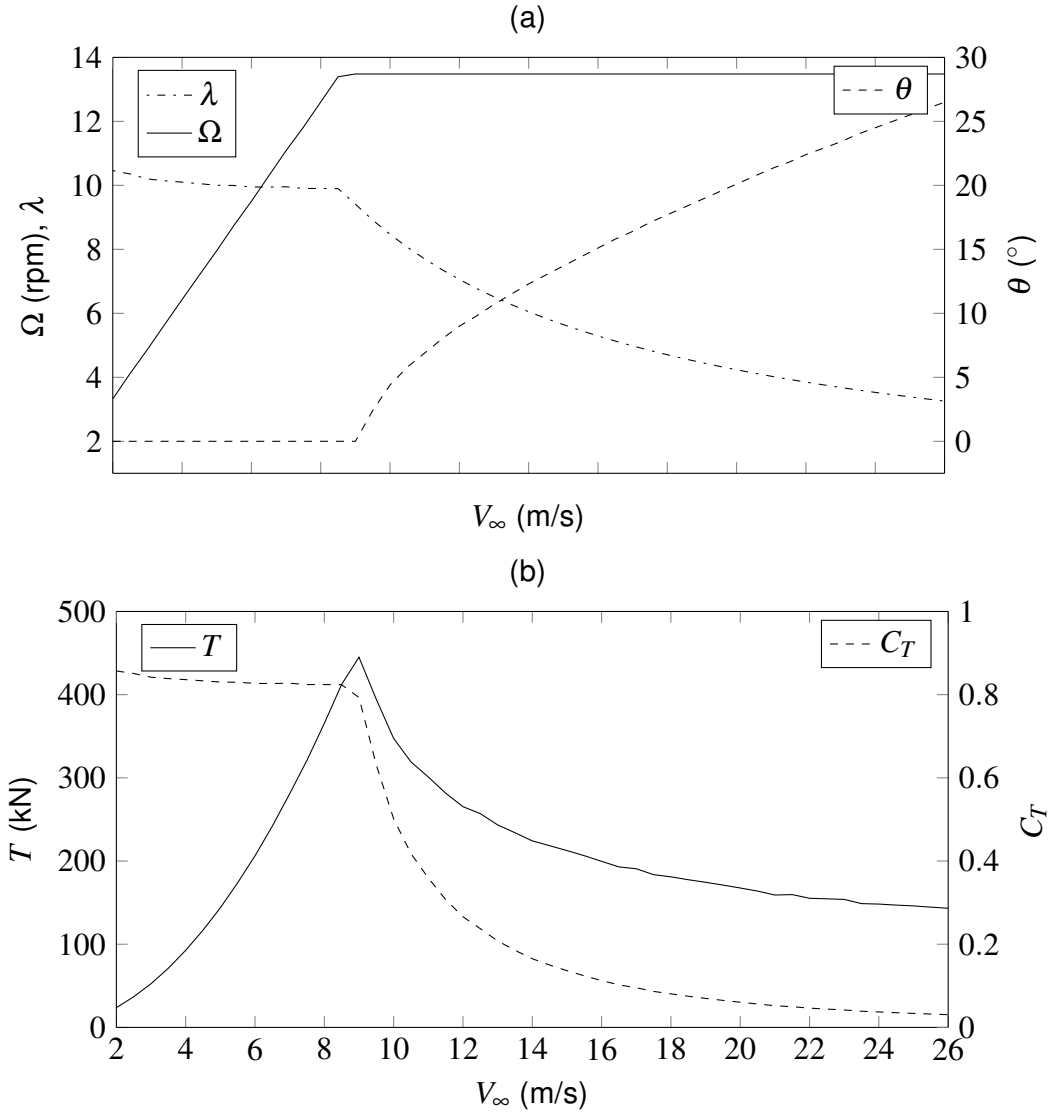

Figure 5.12: Rotor control (a) and thrust (b) characteristics.

The positioning of the true airfoils throughout the blade is shown by its three-dimensional wire-frame plot in Figure 5.13. The unlabelled airfoils shown in this figure are interpolated airfoils. Finally, the rendered Computer-Aided Design (CAD) drawing of this blade is presented at Figure 5.14. In order to generate this drawing, the coordinates of several points in more than one hundred cross sections were exported from MATLAB into a

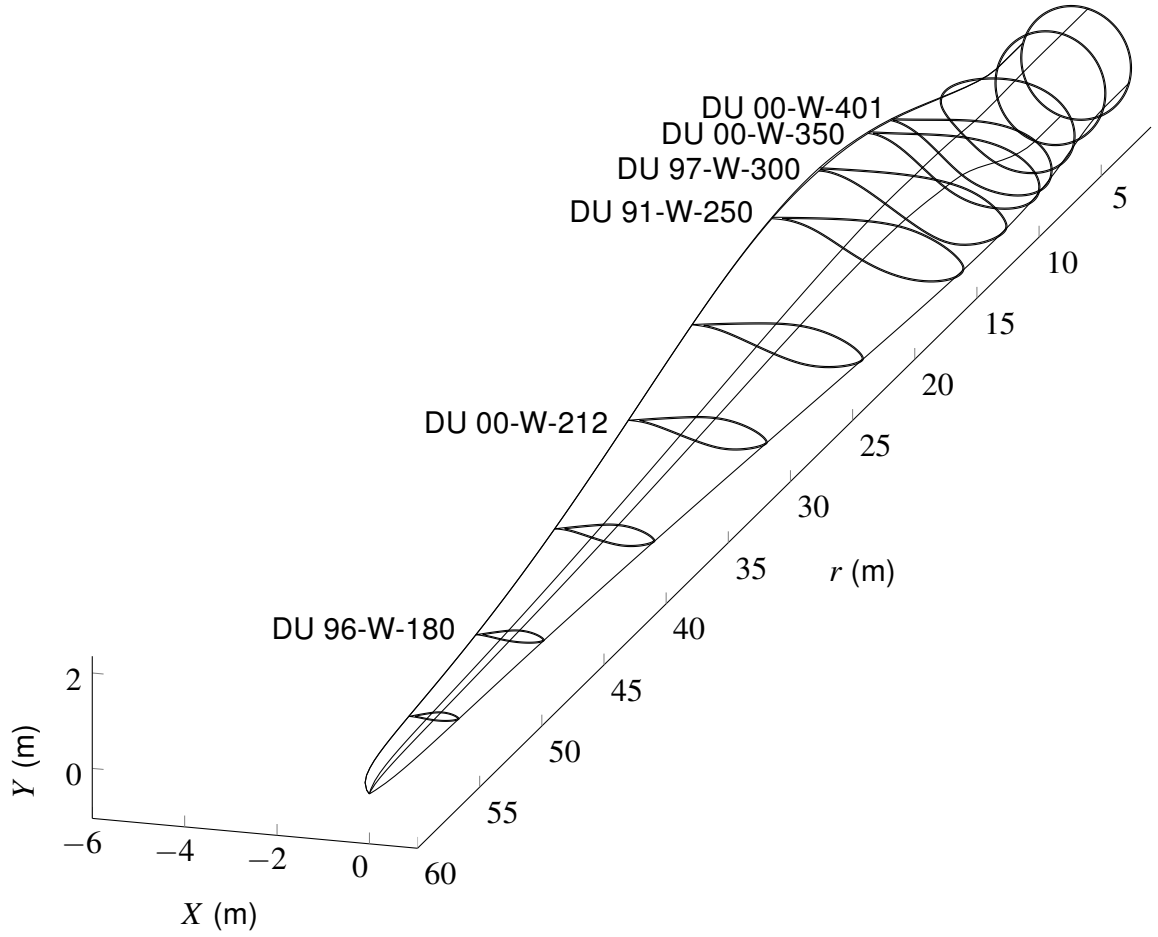

Figure 5.13: Wire-frame of the blade, detailing the spanwise placement of true airfoils.

worksheet, and then imported by a CAD software through the use of a macro programmed in Visual Basic for Applications (VBA).

Figure 5.14: Blade CAD drawing.

6 Conclusion and Future Work

In the present work, a design methodology based on metaheuristics was developed for the multi-objective optimization of the rotor blade geometry, which maximizes the energy production of wind turbines and minimizes the mass of the blade itself. Therefore, at first the multi-objective problem was formulated, with its two objective functions and four constraints. The procedures to calculate the AEP and the blade mass for a given solution were described, in which a BEM model for the first and a simple beam model for the second were applied. The blade geometry representation used in this work was presented, whereupon the parameters of the solution vector correspond to coordinates of control points for the chord, twist and thickness curves. Bézier curve parametrization and monotone piecewise cubic interpolation were applied to determine the geometrical properties at the blade element centers.

A benchmark problem was proposed, which was based on the wind conditions and present wind turbine concepts found in Brazil. This problem was used as a test-bed for the performance comparison of several metaheuristics, and also for the validation of the design methodology defined here. A variable speed pitch-controlled 2.5 MW DDSG turbine with a rotor diameter of 120 m was chosen as concept.

Five different MOEAs were selected for evaluation in solving this benchmark problem: NSGA-II, QMEA, T-MOEA/D, W-MOEA/D and MODE. 30 runs were performed with each metaheuristic, with maximum 15000 function evaluations each. Several performance metrics were computed with the approximated PFs and averaged over the runs of each algorithm. The results have shown that the two best performing techniques in this type of problem are NSGA-II and T-MOEA/D, one having more spread and evenly spaced solutions, and the other having a better convergence in the region of interest. QMEA was the worst MOEA in convergence and MODE the worst one in solutions distribution. As the MODE scheme used in the present work does not incorporate any distance metric, the distribution of solution points in the non-dominated front is really an issue with this approach. But the differences in overall performance were slight, because the algorithms have alter-

nated their positions in the evaluation rank of each metric. This was also evident by the fact that the known PF consisted of solutions from several techniques, with each dominating a different region of the objective space.

The analysis of the blade designs has shown that the human DM is better than the maximum harmonic mean DM for this MOP, given that the solution found by the former was better than the one found by the latter (superior aerodynamic efficiency with equivalent structural performance). Furthermore, the solution selected by human DM has demonstrated to be superior to the extreme solutions, because it provides a better trade-off between aerodynamic and structural performances, which will certainly result in a lower COE. This corroborates the fact that the multi-objective approach for the blade design is better than the mono-objective (considering either AEP maximization or blade mass minimization), because the extreme solutions would be the output of a mono-objective optimization.

The design methodology defined in this work does not perform the actual blade structural design, but it gives as output an aerodynamic design that is more friendly to the structure of the blade, balancing the loads and stresses throughout the blade span, thus avoiding stress concentration points. In this way, this design methodology can reduce the number of aerodynamic-to-structural design loops, thus reducing design time and cost.

Detailed analysis of the best blade design showed that the output of the design methodology is feasible in practice, given that flow conditions and operational features of the rotor are as desired, and also that the blade geometry is very smooth and easy to manufacture. Moreover, this geometry is easily exported to a CAD or Computer-Aided Engineering (CAE) software. Finally, proven by all the topics discussed here, the design methodology defined by the present work was validated, and consequently the general and specific objectives of this dissertation, defined in Section 1.4, were achieved.

However, the developed methodology still presents some shortcomings and limitations that must be addressed in the future. The main ones are discussed in the following items:

- The chosen DM process was not very robust, in the sense that it relies on the experience of the designer. Furthermore, based solely on the technical data it is difficult to state whether one solution is superior to another (for instance, solutions 3 is better than solution 2, stated in Section 5.4), because their cost-benefit cannot be inferred without the COE information. The proper DM strategy would be the selection of the solution with minimum COE.

- The structural model is not accurate enough to support the use of a COE model. To compute the actual blade mass and cost, the structural model should account for shear webs, spar caps and shells with different material properties.
- As discussed in Section 5.4, the positioning of two true airfoils close to one another in the region of maximum chord can cause some bumps to appear in the dimensional thickness distributions. This could be solved in the future with an improved thickness representation, with similar features as the chord and twist representation.
- The constraint handling in the present work also presents some issues. The death penalty applied when geometrical constraints are violated causes high death rates, specially in the first MOEA iterations, what causes the search to be more time consuming. Besides, not all the solutions in the PFs presented in Chapter 5 are feasible, i.e., some of them may violate the maximum angle of attack or the maximum allowable strain constraints.

The computational effort of the MOP handled in this work is substantially high, spending easily more than ten hours for a single run of a MOEA in a considerably fast computer. Also much of the research time was spent in the MOP formulation and in code writing, because one of the primary concerns of the author was that the output of the design methodology would be feasible in practice. The code used in this work is very extensive for a research application, taking valuable time to perform modifications or add new features. For this reasons, further work could not be accomplished in the available time of this research, and so it was left for the future. The main topics for this future research are summarized as follows:

- Apply a more advanced flow model for the rotor performance estimation, such as vortex or hybrid vortex/BEM methods. This would enable the modelling of non-planar blades, allowing features as winglets and swept blades to be taken in account.
- Investigate the proper setting of the angle of attack margin, by a sensitivity analysis of the angle of attack in case of upflow and wind shear. This would result in a more effective angle of attack constraint.
- Apply other MOEA frameworks to the benchmark problem, such as MOEAs based on decision maker's preference, indicator-based, hybrid, memetic, based on co-evolution, and with external archive. This would grow the experimental database on this MOP, and contribute to a continuous evolution of the blade design methodology. Also apply

more advanced MODE schemes that promote the diversity of solutions in the objective space.

- Carry out the parameter tuning of metaheuristics for this problem, which could improve their performance. This could either be accomplished by empirically switching parameters, running the algorithms and measuring their performance repeatedly, or by applying parameter tuning methods, such as the ones described by Smit and Eiben [146].

- Use generational performance metrics, e.g. progress measure [147], generational distance [93], generational non-dominated vector generation [144], and non-dominated vector addition [144], to assess the convergence issues in the algorithms, specially in QMEA.

- Perform correlation analysis of the decision variables and objective values in the known PS, by making use of the R indicator [86] for each combination of them. This would give a better understanding of the proposed MOP, e.g. about how much each decision variable affect each objective function.

- Run the original version of HARP_Opt, from Sale [13], on the benchmark problem proposed in Section 4.4, and compare the resulting blade designs with the ones presented in this dissertation. This would make more evident the actual improvements to the HARP_Opt approach, caused by the modifications and new features outlined in Section 1.5.

6.1 Publications

The following papers, related to this dissertation, were published during the development of the present work:

VIANNA NETO, J. X.; BERNERT, D. L. A.; COELHO, L. S. Improved quantum-inspired evolutionary algorithm with diversity information applied to economic dispatch problem with prohibited operating zones. *Energy Conversion and Management*, v. 52, n. 1, p. 8-14, 2011.

VIANNA NETO, J. X. et al. Wind turbine blade aerodynamic design through quantum-inspired evolutionary algorithm. In: *Proceedings of the European Wind Energy Association (EWEA) 2012 Annual Event*. Copenhagen, Denmark, 2012.

VIANNA NETO, J. X. et al. The wind power market in Brazil - an overview. In: *Proceedings of the European Wind Energy Association (EWEA) 2012 Annual Event*. Copenhagen, Denmark, 2012.

VIANNA NETO, J. X. et al. Projeto e verificação das características aerodinâmicas de três perfis aerodinâmicos voltados à geração eólica nas condições de vento do nordeste brasileiro. In: *XXI Seminário Nacional de Produção e Transmissão de Energia Elétrica (SNPTEE)*. Florianópolis, SC, Brazil, 2011.

References

1 ENDE, M. *Die unendliche Geschichte*. Stuttgart, Germany: Thienemann Verlag, 1979.

2 AGÊNCIA NACIONAL DE ENERGIA ELÉTRICA (ANEEL). *Capacidade de Geração do Brasil*. November 2012. Disponível em: <http://www.aneel.gov.br/aplicacoes/capacidadebrasil/capacidadebrasil.asp>.

3 AMARANTE, O. A. C. et al. *Atlas do Potencial Eólico Brasileiro*. Brasília, DF, Brazil, 2001.

4 MINISTÉRIO DE MINAS E ENERGIA (MME); EMPRESA DE PESQUISA ENERGÉTICA (EPE). *Plano Decenal de Expansão de Energia 2020*. Brasília, DF, Brazil, 2011.

5 CÂMARA DE COMERCIALIZAÇÃO DE ENERGIA ELÉTRICA (CCEE). *Leilões*. November 2012. Disponível em: <http://www.ccee.org.br/>.

6 BURTON, T. et al. *Wind Energy Handbook*. Chichester, West Sussex, United Kingdom: John Wiley & Sons, Ltd., 2001.

7 JURECZKO, M.; PAWLAK, M.; MEZYK, A. Optimisation of wind turbine blades. *Journal of Materials Processing Technology*, v. 167, n. 2, p. 463 – 471, 2005.

8 SELIG, M. S.; COVERSTONE-CARROLL, V. L. Application of a genetic algorithm to wind turbine design. *Journal of Energy Resources Technology*, v. 118, n. 1, p. 22–28, 1996.

9 MÉNDEZ, J.; GREINER, D. Wind blade chord and twist angle optimization using genetic algorithms. In: *Proceedings of the Fifth International Conference on Engineering Computational Technology*. Las Palmas de Gran Canaria, Spain: [s.n.], 2006. Paper 59.

10 LIU, X.; CHEN, Y.; YE, Z. Optimization model for rotor blades of horizontal axis wind turbines. *Frontiers of Mechanical Engineering in China*, v. 2, n. 4, p. 483–488, 2007.

11 XUAN, H. et al. Aerodynamic and aeroacoustic optimization of wind turbine blade by a genetic algorithm. In: *46th American Institute of Aeronautics and Astronautics (AIAA) Aerospace Sciences Meeting and Exhibit*. Reno, Nevada, United States of America: [s.n.], 2008.

12 EKE, G. B.; ONYEWUDIALA, J. I. Optimization of wind turbine blades using genetic algorithm. *Global Journal of Researches in Engineering*, v. 10, n. 7, p. 22–26, 2010.

13 SALE, D. C. *HARP_Opt User's Guide*. Golden, Colorado, United States of America, June 2010. National Renewable Energy Laboratory (NREL), National Wind Technology Center (NWTC).

14 CASAS, V.; PENA, F.; DURO, R. Automatic design and optimization of wind turbine blades. In: *International Conference on Computational Intelligence for Modelling, Control and Automation, and International Conference on Intelligent Agents, Web Technologies and Internet Commerce*. Sydney, Australia: [s.n.], 2006. p. 205–211.

15 BENINI, E.; TOFFOLO, A. Optimal design of horizontal-axis wind turbines using blade-element theory and evolutionary computation. *Journal of Solar Energy Engineering*, v. 124, n. 4, p. 357–363, 2002.

16 ERNST, B. et al. Implementation of the cuckoo search algorithm to optimize the design of wind turbine rotor blades. In: *Proceedings of the European Wind Energy Association (EWEA) 2012 Annual Event*. Copenhagen, Denmark: [s.n.], 2012.

17 VIANNA NETO, J. X. et al. Wind turbine blade aerodynamic design through quantum-inspired evolutionary algorithm. In: *Proceedings of the European Wind Energy Association (EWEA) 2012 Annual Event*. Copenhagen, Denmark: [s.n.], 2012.

18 SALE, D. C. *HARP_Opt: An optimization code for the design of horizontal-axis wind and hydrokinetic turbines*. November 2012. National Wind Technology Center (NWTC) Design Codes. Disponível em: <http://wind.nrel.gov/designcodes/simulators/HARP_Opt/>.

19 PLATT, A. *WT_Perf: A Wind-Turbine Performance Predictor*. November 2012. National Wind Technology Center (NWTC) Design Codes. Disponível em: <http://wind.nrel.gov/designcodes/simulators/wtperf/>.

20 FARIN, G. E. *Curves and surfaces for computer-aided geometric design: a practical guide*. 4. ed. Ann Arbor, United States of America: University of Michigan Press, 1997. (Computer science and scientific computing, v. 1).

21 FRITSCH, F. N.; CARLSON, R. E. Monotone piecewise cubic interpolation. *SIAM Journal on Numerical Analysis*, Society for Industrial and Applied Mathematics, v. 17, n. 2, p. 238 – 246, 1980.

22 MANWELL, J.; MCGOWAN, J.; ROGERS, A. *Wind Energy Explained: Theory, Design and Application*. Chichester, West Sussex, United Kingdom: John Wiley & Sons, Ltd., 2010.

23 HAU, E. *Wind Turbines: Fundamentals, Technologies, Application, Economics*. Heidelberg, Germany: Springer-Verlag GmbH, 2012.

24 FINGERSH, L.; HAND, M.; LAXSON, A. *Wind Turbine Design Cost and Scaling Model*. Golden, Colorado, United States of America, December 2006. National Renewable Energy Laboratory (NREL), Technical Report NREL/TP-500-40566.

25 POLINDER, H. et al. Comparison of direct-drive and geared generator concepts for wind turbines. *IEEE Transactions on Energy Conversion*, v. 21, n. 3, p. 725 –733, 2006.

26 POLINDER, H.; SLOOTWEG, J. G. Design optimization of a synchronous generator for a direct-drive wind turbine. In: *Proceedings of the European Wind Energy Conference and Exhibition*. Copenhagen, Denmark: [s.n.], 2001. p. 1067–1070.

27 TAN, K.; ISLAM, S. Optimum control strategies in energy conversion of PMSG wind turbine system without mechanical sensors. *IEEE Transactions on Energy Conversion*, v. 19, n. 2, p. 392–399, 2004.

28 MUNTEANU, I. et al. *Optimal Control of Wind Energy Systems: Towards a Global Approach*. Heidelberg, Germany: Springer-Verlag GmbH, 2008. (Advances in Industrial Control).

29 WEIBULL, W. A statistical distribution function of wide applicability. *ASME Journal of Applied Mechanics*, v. 18, n. 3, p. 293–297, 1951.

30 INTERNATIONAL ELECTROTECHNICAL COMMISSION (IEC). *Wind Turbines — Part 1: Design requirements*. 3. ed. [S.l.], August 2005. IEC 61400-1.

31 GASCH, R.; TWELE, J. *Wind Power Plants: Fundamentals, Design, Construction and Operation*. Heidelberg, Germany: Springer-Verlag GmbH, 2011. (Electrical Engineering).

32 BETZ, A. *Wind-Energie und ihre Ausnutzung durch Windmühlen*. Göttingen, Germany: Vandenhoeck & Ruprecht, 1926.

33 SCHMITZ, G. Theorie und entwurf von windrädern optimaler leistung. *Wissenschaftliche Zeitschrift der Universität Rostock*, 1955/56. 5. Jahrgang.

34 WILSON, R.; LISSAMAN, P. *Applied aerodynamics of wind power machines*. United States of America: Oregon State University, 1974.

35 FUGLSANG, P.; MADSEN, H. Optimization method for wind turbine rotors. *Journal of Wind Engineering and Industrial Aerodynamics*, v. 80, n. 1, p. 191–206, 1999.

36 KENWAY, G.; MARTINS, J. R. R. A. Aerostructural shape optimization of wind turbine blades considering site-specific winds. In: *Proceedings of the 12th AIAA/ISSMO Multidisciplinary Analysis and Optimization Conference*. Victoria, British Columbia, Canada: [s.n.], 2008.

37 FUGLSANG, L. Integrated design of turbine rotors. In: *Proceedings of the 2008 European Wind Energy Conference & Exhibition (EWEC 2008)*. Brussels, Belgium: [s.n.], 2008.

38 XUDONG, W. et al. Shape optimization of wind turbine blades. *Wind Energy*, v. 12, n. 8, p. 781–803, 2009.

39 BOTTASSO, C.; CAMPAGNOLO, F.; CROCE, A. Multi-disciplinary constrained optimization of wind turbines. *Multibody System Dynamics*, v. 27, n. 1, p. 21–53, 2012.

40 GUIDELINES for Design of Wind Turbines. 2. ed. Copenhagen, Denmark: Det Norske Veritas and Risø National Laboratory, 2009.

41 SPERA, P. D. A. *Wind Turbine Technology: Fundamental Concepts in Wind Turbine Engineering*. 2. ed. New York, United States of America: American Society of Mechanical Engineers, 2009.

42 HANSEN, M. *Aerodynamics of Wind Turbines*. 2, illustrated, revised. ed. London, United Kingdom: Earthscan, 2012.

43 BETZ, A. Schraubenpropeller mit geringstem energieverlust. *Nachrichten von der Gesellschaft der Wissenschaften zu Göttingen, Mathematisch-Physikalische Klasse*, v. 1919, p. 193–217, 1919. Mit einem Zusatz von L. Prandtl.

44 MORIARTY, P. J.; HANSEN, A. C. *AeroDyn Theory Manual*. Golden, Colorado, United States of America, December 2005. National Renewable Energy Laboratory (NREL), Technical Report NREL/EL-500-36881.

45 GLAUERT, H. *The Analysis of Experimental Results in the Windmill Brake and Vortex Ring States of an Airscrew*. Great Britain: H.M. Stationery Office, 1926. (Reports and memoranda, v. 1026). Great Britain Aeronautical Research Committee.

46 ZHANG, Q.; LI, H. MOEA/D: a multiobjective evolutionary algorithm based on decomposition. *IEEE Transactions on Evolutionary Computation*, v. 11, n. 6, p. 712 –731, 2007.

47 ZHOU, A. et al. Multiobjective evolutionary algorithms: A survey of the state of the art. *Swarm and Evolutionary Computation*, v. 1, n. 1, p. 32 – 49, 2011.

48 SCHAFFER, J. D. Multiple objective optimization with vector evaluated genetic algorithms. In: *Proceedings of the 1st International Conference on Genetic Algorithms*. Hillsdale, NJ, United States of America: L. Erlbaum Associates Inc., 1985. p. 93–100.

49 DEB, K. et al. A fast and elitist multiobjective genetic algorithm: NSGA-II. *IEEE Transactions on Evolutionary Computation*, v. 6, n. 2, p. 182 –197, 2002.

50 FONSECA, C.; FLEMING, P. Genetic algorithms for multiobjective optimization: Formulation, discussion and generalization. In: *Proceedings of the 5th International Conference on Genetic Algorithms*. San Francisco, CA, Unites States of America: Morgan Kaufmann Publishers Inc., 1993. p. 416–423.

51 TANINO, T.; TANAKA, M.; HOJO, C. An interactive multicriteria decision making method by using a genetic algorithm. In: *Proceedings of the 2nd International Conference on Systems Science and Systems Engineering*. [S.l.: s.n.], 1993. p. 381–386.

52 ZITZLER, E.; KÜNZLI, S. Indicator-based selection in multiobjective search. In: YAO, X. et al. (Ed.). *Parallel Problem Solving from Nature - PPSN VIII*. Heidelberg, Germany: Springer-Verlag GmbH, 2004, (Lecture Notes in Computer Science, v. 3242). p. 832–842.

53 ELHOSSINI, A.; AREIBI, S.; DONY, R. Strength Pareto particle swarm optimization and hybrid EA-PSO for multi-objective optimization. *Evolutionary Computation*, v. 18, n. 1, p. 127–156, 2010.

54 LI, B.-B.; WANG, L. A hybrid quantum-inspired genetic algorithm for multiobjective flow shop scheduling. *IEEE Transactions on Systems, Man, and Cybernetics, Part B: Cybernetics*, v. 37, n. 3, p. 576 –591, 2007.

55 YANG, D.; JIAO, L.; GONG, M. Adaptive multi-objective optimization based on nondominated solutions. *Computational Intelligence*, v. 25, n. 2, p. 84–108, 2009.

56 ISHIBUCHI, H.; MURATA, T. A multi-objective genetic local search algorithm and its application to flowshop scheduling. *IEEE Transactions on Systems, Man, and Cybernetics, Part C: Applications and Reviews*, v. 28, n. 3, p. 392–403, 1998.

57 DEB, K.; MOHAN, M.; MISHRA, S. Evaluating the epsilon-domination based multiobjective evolutionary algorithm for a quick computation of pareto-optimal solutions. *Evolutionary Computation*, v. 13, n. 4, p. 501 – 525, 2005.

58 WANG, T. et al. Large-scale wind turbine blade design and aerodynamic analysis. *Chinese Science Bulletin*, v. 57, n. 5, p. 466–472, 2012.

59 THIAUX, Y. et al. Load profile impact on the gross energy requirement of stand-alone photovoltaic systems. *Renewable Energy*, v. 35, n. 3, p. 602–613, 2010.

60 MASAZADE, E. et al. A multiobjective optimization approach to obtain decision thresholds for distributed detection in wireless sensor networks. *IEEE Transactions on Systems, Man, and Cybernetics, Part B: Cybernetics*, v. 40, n. 2, p. 444–457, 2010.

61 STEUERNAGEL, O.; POLANI, D. Multiobjective optimization applied to the eradication of persistent pathogens. *IEEE Transactions on Evolutionary Computation*, v. 14, n. 5, p. 759–765, 2010.

62 DEMIR, G. N.; UYAR, A. S.; GÜNDÜZ-ÖGÜDÜCÜ, S. Multiobjective evolutionary clustering of web user sessions: a case study in web page recommendation. *Soft Computing*, v. 14, n. 6, p. 579–597, 2010.

63 WOZNIAK, P. Preferences in multi-objective evolutionary optimisation of electric motor speed control with hardware in the loop. *Applied Soft Computing*, v. 11, n. 1, p. 49–55, 2011.

64 LI, B.-B.; WANG, L. A hybrid quantum-inspired genetic algorithm for multiobjective flow shop scheduling. *IEEE Transactions on Systems, Man, and Cybernetics, Part B: Cybernetics*, v. 37, n. 3, p. 576–591, 2007.

65 WEI, W. et al. A multi-objective HW-SW co-synthesis algorithm based on quantum-inspired evolutionary algorithm. *International Journal of Computational Intelligence and Applications*, v. 7, n. 2, p. 129–148, 2008.

66 KIM, Y.-H.; KIM, J.-H. Multiobjective quantum-inspired evolutionary algorithm for fuzzy path planning of mobile robot. In: *Proceedings of the 2009 IEEE Congress on Evolutionary Computation (CEC 2009)*. Trondheim, Norway: [s.n.], 2009. p. 1185–1192.

67 KIM, J.-H. et al. Preference-based solution selection algorithm for evolutionary multiobjective optimization. *IEEE Transactions on Evolutionary Computation*, v. 16, n. 1, p. 20–34, 2012.

68 PARK, I.-W. et al. Multi-objective quantum-inspired evolutionary algorithm-based optimal control of two-link inverted pendulum. In: *Proceedings of the 2010 IEEE Congress on Evolutionary Computation (CEC 2010)*. Barcelona, Spain: [s.n.], 2010. p. 1–7.

69 HONG, Y.-D. et al. Evolutionary multiobjective footstep planning for humanoid robots. *IEEE Transactions on Systems, Man, and Cybernetics, Part C: Applications and Reviews*, v. 41, n. 4, p. 520–532, 2011.

70 PARK, I.-W.; LEE, K.-B.; KIM, J.-H. Multi-objective evolutionary algorithm-based optimal posture control of humanoid robots. In: *Proceedings of the 2012 IEEE Congress on Evolutionary Computation (CEC 2012)*. Brisbane, Australia: [s.n.], 2012. p. 1–7.

71 XU, B. et al. Multi-tasking agent coalition formation based on quantum multi-objective evolutionary algorithm. *Xitong Gongcheng Lilun yu Shijian/System Engineering Theory and Practice*, v. 32, n. 10, p. 2253–2261, 2012.

72 CHANG, P. C. et al. MOEA/D for flowshop scheduling problems. In: *Proceedings of the 2008 IEEE Congress on Evolutionary Computation (CEC 2008)*. Hong Kong: [s.n.], 2008. p. 1433–1438.

73 PALMERS, P. et al. Massively multi-topology sizing of analog integrated circuits. In: *Conference on Design, Automation Test in Europe (DATE 2009)*. Nice, France: [s.n.], 2009. p. 706–711.

74 YUEN, T. J.; RAMLI, R. Comparison of computational efficiency of MOEA/D and NSGA-II for passive vehicle suspension optimization. In: *Proceedings of the 24th European Conference on Modelling and Simulation (ECMS 2010)*. Kuala Lumpur, Malaysia: [s.n.]. p. 219–225.

75 CHEN, C.-M. et al. Optimizing degree distributions in LT codes by using the multiobjective evolutionary algorithm based on decomposition. In: *Proceedings of the 2010 IEEE Congress on Evolutionary Computation (CEC 2010)*. Barcelona, Spain: [s.n.], 2010. p. 1–8.

76 KONSTANTINIDIS, A. et al. Multi-objective mobile agent-based sensor network routing using MOEA/D. In: *Proceedings of the 2010 IEEE Congress on Evolutionary Computation (CEC 2010)*. Barcelona, Spain: [s.n.], 2010. p. 1–8.

77 CHAN, Y.-H.; CHIANG, T.-C.; FU, L.-C. A two-phase evolutionary algorithm for multiobjective mining of classification rules. In: *Proceedings of the 2010 IEEE Congress on Evolutionary Computation (CEC 2010)*. [S.l.: s.n.], 2010. p. 1–7.

78 WALDOCK, A.; CORNE, D. Multiple objective optimisation applied to route planning. In: *Proceedings of the 2011 Genetic and Evolutionary Computation Conference (GECCO 2011)*. Dublin, Ireland: [s.n.], 2011. p. 1827–1834.

79 VARADARAJAN, M.; SWARUP, K. Solving multi-objective optimal power flow using differential evolution. *IET Generation, Transmission & Distribution*, v. 2, n. 5, p. 720–730, 2008.

80 ALATAS, B.; AKIN, E.; KARCI, A. MODENAR: Multi-objective differential evolution algorithm for mining numeric association rules. *Applied Soft Computing*, v. 8, n. 1, p. 646–656, 2008.

81 QIAN, B. et al. Multi-objective no-wait flow-shop scheduling with a memetic algorithm based on differential evolution. *Soft Computing*, v. 13, n. 8-9, p. 847–869, 2009.

82 SARAVANAN, R. et al. Evolutionary multi criteria design optimization of robot grippers. *Applied Soft Computing*, v. 9, n. 1, p. 159–172, 2009.

83 KITAK, P. et al. Application of the hybrid multiobjective optimization methods on the capacitive voltage divider. *IEEE Transactions on Magnetics*, v. 45, n. 3, p. 1594–1597, 2009.

84 SURESH, K. et al. Multi-objective differential evolution for automatic clustering with application to micro-array data analysis. *Sensors*, v. 9, n. 5, p. 3981–4004, 2009.

85 PAL, S. et al. Linear antenna array synthesis with constrained multi-objective differential evolution. *Progress In Electromagnetics Research B*, v. 21, p. 87–111, 2010.

86 HANSEN, M. P.; JASZKIEWICZ, A. *Evaluating the quality of approximations to the non-dominated set*. Kongens Lyngby, Denmark, March 1998. Technical University of Denmark, Technical Report IMM-REP-1998-7.

87 ZITZLER, E.; THIELE, L. Multiobjective evolutionary algorithms: a comparative case study and the strength pareto approach. *IEEE Transactions on Evolutionary Computation*, v. 3, n. 4, p. 257–271, 1999.

88 ZITZLER, E. et al. Performance assessment of multiobjective optimizers: an analysis and review. *IEEE Transactions on Evolutionary Computation*, v. 7, n. 2, p. 117 – 132, 2003.

89 ESBENSEN, H.; KUH, E. Design space exploration using the genetic algorithm. In: *IEEE International Symposium on Circuits and Systems, ISCAS 1996*. [S.l.: s.n.], 1996. v. 4, p. 500–503.

90 CZYZAK, P.; JASZKIEWICZ, A. Pareto simulated annealing—a metaheuristic technique for multiple-objective combinatorial optimization. *Journal of Multi-Criteria Decision Analysis*, v. 7, n. 1, p. 34–47, 1998.

91 ULUNGU, E. et al. MOSA method: a tool for solving multiobjective combinatorial optimization problems. *Journal of Multi-Criteria Decision Analysis*, v. 8, n. 4, p. 221–236, 1999.

92 VELDHUIZEN, D. A. V. *Multiobjective evolutionary algorithms: classifications, analyses, and new innovations*. Tese (Doutorado), Wright Patterson AFB, OH, United States of America, 1999. AAI9928483.

93 VELDHUIZEN, D. A. V.; LAMONT, G. B. Evolutionary computation and convergence to a pareto front. In: KOZA, J. R. (Ed.). *Late Breaking Papers at the Genetic Programming 1998 Conference*. University of Wisconsin, Madison, Wisconsin, United States of America: Stanford University Bookstore, 1998. p. 221–228.

94 SRINIVAS, N.; DEB, K. Multiobjective optimization using nondominated sorting in genetic algorithms. *Evolutionary Computation*, v. 2, n. 3, p. 221–248, 1994.

95 SCHOTT, J. R. *Fault tolerant design using single and multicriteria genetic algorithm optimization*. Dissertação (Master's Thesis) — Massachusetts Institute of Technology, Department of Aeronautics and Astronautics, Cambridge, Massachusetts, United States of America, 1995.

96 ZITZLER, E. *Evolutionary Algorithms for Multiobjective Optimization: Methods and Applications*. Tese (Doutorado) — ETH Zurich, Switzerland, 1999.

97 SAYIN, S. Measuring the quality of discrete representations of efficient sets in multiple objective mathematical programming. *Mathematical Programming*, v. 87, n. 3, p. 543–560, 2000.

98 DEB, K. *Multi-Objective Optimization using Evolutionary Algorithms*. Chichester, West Sussex, United Kingdom: John Wiley & Sons, Ltd., 2001. (Wiley Interscience Series in Systems and Optimization).

99 WU, J.; AZARM, S. Metrics for quality assessment of a multiobjective design optimization solution set. *Journal of Mechanical Design*, v. 123, n. 1, p. 18–25, 2001.

100 KNOWLES, J.; THIELE, L.; ZITZLER, E. *A Tutorial on the Performance Assessment of Stochastic Multiobjective Optimizers*. Zurich, Switzerland, February 2006. Computer Engineering and Networks Laboratory (TIK), ETH Zurich, TIK Report 214.

101 KNOWLES, J.; NAKAYAMA, H. Multiobjective optimization. In: BRANKE, J. et al. (Ed.). Heidelberg, Germany: Springer-Verlag GmbH, 2008, (Lecture Notes in Computer Science / Theoretical Computer Science and General Issues, v. 5252). cap. Meta-Modeling in Multiobjective Optimization, p. 245–284.

102 HOLLAND, J. *Adaptation in natural and artificial systems: an introductory analysis with applications to biology, control, and artificial intelligence*. Ann Arbor, United States of America: University of Michigan Press, 1975.

103 DEB, K. et al. A fast elitist non-dominated sorting genetic algorithm for multi-objective optimization: NSGA-II. In: SCHOENAUER, M. et al. (Ed.). *Parallel Problem Solving from Nature - PPSN VI*. Heidelberg, Germany: Springer-Verlag GmbH, 2000, (Lecture Notes in Computer Science, v. 1917). p. 849–858.

104 SALAZAR, D.; ROCCO, C. M.; GALVÁN, B. J. Optimization of constrained multiple-objective reliability problems using evolutionary algorithms. *Reliability Engineering & System Safety*, v. 91, n. 9, p. 1057 – 1070, 2006.

105 HAN, K.-H.; KIM, J.-H. Quantum-inspired evolutionary algorithm for a class of combinatorial optimization. *IEEE Transactions on Evolutionary Computation*, v. 6, n. 6, p. 580 – 593, 2002.

106 HAN, K.-H.; KIM, J.-H. Genetic quantum algorithm and its application to combinatorial optimization problem. In: *Proceedings of the 2000 IEEE Congress on Evolutionary Computation (CEC 2000)*. San Diego, CA, Unites States of America: [s.n.], 2000. v. 2, p. 1354 –1360.

107 HAN, K.-H.; KIM, J.-H. Quantum-inspired evolutionary algorithms with a new termination criterion, h epsilon gate, and two-phase scheme. *IEEE Transactions on Evolutionary Computation*, v. 8, n. 2, p. 156 – 169, 2004.

108 CRUZ, A. V. A. da et al. Quantum-inspired evolutionary algorithms and its application to numerical optimization problems. In: PAL, N. et al. (Ed.). *Neural Information Processing*. Heidelberg, Germany: Springer-Verlag GmbH, 2004, (Lecture Notes in Computer Science, v. 3316). p. 212–217.

109 LI, P.; LI, S. Quantum-inspired evolutionary algorithm for continuous space optimization based on bloch coordinates of qubits. *Neurocomputing*, v. 72, n. 1-3, p. 581 – 591, 2008.

110 WANG, L.; TANG, F.; WU, H. Hybrid genetic algorithm based on quantum computing for numerical optimization and parameter estimation. *Applied Mathematics and Computation*, v. 171, n. 2, p. 1141–1156, 2005.

111 VIANNA NETO, J. X.; BERNERT, D. L. A.; COELHO, L. S. Improved quantum-inspired evolutionary algorithm with diversity information applied to economic dispatch problem with prohibited operating zones. *Energy Conversion and Management*, v. 52, n. 1, p. 8–14, 2011.

112 KIM, Y.; KIM, J.-H.; HAN, K.-H. Quantum-inspired multiobjective evolutionary algorithm for multiobjective 0/1 knapsack problems. In: *Proceedings of the 2006 IEEE Congress on Evolutionary Computation (CEC 2006)*. Vancouver, BC, Canada: [s.n.], 2006. p. 2601–2606.

113 MIETTINEN, K. *Nonlinear Multiobjective Optimization*. Dordrecht, Netherlands: Kluwer Academic Publishers, 1998. (International Series in Operations Research & Management Science, v. 12).

114 STORN, R.; PRICE, K. *Differential Evolution – A Simple and Efficient Adaptive Scheme for Global Optimization over Continuous Spaces*. Berkeley, California, United States of America, March 1995. International Computer Science Institute (ICSI), ICSI Technical Report TR-95-012.

115 PRICE, K.; STORN, R.; LAMPINEN, J. *Differential Evolution: A Practical Approach to Global Optimization*. Heidelberg, Germany: Springer-Verlag GmbH, 2005. (Natural Computing Series).

116 STORN, R.; PRICE, K. Differential evolution – a simple and efficient heuristic for global optimization over continuous spaces. *Journal of Global Optimization*, v. 11, n. 4, p. 341–359, 1997.

117 DAS, S.; SUGANTHAN, P. Differential evolution: A survey of the state-of-the-art. *IEEE Transactions on Evolutionary Computation*, v. 15, n. 1, p. 4–31, 2011.

118 CHANG, C.; XU, D.; QUEK, H. Pareto-optimal set based multiobjective tuning of fuzzy automatic train operation for mass transit system. *IEE Proceedings on Electric Power Applications*, v. 146, n. 5, p. 577–583, 1999.

119 LAMPINEN, J. *DE's Selection Rule for Multiobjective Optimization*. Lappeenranta, Finland, July 2001. Technical Report, Lappeenranta University of Technology, Department of Information Technology.

120 ABBASS, H. A.; SARKER, R. The pareto differential evolution algorithm. *International Journal on Artificial Intelligence Tools*, v. 11, n. 04, p. 531–552, 2002.

121 XUE, F.; SANDERSON, A.; GRAVES, R. Pareto-based multi-objective differential evolution. In: *Proceedings of the 2003 IEEE Congress on Evolutionary Computation (CEC 2003)*. Canberra, Australia: [s.n.], 2003. v. 2, p. 862–869.

122 IORIO, A.; LI, X. Solving rotated multi-objective optimization problems using differential evolution. In: WEBB, G.; YU, X. (Ed.). *AI 2004: Advances in Artificial Intelligence*. Heidelberg, Germany: Springer-Verlag GmbH, 2005, (Lecture Notes in Computer Science, v. 3339). p. 861–872.

123 KUKKONEN, S.; LAMPINEN, J. GDE3: the third evolution step of generalized differential evolution. In: *Proceedings of the 2005 IEEE Congress on Evolutionary Computation (CEC 2005)*. Edinburgh, United Kingdom: [s.n.], 2005. v. 1, p. 443–450.

124 ROBIC, T.; FILIPIC, B. DEMO: Differential evolution for multiobjective optimization. In: COELLO, C. C.; AGUIRRE, A. H.; ZITZLER, E. (Ed.). *Evolutionary Multi-Criterion Optimization*. Heidelberg, Germany: Springer-Verlag GmbH, 2005, (Lecture Notes in Computer Science, v. 3410). p. 520–533.

125 KUKKONEN, S.; LAMPINEN, J. An extension of generalized differential evolution for multi-objective optimization with constraints. In: YAO, X. et al. (Ed.). *Parallel Problem Solving from Nature - PPSN VIII*. Heidelberg, Germany: Springer-Verlag GmbH, 2004, (Lecture Notes in Computer Science, v. 3242). p. 752–761.

126 SANTANA-QUINTERO, L. V.; COELLO, C. A. C. An algorithm based on differential evolution for multi-objective problems. *International Journal of Computational Intelligence Research*, v. 1, n. 2, p. 151–169, 2005.

127 LAUMANNS, M. et al. Combining convergence and diversity in evolutionary multiobjective optimization. *Evolutionary Computation*, v. 10, n. 3, p. 263–282, 2002.

128 BABU, B.; JEHAN, M. Differential evolution for multi-objective optimization. In: *Proceedings of the 2003 IEEE Congress on Evolutionary Computation (CEC 2003)*. Canberra, Australia: [s.n.], 2003. v. 4, p. 2696–2703.

129 LI, H.; ZHANG, Q. A multiobjective differential evolution based on decomposition for multiobjective optimization with variable linkages. In: RUNARSSON, T. et al. (Ed.). *Parallel Problem Solving from Nature - PPSN IX*. Heidelberg, Germany: Springer-Verlag GmbH, 2006, (Lecture Notes in Computer Science, v. 4193). p. 583–592.

130 QU, B.; SUGANTHAN, P. Multi-objective evolutionary algorithms based on the summation of normalized objectives and diversified selection. *Information Sciences*, v. 180, n. 17, p. 3170–3181, 2010.

131 ZAMUDA, A. et al. Differential evolution for multiobjective optimization with self adaptation. In: *Proceedings of the 2007 IEEE Congress on Evolutionary Computation (CEC 2007)*. Singapore: [s.n.], 2007. p. 3617–3624.

132 HUANG, V. et al. Multi-objective optimization based on self-adaptive differential evolution algorithm. In: *Proceedings of the 2007 IEEE Congress on Evolutionary Computation (CEC 2007)*. Singapore: [s.n.], 2007. p. 3601–3608.

133 HUANG, V. et al. Multi-objective optimization using self-adaptive differential evolution algorithm. In: *Proceedings of the 2009 IEEE Congress on Evolutionary Computation (CEC 2009)*. Trondheim, Norway: [s.n.], 2009. p. 190–194.

134 TIMMER, W. A.; ROOIJ, R. P. J. O. M. van. Summary of the delft university wind turbine dedicated airfoils. *Journal of Solar Energy Engineering*, v. 125, n. 4, p. 488–496, 2003.

135 ROOIJ, R. P. J. O. M. van; TIMMER, W. A. Roughness sensitivity considerations for thick rotor blade airfoils. *Journal of Solar Energy Engineering*, v. 125, n. 4, p. 468–478, 2003.

136 TIMMER, W. A.; SCHAFFARCZYK, A. P. The effect of roughness at high Reynolds numbers on the performance of aerofoil DU 97-W-300Mod. *Wind Energy*, v. 7, n. 4, p. 295–307, 2004.

137 SESHADRI, A. *NSGA-II: A multi-objective optimization algorithm*. July 2009. MATLAB File Exchange. Disponível em: <http://www.mathworks.com/matlabcentral/fileexchange/10429-nsga-ii-a-multi-objective-optimization-algorithm>.

138 DEB, K.; AGRAWAL, R. B. Simulated binary crossover for continuous search space. *Complex Systems*, v. 9, n. 2, p. 115–148, 1995.

139 ZHANG, Q. *MOEA/D: Matlab code for continuous MOP*. November 2012. Disponível em: <dces.essex.ac.uk/staff/qzhang/moead/moeadmatlab.rar>.

140 REYNOSO-MEZA, G. *Multi-objective Optimization Differential Evolution Algorithm*. November 2012. MATLAB File Exchange. Disponível em: <http://www.mathworks.com/matlabcentral/fileexchange/38962-multi-objective-optimization-differential-evolution-algorithm>.

141 KUKKONEN, S.; LAMPINEN, J. Generalized differential evolution for general nonlinear optimization. In: BRITO, P. (Ed.). *COMPSTAT 2008: Proceedings in Computational Statistics*. Heidelberg, Germany: Physica-Verlag HD, 2008. p. 459–471.

142 KRUISSELBRINK, J. W. *Hypervolume Computation*. November 2012. MATLAB File Exchange. Disponível em: <http://www.mathworks.com/matlabcentral/fileexchange/30785-hypervolume-computation>.

143 ENERCON GMBH. *ENERCON product overview*. November 2012. Disponível em: <http://www.enercon.de/p/downloads/ENERCON_PU_en.pdf>.

144 COELLO, C.; LAMONT, G.; VELDHUIZEN, D. *Evolutionary Algorithms for Solving Multi-Objective Problems*. Heidelberg, Germany: Springer-Verlag GmbH, 2007. (Genetic and evolutionary computation series).

145 AYALA, H. V. H.; COELHO, L. S. A multiobjective genetic algorithm applied to multivariable control optimization. In: MIYAGI, P. E.; HORIKAWA, O.; MOTTA, J. M. (Ed.). *ABCM Symposium Series in Mechatronics*. Rio de Janeiro, RJ, Brazil: The Brazilian Society of Mechanical Sciences and Engineer (ABCM), 2008, (ABCM Symposium Series, v. 3). p. 736–745.

146 SMIT, S. K.; EIBEN, A. Comparing parameter tuning methods for evolutionary algorithms. In: *Proceedings of the 2009 IEEE Congress on Evolutionary Computation (CEC 2009)*. Trondheim, Norway: [s.n.], 2009. p. 399–406.

147 BÄCK, T. *Evolutionary algorithms in theory and practice: evolution strategies, evolutionary programming, genetic algorithms*. Oxford, UK: Oxford University Press, 1996.

148 DEUTSCH, D. Quantum theory, the church-turing principle and the universal quantum computer. *Proceedings of the Royal Society A: Mathematical, Physical and Engineering Sciences*, v. 400, n. 1818, p. 97–117, 1985.

149 NEDJAH, N.; COELHO, L. S.; MOURELLE, L. de M. (Ed.). *Quantum Inspired Intelligent Systems*. Heidelberg, Germany: Springer-Verlag GmbH, 2008. (Studies in Computational Intelligence, v. 121).

150 HAN, K.-H.; KIM, J.-H. On the analysis of the quantum-inspired evolutionary algorithm with a single individual. In: *Proceedings of the 2006 IEEE Congress on Evolutionary Computation (CEC 2006)*. Vancouver, BC, Canada: [s.n.], 2006. p. 2622–2629.

APPENDIX A – Non-dominated Sorting Genetic Algorithm version II

The procedure of NSGA-II is detailed in Pseudocode 2. This algorithm starts with a random parent population $P(0)$ of n individuals, which are sorted with respect to their non-domination level. The non-dominated sort is better understood by interpretation of Figure 3.2(a), of a minimization MOP. Each individual is assigned a rank according to the level of the non-dominated front that it belongs. This procedure will be more detailed later on. Then an offspring population $Q(0)$ of the same size is created, by use of selection, crossover and mutation operators. The selection operator is the usual binary tournament, but the selection criterion is based on the crowded-comparison operator, which, as defined by Deb et al. [49, 103], requires primarily the non-domination rank, and in case of draw it then uses the crowding-distance (which will also be explained hereafter).

Afterwards, the algorithm enters in its main loop. Current parent and offspring populations, $P(t)$ and $Q(t)$, are combined in $R(t)$, of size $2n$, and again sorted based on non-domination. This introduces elitism in NSGA-II, because all parent and offspring individuals are included in $R(t)$. The next generation parent population, $P(t+1)$, is formed by half of the current combined population $R(t)$. The individuals in each non-dominated front, NF_i, are included in $P(t+1)$ in the order of their rank. When the inclusion of the i-th non-dominated front individuals exceeds the size of $P(t+1)$, they are sorted in the descending order of their crowding-distance, and then included in this order until the parent population is filled with exactly n individuals. At last, the next offspring population $Q(t+1)$ is created, again through the use of selection, crossover and mutation operators. This loop repeats itself until the stopping criterion is satisfied.

The non-dominated sort procedure is explained by Pseudocode 3. As previously mentioned, this procedure assigns a rank to each solution of the set A, that corresponds to the level of the non-dominated front that it belongs. Therefore, two parameters are computed for each solution p: n_p, the domination count, which describes the number of solutions that dominate p; and S_p, a set of solutions dominated by p. If n_p is zero, the solution

Pseudocode 2 Non-dominated Sorting Genetic Algorithm version II

Begin of NSGA-II

$t \leftarrow 0$, initialize the generation counter
Generate initial random population $P(0)$ with size n
Sort $P(0)$ based on the non-domination level
Use selection, crossover and mutation to create an offspring population $Q(0)$ also with size n
while not stopping condition **do**
  $R(t) \leftarrow P(t) \cup Q(t)$, combine parent and offspring populations
  Sort $R(t)$ based on the non-domination level
  $P(t+1) \leftarrow \{\}$ and $i \leftarrow 1$
  while $|P(t+1)| + |NF_i| \leq n$ **do**
    Calculate the crowding-distance of individuals in NF_i
    $P(t+1) \leftarrow P(t+1) \cup NF_i$, include the i-th non-dominated front in the parent population
    $i \leftarrow i+1$
  end while
  Sort NF_i in descending order based on the crowding distance
  Include the first $n - |P(t+1)|$ elements of NF_i in $P(t+1)$
  Use selection, crossover and mutation to create the next offspring population $Q(t+1)$
  $t \leftarrow t+1$, update the generation counter
end while

End of NSGA-II

p belongs to the first non-dominated front, NF_1, and a value of 1 will be assigned to its rank (p_{rank}). Now each next front NF_{i+1} will be identified in a loop, by reducing the domination count of each q in S_p by one, for each p in NF_i. By doing that, if any n_q becomes zero, it means that the solution q belongs to the next front NF_{i+1}.

The diversity preservation, or niching, is conducted by NSGA-II through a crowding-comparison approach. This metaheuristic promotes the individuals with higher crowding-distance values in the selection and population reduction phases. This keeps the spread of solutions and helps NSGA-II to explore the fitness landscape. The crowding-distance assignment procedure of the solutions in a non-dominated set A is detailed in Pseudocode 4. The crowding-distance $x^j_{distance}$, of the j-th solution in the sorted set A, is calculated as half of the perimeter of the cuboid formed by its neighbour solutions, with a normalized objective space. As a matter of clarity, this cuboid is shown as a dashed box in Figure 3.2(b). For the extreme solutions x^1 and x^k, k being the number of solutions in A, the crowding-distance value is set as the infinity, so that they are always preferred over the others.

Pseudocode 3 Non-dominated Sort

Begin of sorting procedure of A

for each $p \in A$ **do**
  $NF_1 \leftarrow \{\}$
  $S_p \leftarrow \{\}$
  $n_p \leftarrow 0$
  for each $q \in A$ **do**
    if p dominates q **then**
      $S_p \leftarrow S_p \cup q$, add q to the set of solutions dominated by p
    else
      if q dominates p **then**
        $n_p \leftarrow n_p + 1$, update the domination counter of p
      end if
    end if
  end for
  if $n_p = 0$ **then**
    $p_{rank} \leftarrow 1$, p belongs to the first non-dominated front NF_1
    $NF_1 \leftarrow NF_1 \cup p$
  end if
end for
$i \leftarrow 1$, initialize the front counter
while $NF_i \neq \{\}$ **do**
  $B = \{\}$, initialize the members set of the next front
  for each $p \in NF_i$ **do**
    for each $q \in S_p$ **do**
      $n_q \leftarrow n_q - 1$
      if $n_q = 0$ **then**
        $q_{rank} \leftarrow i + 1$, q belongs to the next non-dominated front NF_{i+1}
        $B \leftarrow B \cup q$
      end if
    end for
  end for
  $i = \leftarrow i + 1$, update the front counter
  $NF_i \leftarrow B$
end while

End of sorting procedure

Pseudocode 4 Crowding Distance Assignment

Begin of crowding distance assignment procedure of A

$k \leftarrow |A|$, number of solutions in A
for each $x \in A$ **do**
$x_{distance} \leftarrow 0$, initialize distance
end for
for each objective F_i **do**
Sort A using the objective values
$x^1_{distance} \leftarrow \infty$ and $x^k_{distance} \leftarrow \infty$, so that extreme points are always selected
for $j = 2 \rightarrow k-1$ **do**
$x^j_{distance} \leftarrow x^j_{distance} + \frac{F_i(x^{j+1}) - F_i(x^{j-1})}{\max(F_i) - \min(F_i)}$, for all other points
end for
end for

End of crowding distance assignment procedure

APPENDIX B – Quantum-inspired Evolutionary Algorithm

Since Deutsch first proposed the Deutsch-Jozsa algorithm in 1985 [148], quantum computation has been widely drawing the attention of many researchers in formulation of new optimization approaches. Quantum computation is a novel inter-discipline that includes quantum mechanics and information science. This emergent research field concentrates on studying quantum computation, which is characterized by certain principles of quantum mechanics such as interference, quantum bits, coherence and superposition of states [149].

Quantum-inspired evolutionary algorithms can be viewed as probability optimization algorithms based on quantum computation concept and theory. Recently, some quantum-inspired evolutionary algorithms have been proposed for some combinatorial [105–107] and continuous [108–110] optimization problems.

Han and Kim [105] proposed the QEA introducing a Q-gate as a variation operator to promote the optimization of the Q-bit individual. QEA uses Q-bits (Q-bit is defined by Han and Kim [105] and means quantum-inspired bit, which is inspired on qubit or quantum bit) as the smallest unit of information for representing individuals. A Q-bit-coded individual probabilistically represents all the states in the search space. The individuals are updated by quantum rotation gates, which can achieve an evolutionary search.

Unlike the classical bit, the Q-bit does not represent only the value 0 or 1 but a superposition of the two. Its state ($|\psi\rangle$) is given by:

$$|\psi\rangle = \alpha|0\rangle + \beta|1\rangle \ , \tag{B.1}$$

where $|0\rangle$ and $|1\rangle$ represent respectively the classical bit values 0 and 1; α and β are complex numbers that specify the probability amplitudes of the corresponding quantum state. Normalization of the state to unity always guarantees:

$$|\alpha|^2 + |\beta|^2 = 1 \ . \tag{B.2}$$

If a superposition is measured with respect to the basis $\{|0\rangle, |1\rangle\}$, the probability to have the value 0 is $|\alpha|^2$ and the probability to have the value 1 is $|\beta|^2$. In classical computing, the possible states of a n-bit system form a vector space of n dimensions, i.e., we have 2^n possible states. However, in a quantum system of n Q-bits, a single string represents all the 2^n classical states at the same time. It is this exponential growth of the state space with the number of particles that suggests a possible exponential speed-up of computation on quantum computers over classical computers. Each quantum operation will deal with all the states present within the superposition in parallel.

The representation of a m-Q-bits individual is defined as follows:

$$\left[\begin{array}{c|c|c|c} \alpha_1 & \alpha_2 & \cdots & \alpha_m \\ \beta_1 & \beta_2 & \cdots & \beta_m \end{array}\right] \tag{B.3}$$

where $|\alpha_i|^2 + |\beta_i|^2 = 1$, $i = 1, 2, \cdots, m$. Q-bit representation has the advantage that it is able to represent a linear superposition of states probabilistically. Furthermore, in this way, the m-Q-bits individual is able to represent the information of 2^m binary states simultaneously.

For the update process of QEA, suitable quantum gate $U(\Delta\theta)$ is usually adopted in compliance with optimization problems. In this work, a quantum rotation gate, such as

$$U(\Delta\theta_i) = \begin{bmatrix} \cos(\Delta\theta_i) & -\sin(\Delta\theta_i) \\ \sin(\Delta\theta_i) & \cos(\Delta\theta_i) \end{bmatrix} \tag{B.4}$$

is adopted as a basic gate of QEA, where $\Delta\theta_i$ is the rotation angle of each Q-bit toward either 0 or 1 state depending on its sign, and again $i = 1, 2, \cdots, m$. The values of $\Delta\theta_i$ should be designed in compliance with the application problem. Then let us briefly review the procedure of QEA in Pseudocode 5. For more details the reader is referred to [105].

In Pseudocode 5, $Q(t) = q_1^t, q_2^t, \cdots, q_n^t$ is a population of n Q-bit individuals at generation t; q_j^t is the j-th $(j = 1, 2, \cdots, n)$ individual defined as

$$q_j^t = \left[\begin{array}{c|c|c|c} \alpha_{j1}^t & \alpha_{j2}^t & \cdots & \alpha_{jm}^t \\ \beta_{j1}^t & \beta_{j2}^t & \cdots & \beta_{jm}^t \end{array}\right] \tag{B.5}$$

and $P(t) = x_1^t, x_2^t, \cdots, x_n^t$ is a set of binary solutions from observing the states of $Q(t)$, where x_j^t is the binary solution by observing q_j^t. A set of n binary solutions $B(t) = b_1^t, b_2^t, \cdots, b_n^t$ is maintained at the generation t, where b_j^t is the best j-th binary solution x_j between the generations 0 and t. The variable b stores the best binary solution among $B(t)$.

Pseudocode 5 Quantum-inspired Evolutionary Algorithm

Begin of QEA

$t \leftarrow 0$ initialize the generation counter
Initialize the population of Q-bits individuals $Q(t)$
Make $P(t)$ by observing the states of $Q(t)$
Convert $P(t)$ from binary to floating point representation $P_r(t)$
Evaluate the solutions given by floating point representation $P_r(t)$
Store the best binary individuals among $P(t)$ into $B(t)$ and its fitness
while not stopping condition **do**
  $t \leftarrow t+1$, update the generation counter
  Make $P(t)$ by observing the states of $Q(t-1)$
  Convert $P(t)$ from binary to floating point representation $P_r(t)$
  Evaluate the solutions given by floating point representation $P_r(t)$
  Update $Q(t)$ using suitable quantum gates (in this work, a quantum rotation gate)
  Store the best binary individuals among $P(t)$ and $B(t-1)$ into $B(t)$ and their fitness
  Store the best binary individual b among $B(t)$
  if global migration condition **then**
    Migrate b to $B(t)$ globally
  else
    if local migration condition **then**
      Migrate b_j^t to $B(t)$ locally
    end if
  end if
end while

End of QEA

In the 'initialize $Q(t)$' step, each pair of Q-bit probability amplitudes, α_{ji}^t and β_{ji}^t, are initialized with $1/\sqrt{2}$, $\forall q_j^t \in Q(t)$. The next step generates a set of binary solutions $P(t)$ where each bit of x_j^t is formed by determining the explicit state of each Q-bit of q_j^t, $|0\rangle$ state or $|1\rangle$ state, according to either $|\alpha_{ji}^t|^2$ or $|\beta_{ji}^t|^2$ of q_j^t. For example, to form a explicit state of the i-th bit of x_j^t, a number h is generated randomly with uniform distribution in the range $[0,1]$. Then, if $h < |\beta_{ji}^t|^2$, the i-th bit of x_j^t is set to be 1, otherwise, it is set to be 0. Each solution $x_j^t \in P(t)$ is a binary string of length m, and is evaluated to give some measure of its fitness. However, before evaluating the solutions, $P(t)$ is converted from binary to floating point representation $P_r(t)$. The initial binary solutions $P(t)$ are stored in $B(t)$, and the best binary solution b among $B(t)$ is then selected and stored. In the while loop, the quantum gate $U(\Delta\theta)$ is used to update $Q(t-1)$ so that fitter states of the Q-bit individuals are generated. The i-th Q-bit value (α_i^t, β_i^t) of q_j^t is updated as

$$\begin{bmatrix} \alpha_i^{t+1} \\ \beta_i^{t+1} \end{bmatrix} = U(\Delta\theta_i^t) \begin{bmatrix} \alpha_i^t \\ \beta_i^t \end{bmatrix} = \begin{bmatrix} \cos(\Delta\theta_i^t) & -\sin(\Delta\theta_i^t) \\ \sin(\Delta\theta_i^t) & \cos(\Delta\theta_i^t) \end{bmatrix} \begin{bmatrix} \alpha_i^t \\ \beta_i^t \end{bmatrix} . \tag{B.6}$$

The best solutions among $P(t)$ and $B(t-1)$ are then selected in the next step, and if the best current solution is fitter than the best stored solution, the best stored solution will be replaced by this current solution.

Figure 3.3 depicts the polar plot of the rotation gate for Q-bit individuals. In this dissertation, the angle parameters and lookup table (see Table B.1) used for the rotation gate of QEA were the same as the ones adopted in [105]. In this way, $\theta_3 = 0.01\pi$, $\theta_5 = -0.01\pi$, and 0 for the rest were used. The magnitude of $\Delta\theta_i$ has an effect on the speed of convergence, but if it is too high, the solutions may diverge or converge prematurely to a local optimum. The sign of $\Delta\theta_i$ determines the direction of convergence [105].

Table B.1: Lookup table of $\Delta\theta_i$, adapted from Han and Kim [105].

x_{ji}^t	b_{ji}^t	$f(x_j^t) \geq f(b_j^t)$	$\Delta\theta_i$
0	0	False	θ_1
0	0	True	θ_2
0	1	False	θ_3
0	1	True	θ_4
1	0	False	θ_5
1	0	True	θ_6
1	1	False	θ_7
1	1	True	θ_8

If the global migration condition is satisfied, the best solution is migrated to $B(t)$ globally. If the local migration condition is satisfied, the best one in a local group in $B(t)$ is migrated to others in the same local group. The migration process can induce a variation of the probabilities of a Q-bit individual. A local group in QEA is defined as the sub-population affected mutually by a local migration, and its size is the number of individuals in the local group [150].

In terms of stopping criterion, a limit of generation counter t_{max} is adopted.